# Emulsion-Based Supracolloidal Materials Stabilized by Specifically Designed Branched Copolymers

**Robert Valentine Bell**

**A thesis submitted in fulfillment of the requirements for the degree of Doctor of Philosophy**

**Department of Materials**

**Imperial College London**

**December 2015**

# Declaration of Originality

I hereby declare that this thesis is my own work, and no material contained in this work has been submitted for any other degree, or at any other institution. Unless appropriately referenced or acknowledged, all work presented in this thesis is my own and was carried out in the laboratories of Imperial College London and University of Warwick.

*Chapter 2* – Dr. Luke Rochford at the University of Warwick (XRD analysis of the calcium phosphate microcapsules), and Dr. Rafael de Rosales at King's College London (donated fluorescein−bisphosphonate conjugate).

*Chapter 3* – Mr. Christopher Parkins at the University of Warwick (FIB/SEM micrographs of the dried HIPE fiber).

*Chapter 4* – Mr. Thomas Heuser at the DWI—Leibniz Institute for Interactive Materials (pH profile of the buffer-acidified solution with time at different urease concentrations), and Mr. Ross Jaggers at the University of Warwick (Confocal micrograph of the fiber).

Robert Valentine Bell (December 2015)

# Copyright

The copyright of this thesis rests with the author and is made available under a Creative Commons Attribution Non-Commercial No Derivatives licence. Researchers are free to copy, distribute or transmit the thesis on the condition that they attribute it, that they do not use it for commercial purposes and that they do not alter, transform or build upon it. For any reuse or redistribution, researchers must make clear to others the licence terms of this work.

# Abstract

The possible applications of branched copolymers are far reaching because of their various combinations of functionality and architectural diversity. More importantly, the domains and chain-end functionalities of the branched copolymers can be readily varied, *via* the simple and scalable Strathclyde route, to optimize/tailor the properties of the polymers for a specific application by careful choice of monofunctional monomers, branching monomers, and chain transfer agents.

In the present thesis, branched copolymers were utilized as emulsifying agents for the production of oil-in-water emulsion droplets. These emulsion droplets were used as a platform to create novel emulsion-based supracolloidal materials. The chemical composition and architectural structure of the branched copolymers were specifically chosen to create stable emulsions and provide the correct functionalities required for the application.

Calcium phosphate (CaP) microcapsules were fabricated by utilizing oil-in-water emulsion droplets, stabilized with branched copolymer, as templates. The branched copolymer was designed to provide a suitable architecture and functionality to produce stable emulsion droplets, and permit the mineralization of CaP at the surface of the oil droplet. These CaP capsules were made fluorescent by post-functionalization of the CaP shell with a fluorescent conjugate.

Oil-in-water emulsion droplets stabilized with Laponite clay disc functionalized with pH-responsive branched copolymers were microfluidically spun into supracolloidal fibers. These supracolloidal fibers can be used as a tool to delivery volatile compounds in a time-controlled manner. The dried fibers created were low-weight porous materials. It was also discovered that these supracolloidal fibers can be utilized as a storage material for emulsion droplets, where emulsion droplets are 'locked' in the fiber structure under acidic condition, and are released from the fiber upon basification of the system. The release of emulsion droplets from the fiber can be time-controlled by programming the transient acidic pH states of the system by combining a fast acidic promoter with a feedback-driven biocatalytically controlled slow generation of base in a close system.

# Acknowledgements

This work would have not been possible without the endless discussions, advice, and collaboration with numerous people at the University of Warwick and Imperial College London. I also would like to thank the Engineering and Physical Sciences Research Council (EPSRC) for supporting my PhD study.

I am very grateful and fortunate to have had the opportunity to work within the BonLAb. I am very thankful to my supervisor Prof. Stefan Bon for giving me the chance to join his group, for his numerous ideas, and his endless support, guidance, advice, and help.

Thank you to my supervisor at Imperial College London, Prof. Molly Stevens, for all the support and advice throughout the years. I would also like to address special thanks to the Weaver group, Rob (University of Liverpool), Rachel and Saif, for the support, precious discussions, and fun times at Imperial College London.

Special thanks to my family, my second family here at the University of Warwick, and friends for everything. Thank you very much Corinna (Post-doc) for all your helpful comments and advice on my thesis and papers. I am very thankful to my '*Chikas*', Marlon, Ross, Yunhua, Corinna, and Joe, for all the support, encouragement, guidance, and happy memories. I will never forget you guys.

Thank you so much to all the members of the BonLab for all the interesting discussions, support, coffee/tea breaks and lunch, and the fun times in the office and lab− Ross, Corinna, Yunhua, Joe, Sam, Rob Y., Brooke, Chris, Rong, Tom, Holly, Andrea, Indee, Patrick, and other students, visitors, undergrads and masters.

Finally, I would like to dedicate this thesis to my first supervisor and a true friend, Dr. Jon Weaver, who sadly passed away. It was an honor, pleasure, and fun working with you. You are and always be missed.

# Publication List

1. **Fabrication of Calcium Phosphate Microcapsules using Emulsion Droplets Stabilized with Branched Copolymers as Templates**

   R. V. Bell, L. A. Rochford, R. T. M. de Rosales, M. Stevens, J. V. M. Weaver, and S. A. F. Bon, *J. Mater. Chem. B*, 2015, **3**, 5544.

2. **Assembly of Emulsion Droplets into Fibers by Microfluidic Wet Spinning**

   R. V. Bell, C. C. Parkins, R. A. Young, C. M. Preuss, M. M. Stevens and S. A. F. Bon, *J. Mater. Chem. A*, 2016, **4**, 813.

3. **Designing Smart Particles for the Assembly of Complex Macroscopic Structures**

   E. Garcia-Tunon, S. Barg, R. Bell, J. V. M. Weaver, C. Walter, L. Goyos and E. Saiz, *Angew. Chem. Int. Ed.*, 2013, **52**, 7805.

4. **Printing in Three Dimensions with Graphene**

   E. Garcia-Tunon, S. Barg, J. Franco, R. Bell, S. Eslava, E. D'Elia, R. C. Maher, F. Guitian and E. Saiz, *Adv. Mater.*, 2015, **27**, 1688.

5. **Reversible Assembly of pH Responsive Branched Copolymer-Stabilised Emulsion *via* Electrostatic Forces**

   A. L. B. Maçon, S. U. Rehman, R. V. Bell and J. V. M. Weaver, *Chem. Commun.*, 2016, **52**, 136.

6. **Complex Ceramic Architectures by Directed Assembly of 'Responsive' Particles**

   E. Garcia-Tunon, G. C. Machado, M. Schneider, S. Barg, R. V. Bell, and E. Saiz, *J. Eur. Ceram. Soc.*, 2016, **doi:10.1016/j.jeurceramsoc.2016.06.050**

## 7. Enzymatic Catalyzed Time-Controlled Release of Emulsion Droplets from Soft Matter Fibers

R. V. Bell, T. Heuser, R. W. Jaggers, C. M. Preuss, M. M. Stevens, A. Walther and S. A. F. Bon, ***In Preparation***.

# Table of Contents

# List of Figures

droplets released from the ‘cake’. (B) Base is added to initiate release of emulsion from the ‘cake’. (C) The cap comes off from the top of the ‘cake’, and allows the release of emulsion droplets from the ‘cake’ (D). (E) Two layers have been released from the ‘cake’ with time (red and white layers). (F) A composite film (‘bag’) remains after all the layers have been released from the ‘cake’. A magnetic stirrer bar can be seen inside the composite film bag. It was used to add weight and to submerge the ‘cake’ in the acidic water. The magnetic stirrer bar was embedded in the ‘cake’ structure during the setting process of the layers. Scale bars represent 0.5 cm.

**Figure 4.18-Appx.** Photograph of microfluidics devices with one (A) and two (B) inlets to the injection inner capillary. Scale bars represent 1 cm. (C) The two inner capillaries (injection and collection inner capillaries) are aligned within the outer capillary to produce a flow-focusing junction. Scale bar represents 100 μm. **167**

# List of Tables

# List of Abbreviations

| | |
|---|---|
| AIBN | 2,2'−Azobis(isobutyronitrile) |
| BPs | Bisphosphonates |
| BCP | Branched copolymer |
| CaP | Calcium phosphate |
| CTA | Chain transfer agent |
| α | Degree of protonation |
| DEA | 2−(Diethylamino) ethyl methacrylate monomer |
| DMF | N,N−Dimethylformamide |
| DDT | 1−Dodecanethiol |
| EDX | Energy dispersive X-ray |
| EG | Ethylene glycol |
| EDGMA | Ethylene glycol dimethacrylate |
| Fluo−BP | Fluorescein−bisphosphonate conjugate |
| FIB/SEM | Focused ion beam scanning electron microscopy |
| FTIR | Fourier transform infrared |
| HIPE | High internal phase emulsion |
| HLB | Hydrophilic-lipophilic balance |
| HA | Hydroxyapatite |
| ICP-OES | Inductively coupled plasma-optical emission spectrometry |
| LCST | Lower critical solution temperature |

| | |
|---|---|
| $\alpha_\eta$ | Mark-Houwink alpha value |
| MPA | 3−Mercaptopropionic acid |
| MAA | Methacrylic acid |
| $M_n$ | Number-average molecular weights |
| O/W | Oil-in-water emulsion |
| pH-BCP-Laponite | pH-BCP functionalized Laponite platelet |
| pH-BCP | pH-Responsive branched copolymers |
| pH-BCPNs | pH-Responsive branched copolymer nanoparticles |
| $Đ$ | Polydispersity |
| PEGMA | Poly(ethyleneglycol) methyl ether methacrylate |
| PNIPAM | Poly(N−isopropyl acrylamides) |
| PVA | Poly(vinyl alcohol) |
| PVP | Poly(vinyl pyrrolidone) |
| $^1$H NMR | Proton nuclear magnetic resonance |
| SEM | Scanning electron microscope |
| SCVP | Self-condensing vinyl polymerization |
| TGA | Thermogravimetric analysis |
| TG | 1−Thioglycerol |
| TD-GPC | Triple-detection gel permeation chromatography |
| W/O | Water-in-oil emulsion |
| $M_w$ | Weight-average molecular weights |

| | |
|---|---|
| XRD | X-ray diffraction |

# Chapter 1

## General Introduction

This chapter is a general introduction to interface and colloidal chemistry, especially to the area of emulsions. The formation, stability, surface chemistry, and applications of emulsions are discussed. Furthermore, the development of hyper branched polymers, and their utilization as emulsifying agents in emulsions is examined. This introduction is followed by the main objective of the thesis, and each chapter is briefly outlined.

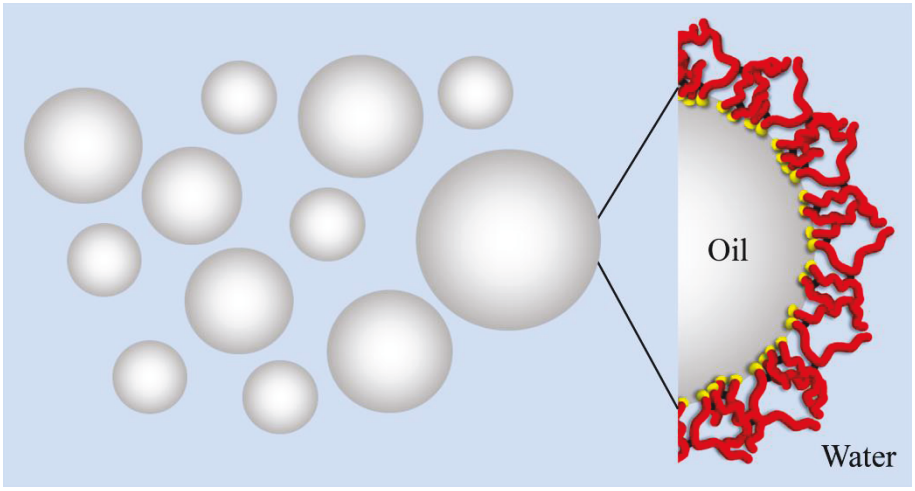


Oil-in-water emulsion droplets stabilized with hyper branched polymers.

## 1.1. Introduction to Colloid Science

Colloid science is the study of heterogeneous systems composed of at least one dispersed phase in a dispersion medium.[1] Each of the constituting phases can be either at a state of solid, liquid or gas. Various examples of colloidal systems are shown in **Table 1.1**. The colloidal domain extends over a range of dimensions from a few nanometers to a few tens of micrometers. At these dimensions, unique physical and chemical properties arise compared to those at molecular and macroscopic levels. The term colloid was developed by Graham in the 1860s.[2,3] He reported that silicic acid gel co-exists between liquid and crystalline states depending on the hydration, solubility and concentrations. Today, colloid science plays an important role in numerous industries, such as pharmaceuticals, food and beverages, bio- and nano-technologies, detergents, agriculture, cosmetics, and to name but a few.

**Table 1.1.** Examples of materials having colloidal domain with phases existing in various states.

| ***Dispersed Phase*** | ***Continuous Phase*** | | |
|---|---|---|---|
| | **Gas** | **Liquid** | **Solid** |
| **Gas** | | foam | solid foam |
| **Liquid** | liquid aerosol | emulsion | gel |
| **Solid** | solid aerosol | sol | solid sol |

Colloids generally can be classified in two categories: *lyophilic* colloids for solvent loving particles, and *lyophobic* colloids for solvent hating particles. Herein, we will concentrate mainly on lyophobic colloids, especially emulsions.

## 1.2. Emulsions

An emulsion is a dispersion of two essentially immiscible liquids, where one liquid is dispersed in a second liquid continuous phase (**Figure 1.1**).

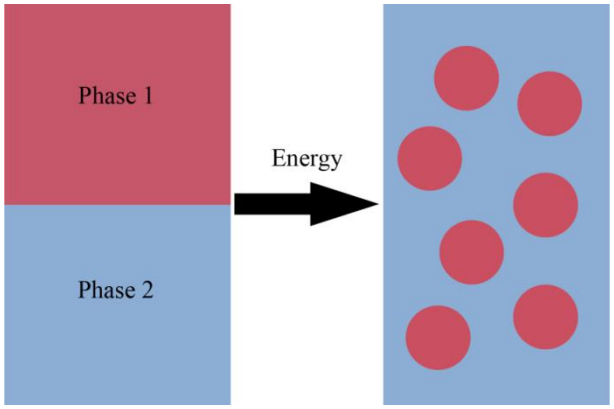


**Figure 1.1.** Schematic representation of the fabrication of emulsion. A dispersion of phase 1 (droplets) in phase 2 (continuous phase).

Emulsions can be classified according to their type, such as oil-in-water emulsion (O/W) or water-in-oil emulsion (W/O). Droplet diameter of emulsions can range from <100 nm to >100 µm (micro- and nano-emulsions: <100 nm, mini-emulsions: 100 nm − 1 µm, macro-emulsions: >1 µm). The formation of emulsion can be described as a subdivision of the dispersed phase into droplets. Then the configuration entropy change ($\Delta S_{conf}$) can be expressed as

$$\Delta S_{conf} = -nk_B [ln\phi + \{(1-\phi)/\phi\} ln(1-\phi)] \quad (1.1)$$

where $n$ is the number of droplets of dispersed phase, $k_B$ is the Boltzmann constant, and $\phi$ is dispersed phase volume fraction. The associated free energy change can be described as the total of the free energy for creating new area of interface $\Delta A\sigma_{1/2}$, and the configurational entropy $\Delta G_{form}$ in the form

$$\Delta G_{form} = \Delta A\sigma_{1/2} - T\Delta S_{conf} \quad (1.2)$$

where $\Delta A$ is the change in interfacial area $A$ (equal to $4\pi r^2$ per droplet of radius $r$) and $\sigma_{1/2}$ is the interfacial tension between phases 1 and 2 at a specific temperature. Substituting **Equation 1.1** into **Equation 1.2** provides an expression for obtaining the maximum interfacial tension between phases 1 and 2.

Emulsions (nano-, mini- and macro-emulsions) are considered kinetically stable systems. The formation of these type of emulsions is not spontaneous ($\Delta G_{form}$ = positive), and energy input is required to fabricate them.[1] Cumminution is the most common method to make emulsions. It involves starting with two bulk

liquids (commonly an oil phase and an aqueous phase), and supplying it with sufficient energy to cause one phase to break into droplets that are dispersed in the second phase. This increases the disorder in the system, which in turn, increases the $\Delta S_{conf}$ ($\Delta S_{conf}$ = positive). In addition, a tremendous increase in the area of the interface between the two phases is generated, which results in a large increase in the interfacial free energy of the system (**Equation 1.2**). Consequently, the emulsion produced is highly thermodynamically unstable relative to the two bulk phases separated by a minimum surface area. It is for this reason that two immiscible liquids, when pure, cannot form an emulsion. A third component, the emulsifiers, is normally added to stabilize this unstable system for a sufficient time. The emulsifying agent diffuses and adsorbs at the newly formed liquid-liquid interfaces during droplet breakdown as an orientated interfacial film. The two main roles of emulsifiers are *(i)* to lower the interfacial tension ($\sigma_{1/2}$) between the two liquids, which in turn reduces $\Delta G_{form}$, and *(ii)* to reduce the rate of coalescence of droplets by forming mechanical, steric, and/or electrical barriers around them. On the other hand, micro-emulsions are considered thermodynamically stable ($\Delta G_{form}$ = negative) and form spontaneously. This results from a sufficiently low interfacial tension ($\sigma_{1/2}$) between the two liquid phases, and therefore, the $\Delta S_{conf}$ term (**Equation 1.2**) is higher in magnitude compared to the $\Delta A\sigma_{1/2}$ term. Micro-emulsions are formed by self-assembly of surfactants, and are essentially swollen micelles with solubilized oil or water, depending on their type.

## 1.3. Stability of Emulsions

Emulsions (except micro-emulsions) are thermodynamically unstable and can undergo four main potential instability mechanisms, some of which may occur simultaneously. These are aggregation, creaming or sedimentation, coalescence and Ostwald ripening (**Figure 1.2**).

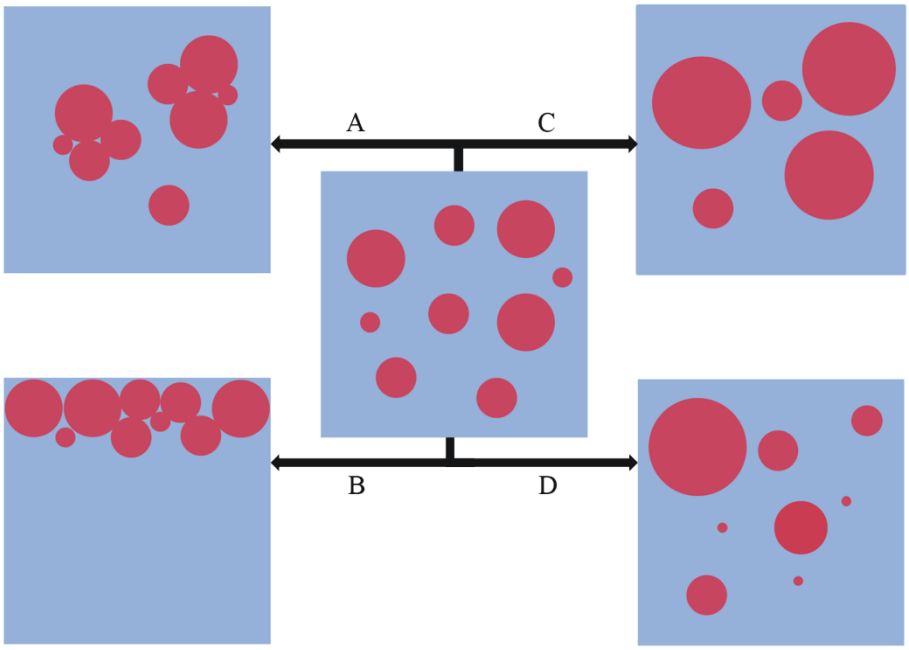


**Figure 1.2.** The four main instability mechanisms of emulsions, (A) aggregation, (B) creaming or sedimentation, (C) coalescence, and (D) Ostwald ripening.

### 1.3.1. Aggregation

Emulsions can be made kinetically stable for a period of time by providing a sufficient energy barrier to prevent aggregation *via* addition of electrostatic charges or steric barrier on the surface of emulsion droplet. In the absence of repulsive interaction, aggregation (coagulation: irreversible aggregation, and flocculation: reversible aggregation) of emulsion droplets arises from a combination of emulsion-emulsion collision driven by Brownian motion (thermal motion) and the attractive forces between emulsions, known as van der Waals forces. The attractive potential energy $V_a$ of two particles in a vacuum at close range was described by Hamaker[4]

$$V_a = -\frac{Aa}{12h} \tag{1.3}$$

(when particle separation is $h<<2a$) where $a$ is the radius of the particle, $h$ is the distance between the particles, and $A$ is the Hamaker constant. The Hamaker constant is a function of the particles' density and electronic polarizability. When particles are dispersed in a medium, the attraction between them is reduced as attractive forces between the particles and the medium are present. As a result, the Hamaker constant can be given by:

$$A = (\sqrt{A_{particle}} - \sqrt{A_{medium}})^2 \quad (1.4)$$

where $A_{particle}$ and $A_{medium}$ is the Hamaker constants for the particle and medium in vacuum, respectively.

#### *1.3.1.1. Electrostatic stabilization*

Electrostatic stabilization is introduced to emulsions by using an emulsifying agent with charged groups, such as carboxylate, sulfonate, phosphate, or ammonium groups. These stabilizers generate an electrical double layer around the emulsion droplet with an equal amount of counter ions located at the surface of the droplet (stern layer), and a diffuse layer of mobile ions outside the stern layer. The electric potential $V_r$ inside the electric double layer is expressed by the following equation:

$$V_r = V_o \frac{a}{r} e^{-k(a-r)} \quad (1.5)$$

where $V_o$ is the surface electric potential, $r$ is the radius of the particle, $a$ is the distance from the surface, and $1/k$ is the thickness of the diffuse layer, known as the Debye length.

Derjaguin and Landau, Verwey, and Overbeek described a model (DLVO theory) to characterized repulsive free energy between electrostatically stabilized particles.[5–7] The DLVO theory is based on the balance of van der Waals attractive forces (Hamaker) with electrostatic repulsive forces. When two charged particles approach each other, owing to Brownian motion, the counter-ion layers of the particles will overlap and results in higher ionic concentration between the particles compared to anywhere else around them. This results in to an increase of free energy of the system, in terms of electrochemical potential osmotic pressure, which in turn brings solvent from outside to the area between the particles, and leads to repulsive forces between the particles. DLVO theory can be utilized to calculate the changes in energy when two particles approach each other by estimating the attractive potential energy $V_a$ and repulsion potential energy $V_r$ as a

function of distance from the surface of a particle. The total interaction energy of the system can be written as:

$$V_t = V_r + V_a \tag{1.6}$$

**Figure 1.3** illustrates the combination of electrostatic (dominates at intermediate separation distance) and Born (dominates at very small separation distance but does not prevent aggregation) repulsion potentials with van der Waals (predominates at small and large separation distance) attraction potential as a function of distance between two particles. There are two minima present, a primary and a secondary minimum. Primary minimum is a result of van der Waals attraction and generally the energy well is so deep that the energy required to separate two particles is considered to be infinite (coagulation−irreversible). The secondary minimum has a shallow energy well and described as a reversible flocculation of particles. The $V_{max}$ is the energy barrier to the primary minimum. The height of the energy barrier is related to the stability of the colloidal system.

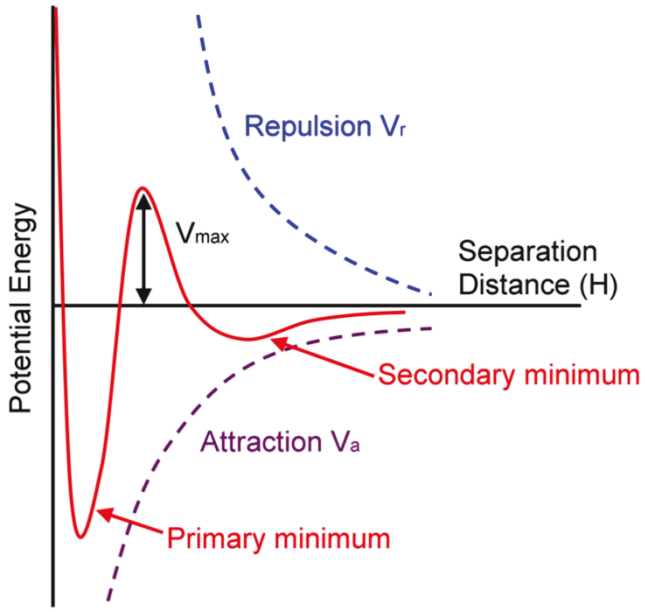


**Figure 1.3.** The total potential energy between two spherical colloidal particles as a function of distance of separation.[8] Reproduced from Reference 8.

#### *1.3.1.2. Steric stabilization*

Steric stabilization in colloidal system was fully established by Napper in the late 1960's.[9–13] Steric stabilization is incorporated in emulsion by using non-ionic emulsifying agent that contain groups such as poly(ethylene oxide) or polyols.

There are two mechanisms to describe the steric stabilization. These are *(i) Osmotic repulsion*: As particles approach each together, their protective polymer chains intermingle. The concentration of polymer chains increases in the overlap area and creates an increase in of osmotic pressure. This results in a concentration gradient between the particles, forcing the medium back in, and thus, keeping the particles apart, and *(ii) Entropic repulsion*: As particles approach one another the polymer chains overlap and the freedom of movement is restricted. This state is unfavourable in free energy terms. The enclosed particles then move apart to a more preferred state.

### 1.3.2. Creaming or Sedimentation

Creaming or sedimentation is the migration of emulsion droplets due to the density difference of the dispersed and the continuous phases.[1] The steady-state velocity $v_s$ of isolated droplets in a diluted system undergoing creaming or sedimentation is expressed as:

$$v_s = \frac{2\pi\Delta\rho g a^2}{9\eta} \tag{1.7}$$

where $\Delta\rho$ is the density difference between the dispersed and continuous phases, $g$ is the acceleration due to gravity, $a$ is the droplet radius, and $\eta$ is the viscosity of the continuous phases. If $a < 1$ μm, creaming or sedimentation is resisted as Brownian motion keeps the emulsion droplets dispersed throughout the system. Creaming or sedimentation may or can also be controlled by matching the densities of the two phases. Moreover, one parameter that can be readily adjusted to reduce $v_s$ is $\eta$. A continuous phase that forms a weak physical gel will reduce $v_s$ to nearly zero.

### 1.3.3. Coalescence

When two emulsion droplets approach each other within a certain distance, the inertial energy of the two droplets causes flattening of the thin film of continuous phase between them.[1] If the net interaction energy between the droplets is repulsive, the thickness of the film between the two droplets will only decrease to certain a degree, and the droplets bounce off each other and separate again.

For coalescence to occur, the thin film between the two droplets needs to rapture. The mechanism for film rapture is related to the presence of oscillatory waves in the film, which are generated thermally or mechanically. As two nodes in the oscillating interfaces approach, a defect may form in the film, leading to rapture. In contrast to standard emulsion system, for Pickering emulsions (see Chapter 1.4.1), the rate of coalescence may be reduced effectively to zero as the monolayer of solid particles at the interface of an emulsion droplet is effectively rigid. Moreover, a very high energy is required to displace a solid particle from an interface.

The situation is different when emulsions are stabilized with surfactants. The stabilization against coalescence is more dependent on the dampening of the oscillatory waves rather than desorption of surfactant from the interface. The formation of the oscillatory waver is accompanied by an increase in local interfacial tension (increase in interfacial area) of the two interfaces comprising the film, and causing a depletion of surfactants at the local interface. The ease in which this expansion of the interfaces occurs is related to the dilation modulus (Gibbs elasticity) $\varepsilon$ of the interface,[14] and can be expressed as

$$\varepsilon = \frac{2d\sigma}{dlnA} \tag{1.8}$$

It is defined as the ratio of the increase in the film tension $2d\sigma$ resulting from an increase in surface area and the relative increment of the area $dlnA$. The greater $\varepsilon$, the more stable emulsion droplets to coalescence. A maximum value of $\varepsilon$ is obtained at a given surfactant concentration as seen in **Figure 1.4**, with $\varepsilon$ eventually reducing to zero at a sufficiently high concentration. This is because the depletion of surfactant at the wave nodes (increase in local interfacial tension)

is replenished by the flow of surfactant in the continuous phase (Marangoni effect) to fill the gaps left by the displaced surfactant molecules. At sufficiently high concentration of surfactant, the rate of displacement of surfactant at the interface is equal to the rate of adsorption from the continuous phase ($\varepsilon = 0$).

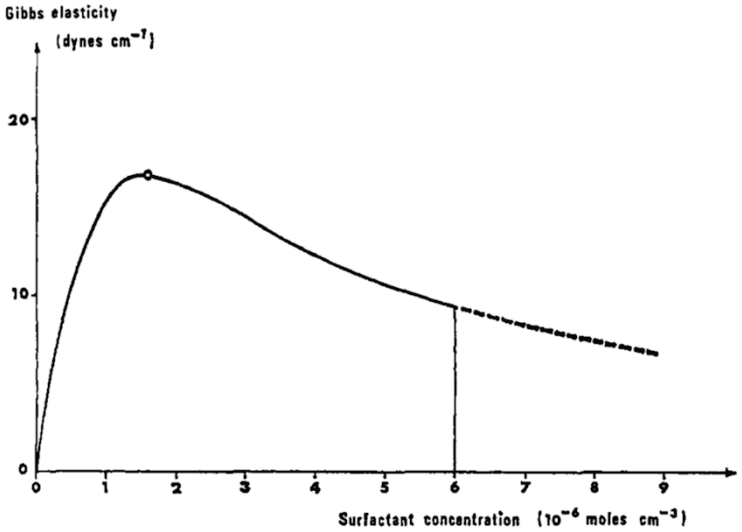


**Figure 1.4.** The Gibbs elasticity of a film with a thickness of $10^{-4}$ cm containing sodium dodecyl sulfate.[14] Reprinted with permission from Reference 14. Copyright (1964) American Chemical Society.

### 1.3.4. Ostwald Ripening

Ostwald ripening is the phenomena in which smaller droplets in solution dissolve and deposit on larger droplets with time.[1] The mechanism is associated with the presence of difference in pressure $\Delta p$ across a curved liquid/liquid interface, as provided by the Laplace equation:

$$\Delta p = \frac{2\sigma}{r} \tag{1.9}$$

where $r$ is the radius of curvature, and $\sigma$ is the interfacial tension.

This implies that $\Delta p$ is higher for smaller droplets than for larger droplets. In turn, this means that the chemical potential of the molecules comprising the droplets is much higher in the smaller droplets. It is this difference in chemical potential between droplets of different sizes, that drives the migration of molecules from smaller droplets across the continuous phase into larger droplets, and hence, reducing the total energy of the system. The Ostwald ripening is enhanced if the

size distribution of the droplets is broader. The high solubility of the dispersed phase in the continuous phase also increases the rate of Ostwald ripening. The rate of Ostwald ripening can be reduced by adding a component to the dispersed phase, which is insoluble in the continuous phase. The reduction of small droplets *via* Ostwald ripening is resisted by a buildup of osmotic pressure of the trapped component in the emulsion droplet.[15]

## 1.4. Type of Emulsions

When emulsifying oil and water mixture, it is important to consider what type of emulsion will be formed (O/W or W/O). By stirring a biphasic (oil and water) mixture in the absence of an emulsifying agent, the liquid with a smaller volume will statistically form the dispersed phase. If the volume ratio of the phases is ~ 1, then the liquid with the lower viscosity will tend to form the dispersed phase. This is owing to a more viscous liquid requires a higher energy input to create droplets, and coalescence of droplets is slower if the continuous phase is more viscous. However, these factors are overridden if an emulsifier is present in the system. The curvature imparted to the oil/water interface by the emulsifying agent is now the dominating factor whether O/W or W/O will be created.[1]

### 1.4.1. Solid Particles as Emulsifying Agents

Emulsions stabilized solely with solid particles, known as Pickering emulsions, were first mentioned by Ramsden in 1903,[16] and later by Pickering in 1907.[17] Both independently reported that solid particles can act as insoluble surfactants to stabilize emulsion droplets. Finkle *et al*. suggested the phenomenon was due to fact that solid particles are partially wettable by both of the phases involved.[18]

In Pickering emulsions, solid particles adhere to the interface between the two immiscible phases, driven by the potential to lower the total free energy of the system. In 1980, Pieranski described a 2-D model of the interactions of a monolayer of polystyrene spheres at a water/air interface.[19] Pieranski noted that polystyrene particles (122.5 nm) are trapped at the interface in a surface energy well greater than the thermal energy $k_BT$ (where $k_B$ is the Boltzmann constant and $T$ is the temperature) by a factor of $10^6$. The stability of the particle at the interface

is determined by the depth of the well. A schematic representation of a spherical particle at the interface of water and air is shown in **Figure 1.5**.

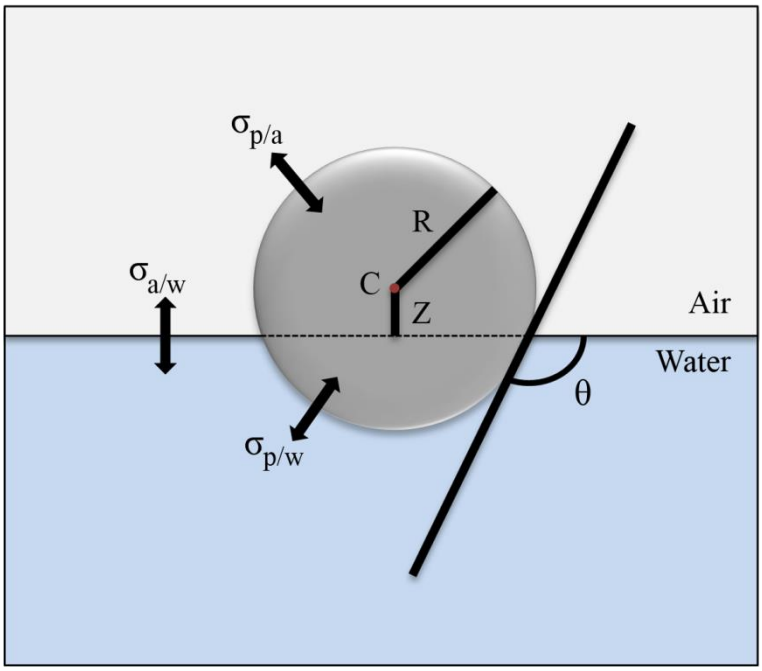


**Figure 1.5.** Schematic representation of a solid particle at a planar air/water interface, immersed partly in the water phase. The $\sigma_{p/a}$, $\sigma_{a/w}$, and $\sigma_{p/w}$ are the interfacial tensions between the solid particle and air, air and water, and solid particle and water, respectively. The radius of the solid particle is R, and the distance from the center *C* of solid particle to the water level *Z*. $\theta$ is the contact angle between the three phases.[1c] Adapted from Reference 1c. Copyright (2015) with permission of The Royal Society of Chemistry.

The energies between the particle and the air, the particle and the water, and between the water and the air are reported in **Equation 1.10, Equation 1.11, Equation 1.12**, respectively:

$$E_{p/a} = \sigma_{p/a}\, 2\pi R^2 (1 + \hat{z}) \tag{1.10}$$

$$E_{p/w} = \sigma_{p/w}\, 2\pi R^2 (1 - \hat{z}) \tag{1.11}$$

$$E_{w/a} = -\sigma_{w/a}\, \pi R^2 (1 - \hat{z}^2) \tag{1.12}$$

where $\sigma_{p/a}$, $\sigma_{p/w}$, $\sigma_{w/a}$, are the surface tensions between particle and air, particle and water, and water and air, respectively. $\hat{z} = z/R$ is the vertical coordinate of the center $C$ with respect to the water level.

The total energy ($E$) is the summation of the energies provided in **Equations 1.10, 1.11, and 1.12**. $E_{unit}$ is introduced to scale the surface energies so that the energy $\tilde{E}$ can be written as:

$$E_{unit} = \pi R^2 \sigma_{w/a} \tag{1.13}$$

$$\tilde{E} = E/E_{unit} = \hat{z}^2 + 2(a-b)\hat{z} + 2a + 2b - 1 \tag{1.14}$$

where $a = \sigma_{p/a} / \sigma_{w/a}$ and $b = \sigma_{p/w} / \sigma_{w/a}$. When $\hat{z} = b - a$ (this is when the vertical coordinate of the center ($C$) position of the particle at the liquid-liquid interface at minimal energy, $z_m$), $\tilde{E}$ has a minimum value ($\tilde{E}_{min}$):

$$\tilde{E}_{min} = 2a + 2b - 1 - (a-b)^2 \tag{1.15}$$

Therefore, $\Delta E_a = E_a - \tilde{E}_{min}$ and $\Delta E_w = E_w - \tilde{E}_{min}$ represent the total energy required to move the particle to air and water, respectively (**Figure 1.6**).

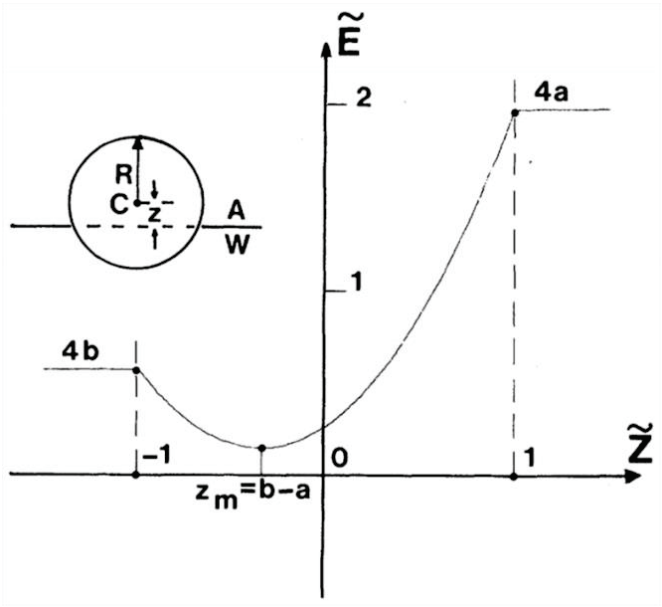


**Figure 1.6.** The surface energy well of a solid particle at the interface of air and water phases with different $\hat{z}$ value. The energies of the well edges, $E_a = 4a$ (solid particle in air) and $E_w = 4b$ (solid particle in water).[19] Reproduced from Reference 19. Copyright (1980) with permission of the American Physical Society.

The model reported by Pieranski was only based on planar interface and does not consider the contact angle of spherical particles at the interface when emulsion droplet is formed. Clint and Taylor adapted this 2-D model by incorporating contact angle in the model.[20] In **Figure 1.5**, for a spherical particle of radius $R$ having a contact angle $\theta$ measured in the water, the area of contact between particle and water is:

$$A_{contact\ p/w} = 2\pi R^2 (1 + cos\theta) \tag{1.16}$$

The missing flat area of water due to the presence of the particle:

$$A_{missing\ a/w} = \pi R^2 (1 - cos^2\theta) \tag{1.17}$$

Therefore, the free energy required to remove the particle from the interface into air is:

$$E = 2\pi R^2 (1 + cos\theta) (\sigma_{p/a} - \sigma_{p/w}) + \pi R^2 (1 - cos^2\theta)\sigma_{a/w} \tag{1.18}$$

The Young's equation for equilibrium at the three-phase contact line is:

$$\sigma_{p/a} - \sigma_{p/l} = \sigma_{w/a}\, cos\theta \tag{1.19}$$

Therefore, **Equation 1.18** simplifies to:

$$E = \pi R^2 \sigma_{w/a} (1 \pm cos\theta)^2 \tag{1.20}$$

The sign in the bracket is negative if $\theta < 90^o$, when the particle is removed into the water and positive for $\theta > 90^o$, when it is removed into the air phase. The radius $R$ of a particle and the surface tension between the two phases $\sigma_{w/a}$ are generally known. Due to its simplicity, this equation is often used to calculate the energy in which a particle could be held at an interface.

The formation, structure, and stability of Pickering emulsions are reported largely through the work of Binks et al.[21] The wettability of particles greatly determines the emulsion type that is created. For solid particles with $\theta < 90^o$, O/W emulsions are formed, for $\theta > 90^o$, W/O emulsions are formed (**Figure 1.7**).

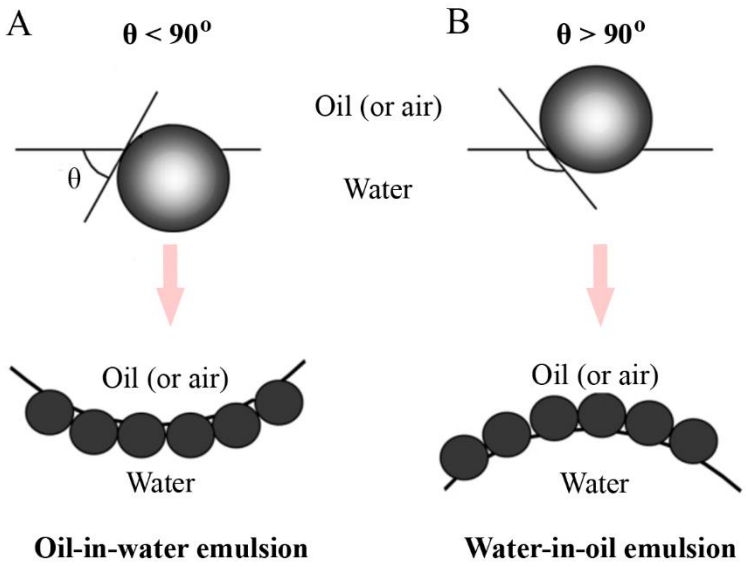


**Figure 1.7.** The position of a solid particle at a planar oil /water interface for a contact angle less than 90° (A), and greater than 90° (B). For $\theta < 90°$, oil-in-water Pickering emulsions are created. For $\theta > 90°$, water-in-oil Pickering emulsions are formed.[21] Altered from Reference 21. Copyright (2002) with permission from Elsevier.

Particles, such as silica particles,[22,23] Laponite clay,[24] functionalized titania,[25] functionalized $Al_2O_3$ and SiC ceramics,[26] micro-gel particles,[27,28] and Janus particles,[29] have been used to fabricate Pickering emulsions. Stimuli responsive particles have been utilized to produce Pickering emulsions that can demulsify on demand with external stimuli by changing the wettability properties of the particles. Armes *et al*. and Ngai *et at*. have reported pH-responsive Pickering emulsions,[30,31] and pH-temperature dual responsive Pickering emulsions,[32] respectively. Furthermore, Pickering stabilization has given way to fabricate novel hierarchical colloidal structures as shown in **Figure 1.8**.

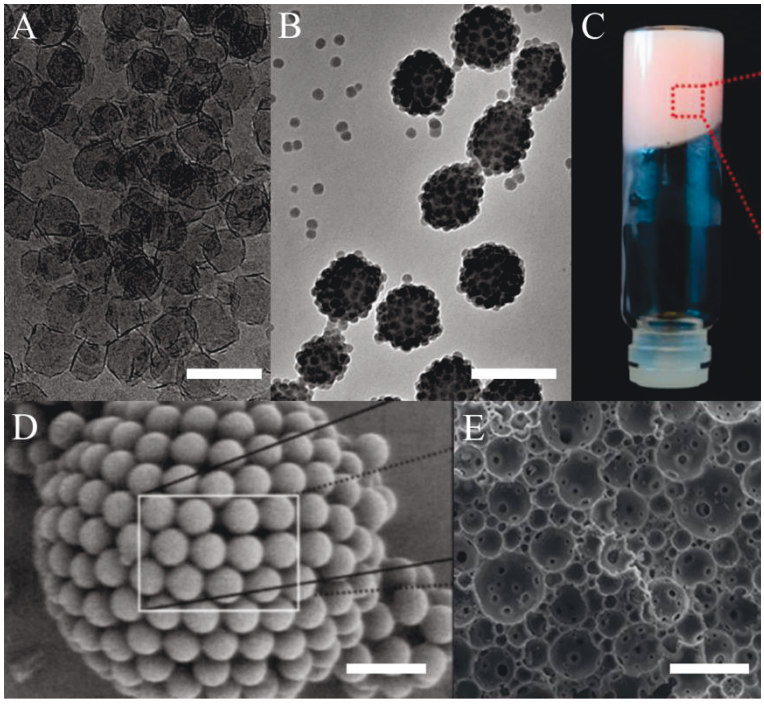


**Figure 1.8.** Laponite (A) and spherical silica (B) armored particles. Scale bars represent 100 nm and 200 nm, respectively.[33,34] [(A)]Altered with permission from Reference 33. Copyright (2011) American Chemical Society. [(B)]Altered with permission from Reference 34. Copyright (2008) American Chemical Society. (C) High internal phase emulsion hydrogel stabilized with nanogel particles.[35] Adapted from Reference 35. Copyright (2013) with permission of The Royal Society of Chemistry. (D) Colloidosome. Scale bar represents 2 μm.[36] Adapted from Reference 36. Copyright (2002) with permission of The American Association for the Advancement of Science. (E) Highly porous ceramic macrostructure fabricated from Pickering emulsions. Scale bar represents 100 μm.[26] Adapted from Reference 26. Copyright (2013) with permission of John Wiley and Sons.

### 1.4.2. Surfactants

Surfactants (surface-active-agents) are generally organic molecules, when dissolved in a solvent at low concentration, have the ability to adsorb at interfaces and form oriented monolayers at the interface.[1] Their adsorption behavior is attributed to their amphiphilic nature, which combines both a polar and a non-polar group into a single molecule. To accommodate for their dual nature, surfactants resides at the interface so that their lyophobic moiety ('tail') and lyophilic domain ('head') are located in the oil phase and water phase, respectively. The adsorption process is associated with energetic changes as the free energy of a surfactant located at an interface is lower than a surfactant solubilized in the bulk phase (hydrophobic effect). Therefore, the accumulation of surfactant at the interface is a spontaneous process and results in a reduction of the

interfacial tension. The head and tail groups of surfactants can have numerous structural and chemical variations. The head group can be charged (negative, positive, or zwitterionic) or neutral, small and compact in size or a polymeric chain. The tail group is usually a single or double, linear or branched hydrocarbon chain, but may also contain fluorocarbon, or siloxane, or contains aromatic groups.

Surfactants will tend to force curvature of the liquid/liquid interface to determine the type of emulsion that will be created (O/W or W/O). The preferred curvature depends on the structure of the surfactant. The changes in film curvature can be address quantitatively in terms of geometric requirements. This concept was introduced by Mitchell and Ninham,[37] and Israelachvili,[38] and describes that the aggregation of surfactants is controlled by a balanced molecular geometry. The geometric treatment separates the overall free energy of association to three important geometric terms (**Figure 1.9**).

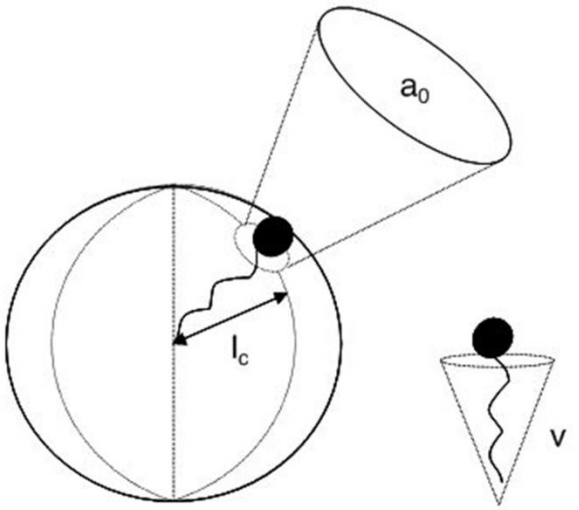


**Figure 1.9.** The critical packing parameter $P_c$ ($P_c = v/a_o l_c$) relates to the area of the head group $a_o$, the extended length $l_c$ and the volume of the hydrophobic tail of a surfactant molecule $v$ into a dimensionless number.[39] Adapted from Reference 39. Copyright (2010) with permission of John Wiley and Sons.

The formation of a spherical micelle needs the maximum extended chain length of the tail in the micelle core $l_c$ to be equal to the radius of the micelle's core $R_{mic}$. Therefore, for a specific shape, an aggregation number $N$ can be expressed either by the ratio of micellar core volume $V_{mic}$ and that for the volume of the hydrophobic tail $v$,[40]

$$\mathrm{N} = \frac{V_{mic}}{v} = \frac{\frac{4}{3}\pi R_{mic}^3}{v} \tag{1.21}$$

or the ratio between the micellar area $A_{mic}$ and the cross-sectional area $a_o$:

$$\mathrm{N} = \frac{A_{mic}}{a_o} = \frac{4\pi R_{mic}^2}{a_o} \tag{1.22}$$

Equating equations (1.21) and (1.22):

$$\frac{v}{a_o R_{mic}} = \frac{1}{3} \tag{1.23}$$

Since $l_c$ cannot exceed $R_{mic}$ for a spherical micelle:

$$\frac{v}{a_o l_c} \leq \frac{1}{3} \tag{1.24}$$

More generally, this defines a critical packing parameter $P_c$ as the ratio:

$$P_C = \frac{v}{a_o l_c} \tag{1.25}$$

In terms of micro-emulsions, the preferred curvature is governed by the relative areas of the head group $a_o$ and the tail group $v/l_c$. If $P_c < 1$, oil-in-water micro-emulsion is formed, and if $P_c > 1$, water-in-oil micro-emulsion is created.[41] The same rules can also be applied for nano-, mini, and macro-emulsions.

Another concept relating to interfacial packing of surfactant and film curvature is the hydrophilic-lipophilic balance (HLB). In 1949, Griffin first introduced this concept and derived an empirical equation for non-ionic alkyl polyglycol esters based on the surfactant chemical composition:

$$HLB = \frac{E_j wt\% + OHwt\%}{5} \tag{1.26}$$

where $E_j$ *wt%* and *OH wt%* are the weight percent of ethylene oxide and hydroxide groups, respectively.[42]

Ten years later, Davies proposed a more general equation that associates a constant to the different hydrophilic and hydrophobic groups:

$$HLB = [(n_H H) - (n_L L)] + 7 \quad (1.27)$$

where $H$ and $L$ are the constant assigned to the hydrophilic and hydrophobic groups, respectively. $n_H$ and $n_L$ are the number of hydrophilic and hydrophobic groups per surfactant molecule, respectively.[43] For HLB < 10 (lipid soluble surfactants), W/O micro-emulsions are formed, and for HLB > 10 (water soluble surfactants) O/W micro-emulsions are produced. The effect of surfactant on molecular geometry and system conditions on the HLB numbers and packing parameter are shown in **Figure 1.10**.

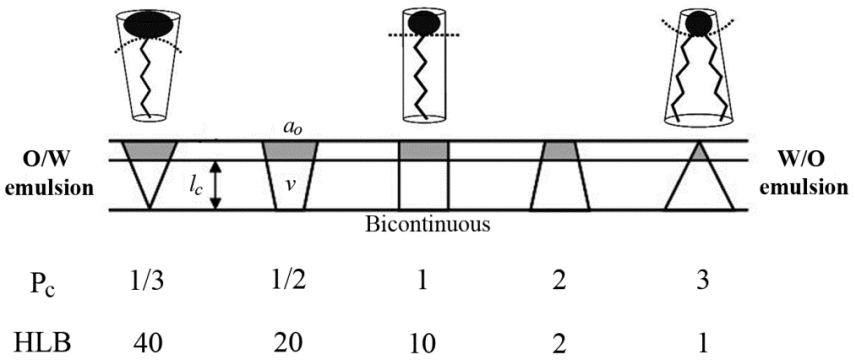


**Figure 1.10.** The preferred liquid/liquid curvature with packing parameter ($P_c$) value and HLB number.[44] Adapted from Reference 44. Copyright (2010) with permission of John Wiley and Sons.

Emulsions that are stabilized with surfactants that are capable to response to external stimuli, such as pH,[45] temperature,[46] light,[47,48] and $CO_2$,[49] have been reported. New advances in polymeric surfactants, especially branched polymers, have gained much attention in recent years in the field of stimuli responsive emulsions due to their unique and versatile properties. Branched polymers will be further discussed in the next chapter (Chapter 1.5).

## 1.5. Branched Polymers

The preparation of architecturally and compositionally controlled branched polymers has been a continuous challenge for polymer chemists. However,

research and development in the area of branched polymers have remained active because of their unique and versatile properties that can have potential applications in numerous fields. These several unique properties (compared to their linear analogues) include low solution and melt viscosities, higher solubility, greater surface adhesion, tunable solution behavior, and higher concentration of end groups.[50,51] **Figure 1.11** demonstrates the different architecture structures of branched polymers.

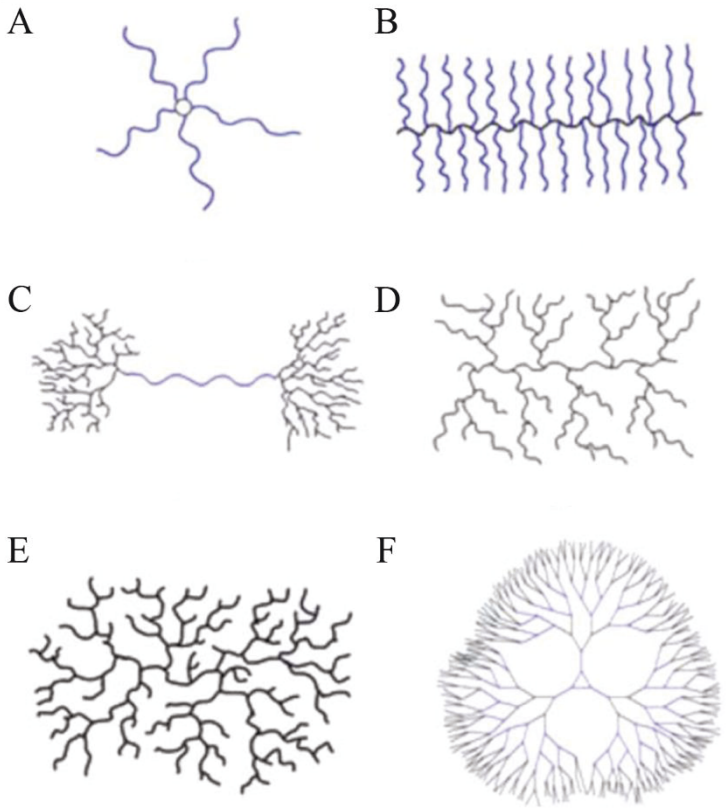


**Figure 1.11.** Schematic representation of various architecture structures of branched polymers.(A) Stars, (B) brush, (C) pompom, (d) dendrigraft, (e) hyper branched, and (f) dendrimers.[50] Adapted from Reference 50. Copyright (2010) with permission of The Royal Society of Chemistry.

Dendrimers are special type of branched polymers as they have a perfect branched architecture structure with high degrees of symmetry and defined size.[52,53] Although dendrimers exhibit fascinating properties and behaviours on account to their perfect structure, the production of dendrimers requires laborious multiple steps synthesis with drastic purification between steps. Also, dendrimers are limited in size due to stepwise syntheses (13 nm in size, or $4^{th} - 5^{th}$ generation). This labour intensive syntheses make their production costly and time consuming, and therefore, not suitable for scale-up.[52,53]

Hyper branched polymers also exhibit these unique properties mentioned above. However, there are some drawbacks associated with hyper branched polymers. These include broad molecular weight distribution, irregular branching, and uneven distribution of functional groups throughout the polymer.[54] Although its drawbacks, the synthesis of hyper branched polymer *via* radical polymerization is still the most versatile and scalable method to produce functional hyper branched polymers. Nevertheless, hyper branched polymers offer a unique opportunity in terms of providing undemanding and generic syntheses to vast applications, where control/precision on functional groups placement and structure is not critical.

## 1.6. Hyper Branched Polymers

In 1990, Kim and Webster (Du Pont) described the first preparation of hyper branched polymers by one-step polycondensation of $AB_2$-type monomers.[55,56] This method involves coupling of 3,5−dibromophenyl boronic acid, in the presence palladium triphenylphosphine catalyst, under modified Suzuki reaction. However, this method only allowed ~ 50 % of branching to be incorporated in the polymer, making it inefficient. Furthermore, there was no control over the size and structure of the hyper branched polymers. Fréchet *et al*. recognized the importance of vinyl monomers in the synthesis of hyper branched polymers, and in 1995, Fréchet *et al*. introduced a more generic approach to synthesize hyper branched polymers using step-growth/condensation polymerization, known as self-condensing vinyl polymerization (SCVP) (**Figure 1.12**).[57] This method allowed the production of hyper branched polymers using vinyl monomers. The vinyl monomer contains an extra functional group, which is able to initiate polymerization to other vinyl monomers. The propagation can take place either at the initiating center or at the double bond because they have similar reactivity, leading to hyper branched polymers. The polymerization is time dependent because a broad molecular weight distribution was obtained at high conversion. Therefore, Fréchet and coworkers introduced a controlled type of SCVP, such as cationic polymerization and group transfer, to synthesized hyper branched polymers with a narrow molecular weight distribution.[58] Although compositional diversity is achievable with these methods, expensive tailored vinyl monomers are required to introduce branching, which might limit its scale up viability.

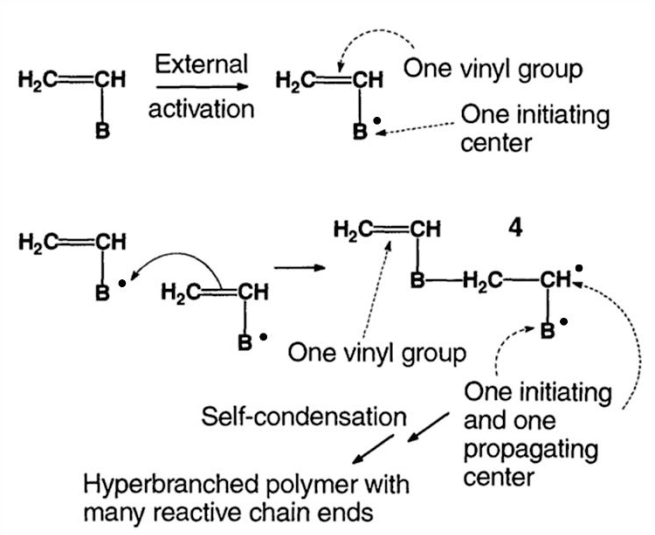


**Figure 1.12.** The basic concept of self-condensing vinyl polymerization.[57] Modified from Reference 57. Copyright (1995) with permission of The American Association for the Advancement of Science.

In 2000, Sherrington and co-workers reported a route to produce hyper branched vinyl polymers, known as the Strathclyde route (Thiol-regulated free radical polymerization), as shown in **Figure 1.13**.[59] The advantages of this method over the previous routes are; it is a one-step reaction, generic, facile, cost effective, and versatile to most readily available vinyl monomers and scalable.[60–62]

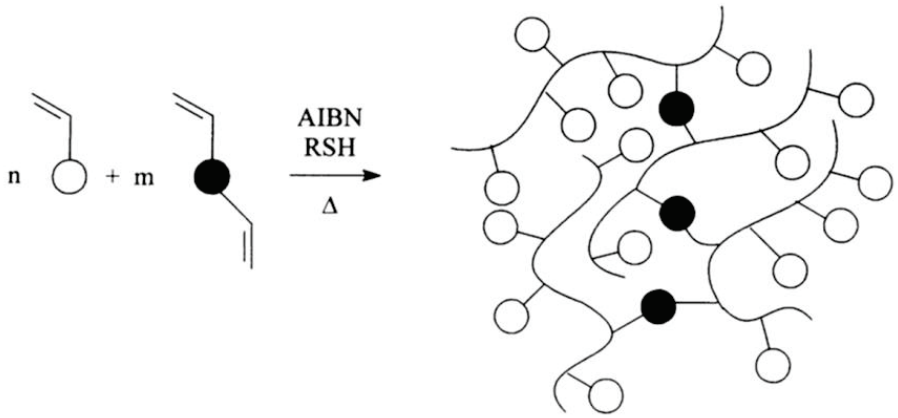


**Figure 1.13.** Schematic representation of the Starthclyde route. The white components represent monofunctional monomer, black components symbolize bifunctional monomer, AIBN is the initiator, and RSH represents chain transfer agent.[59] Reprinted from Reference 59. Copyright (2000) with permission from Elsevier.

The Strathclyde route uses bifunctional monomers as the branching units in standard free radical polymerization. Polymer gelation is avoided by addition of chain transfer agent (CTA). The CTA limits the degree of polymerization of the

primary kinetic chain so that on average, only one branching unit is incorporated per primary polymer chain. Compared to the analogous process in the absence of CTA, polymer gelation is reached at less than 20 % conversion of monomer to polymer in a very dilute polymerization solution.[63] The degree of branching can be varied by altering the molar ratio of the mono- and bi- functional monomers, with equimolar concentrations of CTA to the branching monomer. The Strathclyde route is a non-controlled polymerization, and therefore, the molecular weight and branched structure of the hyper branched polymer cannot be controlled with precision. Isaure *et al*. introduced a copper-based controlled polymerization (atom transfer radical polymerization) to synthesized hyper branched polymers.[64] The copolymerization of methyl methacrylate (monofunctional monomer) and ethylene glycol dimethacrylate (branching unit) yielded a soluble hyper branched polymer in a one-step reaction. Polymer gelation was prevented by having a low concentration of the branching unit, and molar ratio of the branching monomer to initiator must be $\leq 1$. If molar ratio exceeds 1, polymer gel is created. Li and Armes confirmed that if the branched copolymer was synthesized by controlled polymerization, the constituent primary chains of the hyper branched polymer would have similar molecular weight and molecular weight distribution to the linear polymer synthesized without branching units.[65] The Strathclyde route has been further extended to other controlled polymerization processes, such as group transfer polymerization, reverse addition fragmentation chain transfer polymerization[66] and oxyanionic polymerization.[67] The conventional Strathclyde route is still the most convenient method to produced generic hyper branched polymers with architecturally and compositional diversity, in terms of synthetic ease and scalability.

### 1.6.1. Stimuli Responsive Hyper Branched Polymers

One area of hyper branched polymers that is showing growing interest is responsive branched copolymers. These branched copolymers have the ability to change their conformation reversibly with external stimuli.

In 2008, Weaver *et al*. have exploited the conventional Strathclyde route to synthesize pH-responsive branched copolymer nanoparticles (pH-BCPNs).[68] The preparation of pH-BCPNs was generic, scalable, and tolerant of functionality. pH-

BCPNs show some properties similar to shell cross-linked micelles but unlike these materials they are prepared in one-pot and do not require time consuming assembly and potential toxic cross-linking reagents.[69] The synthesis involves conventional free radical polymerization of a pH-responsive tertiary amine, 2−(diethylamino) ethyl methacrylate monomer (DEA), with a permanent hydrophilic macromonomer, poly(ethyleneglycol) methyl ether methacrylate (PEGMA). Ethylene glycol dimethacrylate (EDGMA) was used as the branching monomer and the CTA to prevent polymer gelation (1−dodecanethiol (DDT) or 1−thioglycerol (TG)). A range of different polymer architectures with controllable compositions and chain-ends are defined by the choice of CTA (**Figure 1.14A**).

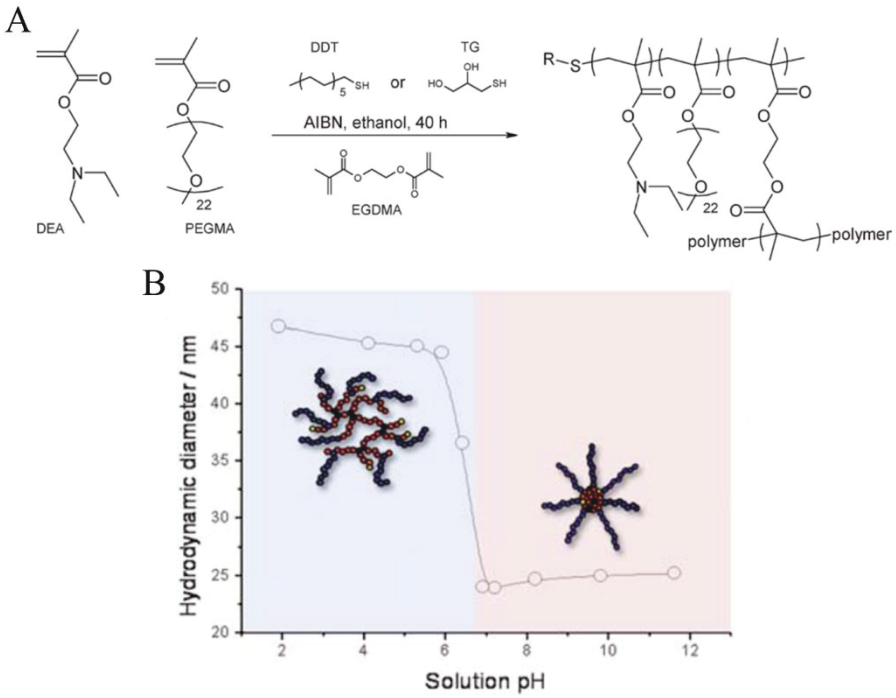


**Figure 1.14.** (A) Synthesis of pH-BCPNs.[68] Adapted from Reference 68. Copyright (2008) with permission of The Royal Society of Chemistry (B) Variation of hydrodynamic diameter with solution pH for pH-BCPNs ($PEGMA_5/DEA_{95}$-$EGDMA_{15}$-$DDT_{15}$). Red components are DEA, blue components are PEGMA, black constituents represent the branching units, and the yellow components are DDT.[70] Adapted from Reference 70. Copyright (2010) with permission of The Royal Society of Chemistry.

These pH-BCPNs are soluble molecularly in both acidic and basic aqueous solution due the presences of the permanently hydrophilic PEGMA. Light scattering as a function of pH was used to determine the hydrodynamic diameter of the pH-BCPNs. Below pH 7 ($pK_a$ of pH-BCPNs), the pH-BCPNs showed a

hydrated, hydrophilic structure due to extensive protonation of the tertiary amine of the DEA residues. On addition of base (pH > 7), the DEA domains become hydrophobic because the tertiary amines are deprotonated. The pH-BCPNs form a compact, amphiphilic, and core-shell structure (**Figure 1.14B**). This observation also confirms that pH-BCPNs have unimolecular structure at basic pH. Interestingly, while free radical polymerization is 'uncontrolled', in terms of molecular weight and polydispersity of primary chains, the particle size distribution of the pH-BCPNs at basic aqueous solution were relatively narrow. The pH-dependent uptake and release of hydrophobic active (pyrene) of pH-BCPNs can be tuned by varying the degree of branching, and hydrophobicity and concentration of end groups (CTA) of the branched copolymers.

Rimmer *et al*. have reported temperature responsive branched copolymers. These temperature responsive branched copolymers, poly(N−isopropyl acrylamides) (PNIPAM) with peptide-end groups, form colloidally stable dispersions of sub-micron particles above the lower critical solution temperature (LCST).[71] The polymer transitions from an open coil and highly solvated state to a more compact globular and less solvated state above its LCST (**Figure 1.15A**). The stability of the colloidal dispersion originates from the hydrophilic/polar end groups, which forms the corona of the particle.

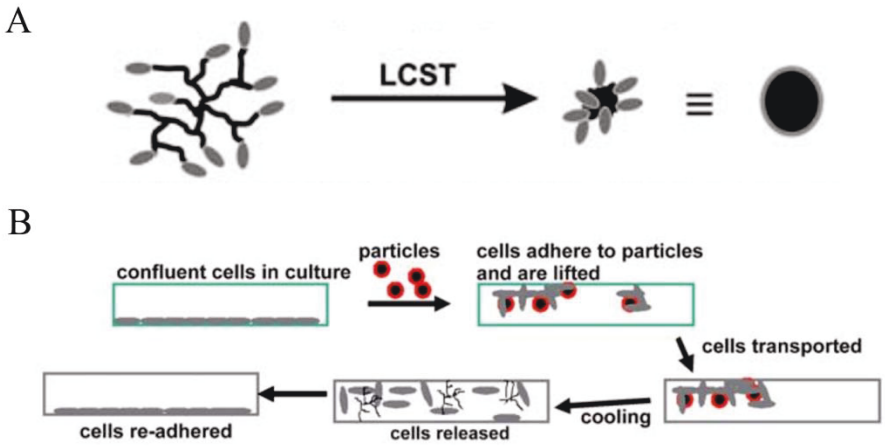


**Figure 1.15.** (A) Schematic representation of the two states of temperature responsive branched copolymer PNIPAM with hydrophilic/polar chain-end groups. The branched copolymer forms a particulate dispersion above its LCST and stabilized by it polar end groups.[50] (B) A schematic representation of the transport and release process of branched copolymers PNIPAM containing cell binding end groups.[50] All adapted from Reference 50. Copyright (2010) with permission of The Royal Society of Chemistry.

Branched PNIPAM copolymers (acid functionalized) have shown they have the ability to enter cells when they are in their globular state and no cell-uptake when they are in their open coil state.[71] Furthermore, branched PNIPAM copolymers (containing cell binding end groups) have the ability to bind and lift/transport cells in their globular state, and release cells in their open coil state (**Figure 1.15B**).[72,73] The two polymer states are controlled by an external stimulus, temperature. Branched copolymers have also been utilized in protein purification and *in vivo* $^{19}F$ magnetic resonance imaging because of their high concentration of end groups.[74–76]

### 1.6.2. Stimuli Responsive Branched Copolymers as Emulsifying Agents

In 2009, Woodward *et al*. demonstrated that pH-BCPNs based on PEGMA and DEA (5:95 molar ratios) can be used to create stable pH-responsive oil-in-water emulsions efficiently at basic pH (droplet size distribution of 8.4 − 12.5 μm), and trigger de-emulsification at acidic pH.[77] The droplet stabilization at basic pH is due to three potential synergistic mechanisms: *(i)* the amphiphilic properties from the hydrophobic core and hydrophilic shell promotes efficient interfacial adsorption, *(ii)* the formation of core-shell of pH-BCPNs allow them to behave as a Pickering stabilizer, and *(iii)* the high concentration of polymer chain-ends can be tailored to interact with either favorably or unfavorably with internal droplet phase, thus facilitating either enhanced or reduced interfacial adsorption.

It was initially thought that the main reason for de-emulsification of droplets at acidic pH was the protonation of the tertiary amine on the DEA residues (cationic and hydrophilic). The change in pH-BCPNs wettability would cause desorption of pH-BCPNs from the interface and trigger de-emulsification. However, it was discovered that the extent of de-emulsification is also highly dependent on both chain-end hydrophobicity and the length of branching unit. In one end of the spectrum, pH-BCPNs with hydrophobic CTA (DDT) and short branching unit produced stable emulsion in acidic solution, so no de-emulsification was observed upon acidification. In the other end, pH-BCPNs with hydrophilic CTA (TG or 3−mercaptopropionic, MPA) and long branching unit showed complete demulsification in acidic conditions. The combination of hydrophilic CTA and

short branching produced stable emulsion droplets that only partially demulsify in acidic condition (**Figure 1.16**).

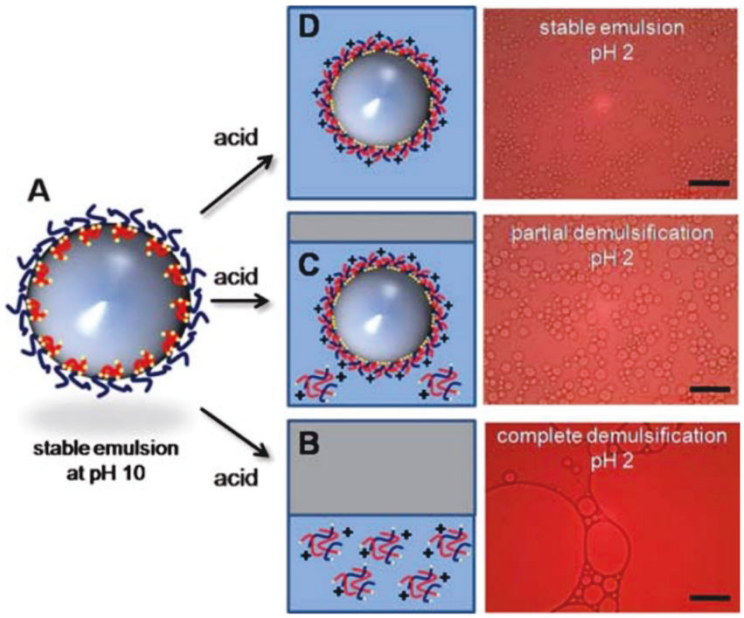


**Figure 1.16.** Schematic illustration of de-emulsification degree of pH-BCPNs stabilized emulsion. (A) Stable emulsion at basic pH, (B) complete de-emulsification of emulsion stabilized with pH-BCPNs containing hydrophilic CTA and long branching unit, (C) partially demulsify emulsion with pH-BCPNs with hydrophilic CTA and short branching unit, (D) stable emulsion stabilized with pH-BCPNs with hydrophobic CTA and short branching unit.[70] Adapted from Reference 70. Copyright (2010) with permission of The Royal Society of Chemistry.

In contrast to emulsions that can trigger de-emulsification at acidic pH, a new class of branched copolymers have been synthesized to produce highly stable pH-responsive emulsions, in which emulsion droplets can form supramolecular structures at acidic pH. The careful design of these branched copolymers provides functionality on the surface of the emulsion droplets, which can manipulate emulsion droplets to assemble or disassemble in response to pH.[78] The branched copolymer was composed of PEGMA macromonomer, methacrylic acid (MAA) with DDT chain-ends and EGDMA as the branching unit (**Figure 1.17A and Figure 1.17B**). The architecture and composition of these copolymers were chosen to provide *(i)* simultaneous steric stabilization from the PEGMA domains at basic and acidic pH, and electrostatic stabilization at basic pH from the MAA domains, *(ii)* the ability to form inter hydrogen-bonding between ethylene glycol (EG) : MAA residues in acidic solution, and *(iii)* the branched architecture of the polymer ensures multiple potential attachment points to the oil phase. A stable oil-

in-water emulsion droplets were produced at basic pH (average droplet size = 9.2 μm), existing as a free-flowing state dispersion (**Figure 1.17D**). Lowering the pH of the solution, allows protonation of MAA residues. The neutralization of the MAA residues is accompanied by the production of extensive hydrogen bonding between EG and MAA residues. This extensive H-bonding exists as intra and inter hydrogen bonding around surface of droplets (**Figure 1.17C**).

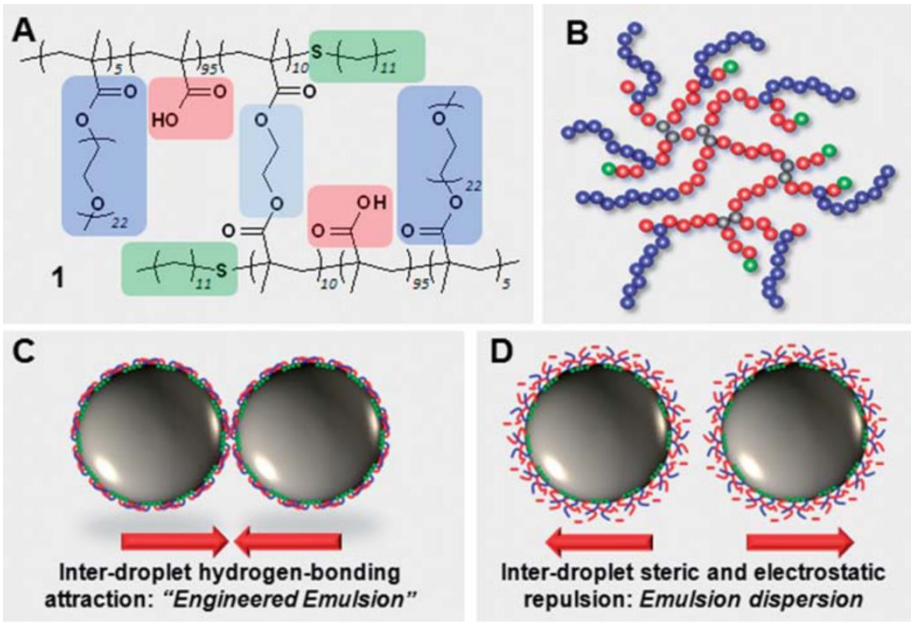


**Figure 1.17.** Schematic representation of the chemical (A) and architecture (B) structures of branched copolymer based on PEGMA and MAA with DDT chain-ends. The formation (C) and deformation (D) of inter-droplet hydrogen bonds between EG (blue) and MAA (red) residues on the surface of emulsion droplets.[79] Reproduced from Reference 79. Copyright (2010) with permission of The Royal Society of Chemistry.

Providing the concentration of emulsion droplets in the solution is sufficiently high, this inter-droplet hydrogen bonding forms multiple cooperative bonding sites between droplets and produces self-supporting, monolithic emulsion assembly known as 'Engineered emulsions' (**Figure 1.18**). Since the extensive hydrogen bonding is responsive to the pH of the solution, the free-standing structure of the 'Engineered Emulsion' can be readily disassembled to discrete free-flowing droplets. The disassembly process is driven by the removal of hydrogen bonds and the reoccurrence of electrostatic repulsion from the anionic MAA residues. The process of making Engineered Emulsion can be scaled up using a homogenous pH-switch, gluconic acid δ−lactone, as a proton source.[79]

Magneto-responsive emulsions can be fabricated by simply encapsulating oleophilic magnetic nanoparticles in the oil phase of the emulsions.[80]

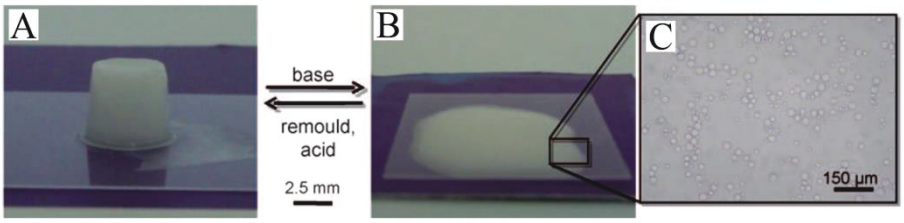


**Figure 1.18.** Engineered emulsions' reversible assembly (A) and disassembly (B) in acidic and basic pH, respectively. (C) Light micrograph of disassembled Engineered emulsions.[78] Adapted from Reference 78. Copyright (2009) with permission of John Wiley and Sons.

In 2011, Woodward *et al*. synthesized a series of compositional controlled branched copolymer based on MAA and PEGMA. All of the branched copolymer with different composition can be used as efficient emulsifiers for the production of stable emulsion droplets at basic pH. It was demonstrated that variation of EG : MAA ratio can control the kinetics of inter-droplet interactions. The aggregation kinetics showed that equimolar ratio of EG : MAA promotes the fastest aggregation, and that excess MAA residue maintains droplet aggregation but at a slower rate in acidic pH. In the other hand, excess PEGMA residues completely stop inter-droplet hydrogen bonding at acidic pH, thus, preventing droplet aggregation. Binary mixture of contra-functionalized droplets, such as 100 % MAA droplets and 100 % EG droplets, present evidence of selective aggregation although yields were low.[81]

Branched copolymers have been utilized as an emulsifying agent for the production of inorganic-organic capsules by hydrolyzing the methoxy silane residues present in the branched copolymers, to form a silica shell.[82] Mei et al. modified this branched copolymer by adding pH-responsive domains, such as tertiary amine, 2−(dimethylamino) ethyl methacrylate and MAA. The pH-responsive branched copolymer was used to create electrostatically gated membrane in inorganic protocells. The pH-responsive branched copolymers generated an ultrathin elastic membrane at the interface of water-in-oil Pickering emulsions that exhibits selective release and uptake of small molecules.[83] Furthermore, branched copolymers has been utilized as a surfactant in the

fabrication of porous materials,[26,84] 'dry' emulsions,[85] and printable 3D graphene structures.[86]

## 1.7. Objectives and Outline of the Thesis

The aim of this thesis is to utilize branched copolymers as emulsifying agents to create emulsions that can act as a platform for the production of unique novel supracolloidal materials. The chemical composition and architectural structure of the branched copolymers were chosen and varied to ensure stable emulsions were produced, and more importantly, to provide the correct functionalities on the interface of the emulsion droplets that were required for the application.

A brief overview of this thesis is presented below.

***Chapter 2*** demonstrates the use of oil-in-water emulsion droplets, stabilized with branched copolymer, as templates to fabricate calcium phosphate (CaP) microcapsules. The method presented is versatile and time-efficient compared to previously reported methods. The branched copolymer was designed to provide a suitable architecture and functionality to produce stable emulsion droplets, and permit the mineralization of CaP at the surface of the oil droplet when incubated in a solution containing calcium and phosphate ions. These CaP capsules were made fluorescent by post-functionalization of the CaP shell with a fluorescein−bisphosphonate conjugate.

***Chapter 3*** illustrates microfluidically spun supracolloidal fibers made from emulsion droplets stabilized with Laponite clay disc functionalized with pH-responsive branched copolymers. The proton diffusion into the stream of emulsion droplets induces the reversible self-assembly process leading to the formation of a continuous supracolloidal fiber. The production of stripy Janus type fibers (two and three stripes), magnetic fibers, and fibers of controlled length suggest the versatility of the material and method. These supracolloidal fibers can be used as a tool to delivery volatile compounds, where the evaporation rate of the volatile compounds can be tuned as a function of ionic crosslinking degree. The dried fibers produced are low-weight highly porous materials.

In ***Chapter 4***, we discovered that these supracolloidal fibers can be utilized as a storage material for emulsion droplets, where emulsion droplets are 'locked' in the fiber structure under acidic condition, and are released from the fiber upon basification of the system. The release of emulsion droplets from the fiber can be time-controlled by programming the transient acidic pH states of the system by combining a fast acidic promoter with a feedback-driven biocatalytically controlled slow generation of base in a close system. These fibers show autonomous dynamics and self-regulation properties. Fabrication and release profiles of other supracolloidal structures have been demonstrated to suggest the versatility of the material.

## 1.8. References


1 (a) R. J. Hunter, *Foundations of Colloids Science*, Oxford University Press Inc., 2nd Ed., **2001**. (b) T. Cosgrove, *Colloid Science: Principles, Methods and Applications*, 2nd Ed., **2010**. (c) T. Ngai and S. A. F. Bon, *Particle-Stabilized Emulsions and Colloids: Formation and Applications*, **2015**. (d) P. C. Hiemenz and R. Rajagopalan, *Principles of Colloid and Surface Chemistry*, 3rd Ed., **1997**.

2 T. J. Graham, *J. Chem. Soc., Trans.*, 1864, **17**, 368.

3 T. J. Graham, *J. Chem. Soc., Trans.*, 1864, **17**, 318.

4 H. C. Hamaker, *Physica*, 1937, **4**, 1058.

5 B. Deryagin and L. Landau, *Acta Physicochim. U.R.S.S*, 1941, **14**, 633.

6 E. J. W. Verwey, *J. Phys. Chem.*, 1947, 51, 631.

7 J. T. G. Overbeek, *J. Colloid Interface Sci.*, 1977, **58**, 408.

8 H. McKenzie, *Particle Encapsulation and Modification to Afford Hierarchical Composite Materials*, PhD thesis, University of Warwick, **2014**.

9 D. H. Napper, *J. Colloid Interface Sci.*, 1969, **29**, 168.

10 D. H. Napper, *J. Colloid Interface Sci.*, 1970, **32**, 106.

11 D. H. Napper, *J. Colloid Interface Sci.*, 1970, **33**, 384.

12 D. H. Napper and A. Netschey, *J. Colloid Interface Sci.*, 1971, **37**, 528.

13 D. H. Napper, *J. Colloid Interface Sci.*, 1977, **58**, 390.

14 M. van den Tempel, J. Lucassen and E. H. Lucassen-Reynders, *J. Phys. Chem.*, 1965, **69**, 1798.

15 T. Delmas, H. Piraux, A.-C. Couffin, I. Texier, F. Vinet, P. Poulin, M. E. Cates and J. Bibette, *Langmuir*, 2011, **27**, 1683.

16 W. Ramsden, *Proc. R. Soc. Lond.*, 1903, **72**, 156.

17 S. U. Pickering, *J. Chem. Soc. Trans.*, 1907, **91**, 2001.

18 P. Finkle, H. D. Draper and J. H. Hildebrand, *J. Am. Chem. Soc.*, 1923, **45**, 2780.

19 P. Pieranski, *Phys. Rev. Lett.*, 1980, **45**, 569.

20 J. H. Clint and S. E. Taylor, *Colloids and Surfaces*, 1992, **65**, 61.

21 B. P. Binks, *Curr. Opin. Colloid Interface Sci.*, 2002, **7**, 21.

22 B. P. Binks and S. O. Lumsdon, *Phys. Chem. Chem. Phys.*, 1999, **1**, 3007.

23 B. P. Binks and S. O. Lumsdon, *Langmuir*, 2000, **16**, 8622.

24 N. P. Ashby and B. P. Binks, *Phys. Chem. Chem. Phys.*, 2000, **2**, 5640.

25 V. O. Ikem, A. Menner and A. Bismarck, *Langmuir*, 2010, **26**, 8836.

26 E. Garcia-Tunon, S. Barg, R. Bell, J. V. M. Weaver, C. Walter, L. Goyos and E. Saiz, *Angew. Chemie Int. Ed.*, 2013, **52**, 7805.

27 Z. Li, T. Ming, J. Wang and T. Ngai, *Angew. Chemie Int. Ed.*, 2009, **48**, 8490.

28 Z. Li and T. Ngai, *Langmuir*, 2010, **26**, 5088.

29 N. Glaser, D. J. Adams, A. Böker and G. Krausch, *Langmuir*, 2006, **22**, 5227.

30 E. S. Read, S. Fujii, J. I. Amalvy, D. P. Randall and S. P. Armes, *Langmuir*, 2004, **20**, 7422.

31 S. Fujii, E. S. Read, B. P. Binks and S. P. Armes, *Adv. Mater.*, 2005, **17**, 1014.

32 T. Ngai, S. H. Behrens and H. Auweter, *Chem. Commun.*, 2005, 331.

33 R. F. A. Teixeira, H. S. McKenzie, A. A. Boyd and S. A. F. Bon,

*Macromolecules*, 2011, **44**, 7415.

34 P. J. Colver, C. A. L. Colard and S. A. F. Bon, *J. Am. Chem. Soc.*, 2008, **130**, 16850.

35 Y. Chen, N. Ballard and S. A. F. Bon, *Chem. Commun.*, 2013, **49**, 1524.

36 A. D. Dinsmore, M. F. Hsu, M. G. Nikolaides, M. Marquez, A. R. Bausch and D. A. Weitz, *Science*, 2002, **298**, 1006.

37 D. J. Mitchell and B. W. Ninham, *J. Chem. Soc. Faraday Trans. 2*, 1981, **77**, 601.

38 J. N. Israelachvili, *Intermol. Surf. forces. Acad. Press.*, London, 1985, **251**.

39 J. Eastoe, *Colloid Science: Principles, Methods and Applications*, 2nd Ed., **2010**.

40 J. N. Israelachvili, D. J. Mitchell and B. W. Ninham, *J. Chem. Soc. Faraday Trans. 2*, 1976, **72**, 1525.

41 R. Aveyard, B. P. Binks, S. Clark and J. Mead, *J. Chem. Soc. Faraday Trans. 1*, 1986, **82**, 125.

42 W. C. Griffin, *J. Cosmetics Chemists*, 1949, **1**, 311.

43 J. T. Davies, *Proc. 2nd Int. Congr. Surf. Act.,* Butterworths, London, 1959, **1**.

44 J. Eastoe, *Colloid Science: Principles, Methods and Applications*, 2nd Ed., **2010**.

45 A. M. Mathur, B. Drescher, A. B. Scranton and J. Klier, *Nature*, 1998, **392**, 367.

46 A. Y. C. Koh and B. R. Saunders, *Chem. Commun.*, 2000, **6**, 2461.

47 A. Vesperinas, J. Eastoe, P. Wyatt, I. Grillo, R. K. Heenan, J. M. Richards and G. A. Bell, *J. Am. Chem. Soc.*, 2006, **128**, 1468.

48 S. Khoukh, P. Perrin, F. B. de Berc and C. Tribet, *ChemPhysChem*, 2005, **6**, 2009.

49 Y. Liu, P. G. Jessop, M. Cunningham, C. A. Eckert and C. L. Liotta, *Science*, 2006, **313**, 958.

50 R. M. England and S. Rimmer, *Polym. Chem.*, 2010, **1**, 1533.

51 C. Gao and D. Yan, *Prog. Polym. Sci.*, 2004, **29**, 183.

52 D. A. Tomalia and J. M. J. Frechet, *J. Polym. Sci. Part A: Polym. Chem.*, 2002, **40**, 2719.

53 D. A. Tomalia and J. M. J. Frechet, *Dendrimers and other Dendritic Polymers*, John Wiley & Sons Ltd., Sussex, UK, **2001**.

54 S. Unal, I. Yilgor, E. Yilgor, J. P. Sheth, G. L. Wilkes and T. E. Long, *Macromolecules*, 2004, **37**, 7081.

55 Y. H. Kim (Du Pont), US4857630 A, **1989**.

56 Y. H. Kim and O. W. Webster, *J. Am. Chem. Soc.*, 1990, **112**, 4592.

57 J. M. J. Frechet, M. Henmi, I. Gitsov, S. Aoshima, M. R. Leduc and R. B. Grubbs, *Science*, 1995, **269**, 1080.

58 C. J. Hawker, J. M. J. Frechet, R. B. Grubbs and J. Dao, *J. Am.Chem. Soc.*, 1995, **117**, 10763.

59 N. O'Brien, A. McKee, D. C. Sherrington, A. T. Slark and A. Titterton, *Polymer*, 2000, **41**, 6027.

60 P. A. Costello, I. K. Martin, A. T. Slark, D. C. Sherrington and A. Titterton, *Polymer*, 2002, **43**, 245.

61 F. Isaure, P. A. G. Cormack and D. C. Sherrington, *J. Mater. Chem.*, 2003, **13**, 2701.

62 F. Isaure, P. A. G. Cormack and D. C. Sherrington, *Macromolecules*, 2004,

**37**, 2096.

63 A. Matsumoto, *Adv. Polym. Sci.*, 1995, **123**, 44.

64 F. Isaure, P. A. G. Cormack, S. Graham, D. C. Sherrington, S. P. Armes and V. Bütun, *Chem. Commun.*, 2004, 1138.

65 Y. Li and S. P. Armes, *Macromolecules*, 2005, **38**, 8155.

66 B. Liu, A. Kazlauciunas, J. T. Guthrie and S. Perrier, *Macromolecules*, 2005, **38**, 2131.

67 Y. Li and S. P. Armes, *Macromolecules*, 2005, **38**, 5002.

68 J. V. M. Weaver, R. T. Williams, B. J. L. Royles, P. H. Findlay, A. I. Cooper and S. P. Rannard, *Soft Matter*, 2008, **4**, 985.

69 K. B. T. Ii, T. Kowalewski and K. L. Wooley, *J. Am. Chem. Soc.*, 1996, **118**, 7239.

70 J. V. M. Weaver and D. J. Adams, *Soft Matter*, 2010, **6**, 2575.

71 S. Rimmer, S. Carter, R. Rutkaite, J. W. Haycock and L. Swanson, *Soft Matter*, 2007, **3**, 971.

72 S. Hopkins, S. Carter, S. MacNeil and S. Rimmer, *J. Mater. Chem.*, 2007, **17**, 4022.

73 J. Shepherd, P. Sarker, K. Swindells, I. Douglas, S. MacNeil, L. Swanson and S. Rimmer, *J. Am. Chem. Soc.*, 2010, **132**, 1736.

74 S. Carter, S. Rimmer, A. Sturdy and M. Webb, *Macromol. Biosci.*, 2005, **5**, 373.

75 S. Carter, S. Rimmer, R. Rutkaite, L. Swanson, J. P. Fairclough, A. Sturdy and M. Webb, *Biomacromolecules*, 2006, **7**, 1124.

76 K. J. Thurecht, I. Blakey, H. Peng, O. Squires, S. Hsu, C. Alexander and A. K. Whittaker, *J. Am. Chem. Soc.*, 2010, **132**, 5336.

77 R. T. Woodward, R. A. Slater, S. Higgins, S. P. Rannard, A. I. Cooper, B. J. L. Royles, P. H. Findlay and J. V. M. Weaver, *Chem. Commun.*, 2009, 3554.

78 J. V. M. Weaver, S. P. Rannard and A. I. Cooper, *Angew. Chem. Int. Ed.*, 2009, **48**, 2131.

79 R. T. Woodward, L. Chen, D. J. Adams and J. V. M. Weaver, *J. Mater. Chem.*, 2010, **20**, 5228.

80 R. T. Woodward, C. I. Olariu, E. A. Hasan, H. H. P. Yiu, M. J. Rosseinsky and J. V. M. Weaver, *Soft Matter*, 2011, **7**, 4335.

81 R. T. Woodward and J. V. M. Weaver, *Polym. Chem.*, 2011, **2**, 403.

82 R. L. Harbron, T. O. McDonald, S. P. Rannard, P. H. Findlay and J. V. M. Weaver, *Chem. Commun.*, 2012, **48**, 1592.

83 M. Li, R. Harbron, J. Weaver, B. Binks and S. Mann, *Nat. Chem.*, 2013, **5**, 529.

84 R. T. Woodward, C. Hight, U. Yildiz, N. Schaeffer, E. M. Valliant, J. R. Jones, M. M. Stevens and J. V. M. Weaver, *Soft Matter*, 2011, **7**, 7560.

85 B. O. Carter, J. V. M. Weaver, W. Wang, D. G. Spiller, D. J. Adams and A. I. Cooper, *Chem. Commun.*, 2011, **47**, 8253.

87 E. García-Tuñon, S. Barg, J. Franco, R. Bell, S. Eslava, E. D'Elia, R. C. Maher, F. Guitian and E. Saiz, *Adv. Mater.*, 2015, **27**, 1688.

# Chapter 2

## Fabrication of Calcium Phosphate Microcapsules Using Emulsion Droplets Stabilized with Branched Copolymers as Templates [§]

We report on a versatile and time-efficient method to fabricate calcium phosphate (CaP) microcapsules by utilizing oil-in-water emulsion droplets stabilized with synthetic branched copolymer (BCP) as templates. The BCP was designed to provide a suitable architecture and functionality to produce stable emulsion droplets, and permit the mineralization of CaP at the surface of the oil droplet when incubated in a solution containing calcium and phosphate ions. The CaP shells of the microcapsules were established to be calcium deficient hydroxyapatite with incorporated chlorine and carbonate species. These capsule walls were made fluorescent by decoration with a fluorescein−bisphosphonate conjugate.

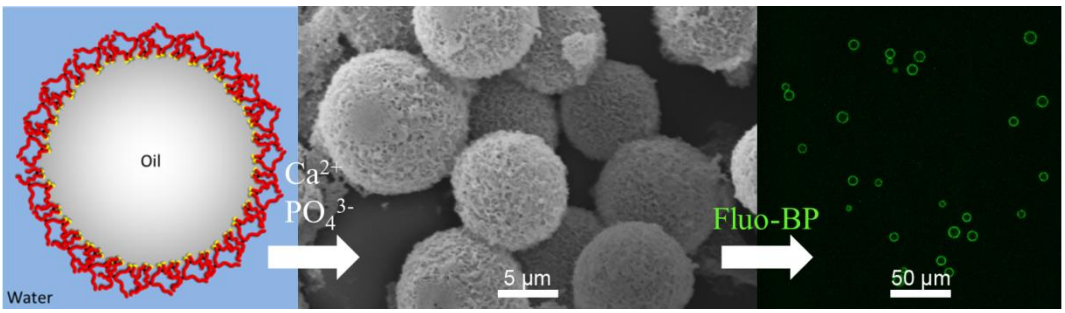


[§]Parts of the chapter were reproduced from R. V. Bell, L. A. Rochford, R. T. M. de Rosales, M. Stevens, J. V. M. Weaver, and S. A. F. Bon, *J. Mater. Chem. B*, 2015, **3**, 5544 by permission of The Royal Society of Chemistry (Copyright 2015).

## 2.1. Introduction

Calcium phosphate (CaP) materials have drawn particular interest in the areas of medicine and health care due to the similarities of composition and structure to the inorganic constituents of hard tissues in vertebrates, such as bone and teeth.[1] Bone is an inorganic-organic biocomposite of which 70 wt% is inorganic, 20 wt% is organic, and the remaining 10 wt% is attributed to water. The inorganic phase of bone is a non-stoichiometric carbonated multi-ion substituted apatite with calcium to phosphorous ratio between 1.37 and 1.87 that exhibits a similar crystal structure to hydroxyapatite (HA).[2] The inorganic component offers the compressive strength and stiffness of bone. Oppositely, the organic phase of the bone, composed predominantly of type I collagen, provides elasticity and fracture toughness to the bone matrix.[2] The physicochemical properties of CaP, as in its bioactivity, biocompatibility, biodegradability and osteoconductivity,[3] allow it to be widely utilized in bone fillers,[4,5] bone tissue engineering scaffolds,[6–8] bioactive coatings and composites,[9] and drug/protein/gene delivery systems.[10–17]

The specific structure of CaP (composition *(i)* or surface *(ii)*) can be tuned to optimize the desired material properties for a specific end application by:

*(i)* The chemical composition of CaP can be modified by utilizing the ability of the apatite structure to accept numerous ionic substituents. CaP, such as HA ($Ca_{10}(PO_4)_6(OH)_2$), is a member of the apatite minerals.[18] Apatites are represented by the general formula $M_{10}(XO_4)_6Y_2$, where M is bivalent ion, $XO_4$ a trivalent ion, and Y a monovalent ion.[18] **Figure 2.1** shows the crystal structure of HA, and can be describe as a hexagonal stack of $PO_4^{3-}$ groups producing two kinds of tunnel parallel to the *c* axis. The first kind of tunnel is occupied by $Ca^{2+}$ (Ca(I) site) ions whereas the second one, which is lined by oxygen (from the phosphate groups) and other calcium ions (Ca(II) site), is occupied by $OH^-$ ions. The diameter of the tunnels (3 Å) gives the apatite with ion exchanger properties, and can also act as a host to small molecules. Divalent and monovalent cations can substitute for $Ca^{2+}$, and anions may substitute for $OH^-$ groups. Additionally, some trivalent ions can substitute for $OH^-$, $PO_4^{3-}$ or both, which is referred to as A, B, and AB type substitution, respectively.[18]

CaP, in particular HA, has been used in fluorescence labeling or imaging by doping its crystal structure with lanthanides.[19–22] Furthermore, it has been demonstrated that the incorporation of silver or fluoride ions provides anti-bacterial properties.[23,24] Next to applications related to health care, HA has also been employed as a low cost absorbent for heavy metal pollutants because of its high sorption efficiency for divalent heavy metals ions, low water solubility, and high stability under reducing and oxidizing conditions.[25–29]

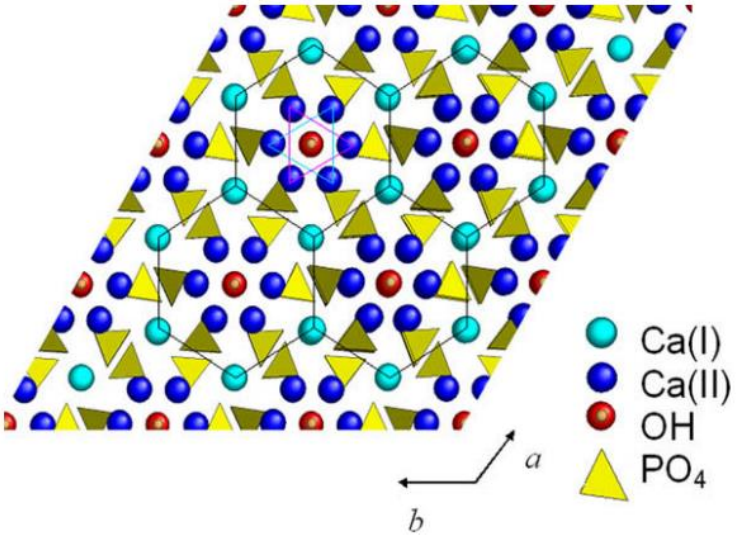


**Figure 2.1.** Crystal structure of HA along the c-axis. The Ca(I) columns are connected in hexagonal networks (black line). The staggered Ca(II) atoms are connected in triangular shapes (cyan and magenta lines) that are on the same plane, but the height with respect to the c-axis is not similar. HA crystal structure has two types of tunnels. The first tunnel is occupied by $Ca^{2+}$ (Ca(II)) ions whereas the second one, is occupied by $OH^-$ ions.[30] Reprinted from Reference 30. Copyright (2010) with permission from Elsevier.

*(ii)* The surface of CaP can be functionalized through chemi- or physisorption. CaP possesses three main sorption sites on its apatite structure, which are, positively charged calcium sites, negatively charged phosphate sites, and hydroxyl sites. CaP therefore has been used in column chromatography for separation of biomolecules,[31–33] in catalysis,[34,35] as organic absorbent,[36] and in imaging[37–39].

Micro/nanostructure capsules possess many intriguing characteristics, for example low density, high surface area to volume area, good flowability, and low coefficients of thermal expansion and refractive index. Also, they have hollow core which can acts as a storage space for various substances or a reaction

chamber, and the shell structure can contain paths to provide a control release system. Due to these advantages, micro/nanostructure capsules are attractive to many applications.[40,41] Capsule walls made from CaP are attractive for reasons mentioned above. Capsules with a CaP shell have been produced by various synthesis routes. One of the approaches widely employed is to use solid particles as a template, around which the CaP capsule wall is being constructed. Solid templates are readily available in a wide range of sizes and shapes, with a narrow size distribution if required. Solid templates, such as glass microspheres,[42–45] calcium carbonate,[46–48] polymeric nanoparticles[49] have been used to fabricate CaP capsules. A substantial drawback of this method is the removal of the solid core template, as it often requires the use of high temperatures and/or acid. These harsh conditions can lead to deterioration of mechanical robustness of the capsule and alter the permeability properties of the wall. Furthermore, refilling the hollow core can only be achieved once the solid template has been removed, and loading the hollow core in an efficient way may arise to some challenges. To minimize the drawbacks of using solid templates, routes based on using soft templates have been explored. Organized systems such as yeast cells,[50] micelles,[11,51–54] liposomes,[55–58] and colloidosomes[59] have been employed for preparing CaP capsules. Template free routes have also been presented to produce hollow CaP capsules.[60–64] The latter system relies on CaP nanoparticles as building blocks to arrange and self-assemble, into supracolloidal structures.

One of the soft templating routes which is especially attractive is the use of emulsion droplets as templates. Liquid cores are easily removed by gentle evaporation or dissolution in a common solvent after the CaP shell formation. More importantly, the emulsion droplet can be pre-loaded with the desired active materials efficiently and with ease, prior to the formation of the CaP shell. Furthermore, the production of emulsion droplets is straightforward and the droplet size distributions can be controlled. Böker and co-workers have presented an emulsion templating route to produce CaP capsules by incubating oil droplets stabilized with protein (that is ferritin or hydrophobin) in an aqueous calcium-phosphate solution.[65–67] The incubation process allows mineralization of CaP at the surface of the oil droplets, resulting in CaP capsules. The procedure is straightforward, requires mild conditions with no organic solvents needed, and all

reactants are non-toxic. However, the mineralization process to produce the CaP capsules required a long incubation period (24 – 28 days), in which the mineralization solution had to be exchanged regularly. Furthermore, the use of ferritin and hydrophobin proteins as stabilizer, and the potential addition of an enzyme to reduce the mineralization period, is costly.

Herein, we demonstrate the fabrication of CaP capsules by utilizing oil-in-water emulsions stabilized with a synthetic branched copolymer (BCP) made by free radical polymerization. The BCP has the right architecture and functionality to produce stable oil droplets, and allows formation of the CaP mineral at the surface of the oil droplets. We believe our method provides a versatile and robust platform in the fabrication of CaP capsules, as the BCP is readily synthesized in large quantities at low cost, and incubation periods are reduced to 72 hours. In addition, we demonstrate a simple post-treatment of the CaP capsules to render them fluorescent upon reaction with a bisphosphonate conjugate containing fluorescein.

## 2.2. Results and Discussion

### 2.2.1. Synthesis and Characterization of Branched Copolymer

The amphiphilic BCP based on methacrylic acid (MAA) with hydrophobic dodecane chain ends was synthesized by thiol-regulated free radical polymerization, as previously reported by Weaver and co-workers (**Figure 2.2A and Figure 2.2B**).[68] The synthesis process gave a high yield with a monomer conversation to polymer of 98 %. MAA moiety was chosen to provide electrostatic stabilization in basic solution for the emulsion droplets, and its ability to chelate to calcium ions, which in turn allows the mineralization of CaP mineral at the surface of the oil droplets. 1−Dodecanethiol (DDT) was employed as a chain transfer agent to provide hydrophobic chain ends, and to mimic the oil phase of the emulsion droplet, here dodecane, for strong oil-droplet surface adsorption. The branched architecture of the BCP provided by the branching agent, ethylene glycol dimethacrylate (EGDMA), ensures multiple potential points of attachment to the droplet surface.

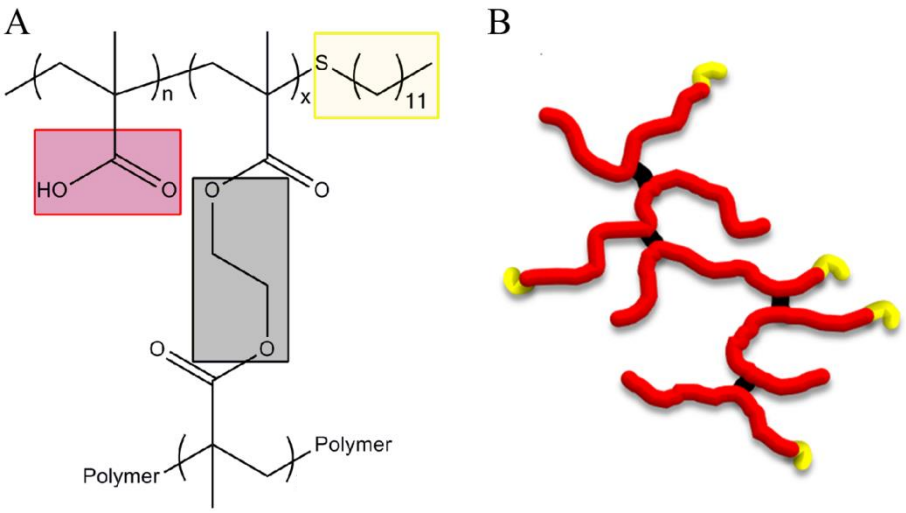


**Figure 2.2.** (A) Chemical structure of the BCP. (B) Schematic illustration of the BCP architecture. The red color represents the main domain of the BCP, MAA, the black color represents the branching unit, EGDMA, and the yellow color represents the hydrophobic chain ends, DDT.

The carboxylic groups of the MAA domain were esterified to determine the relative molar ratios of the co-monomers and chain transfer agent in BCP. The carboxylic groups were esterified using trimethylsilyl diazomethane, and the $^{1}$H NMR spectrum of the esterified-BCP was used to calculate the comonomer ratios

of the final BCP from the extra peak arising from the methyl group on the ester (peak 'h'). The $^{1}$H NMR spectra of the BCP and the esterified-BCP are shown in **Figure 2.3A and Figure 2.3B**, respectively. The target and actual compositions of the BCP can be seen in **Table 2.1**.

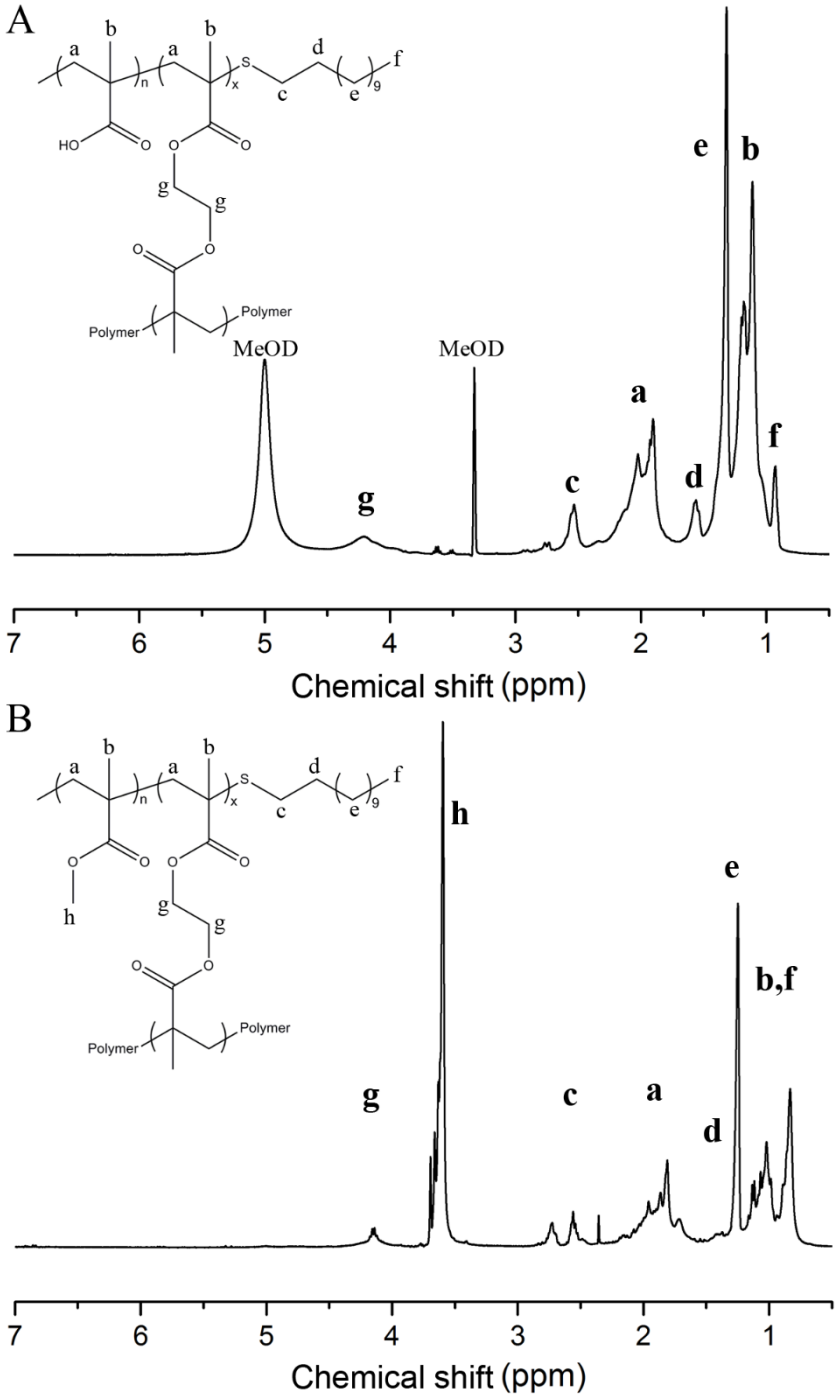


**Figure 2.3.** $^{1}$H NMR spectra of (A) BCP in $CD_3OD$, and (B) esterified BCP in $CDCl_3$. The appearance of peak 'h' (methyl from the ester group) confirms esterification of the BCP.

Triple-detection gel permeation chromatography (TD-GPC) analysis in a DMF eluent was used to analyze the molecular parameters of the BCP. The molecular parameters of the BCP are shown in **Figure 2.4** and **Table 2.1**. The number-average molecular weights ($M_n$) and weight-average molecular weights ($M_w$) values of the BCP were comparable with previous studies.[68] The polydispersity ($Đ$) of the BCP has a broad distribution, which is indicative of a free radical polymerization process. The Mark-Houwink ($\alpha_\eta$) value of 0.23 represents a relatively compact conformation, which is expected for polymers with branched architecture.[68–70]

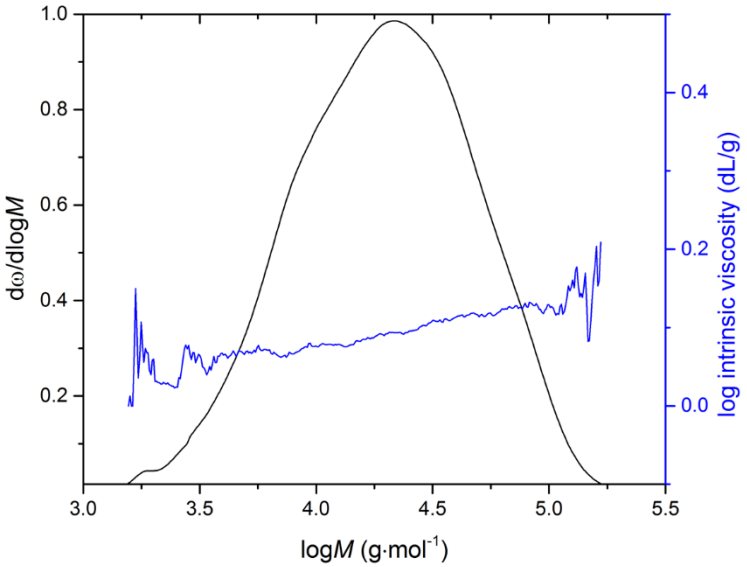


**Figure 2.4.** The TD-GPC chromatograms of the BCP. Molecular weight distribution of the BCP (black line), and molecular weight vs. intrinsic viscosity plot of the BCP (blue line).

**Table 2.1.** Composition and molecular parameters of the BCP.

| Target polymer composition[a] | Actual polymer composition[b] | Conversion (%)[c] | $M_n$ (g·mol$^{-1}$)[d] | $M_w$ (g·mol$^{-1}$)[d] | $Đ$[d] | $\alpha_\eta$[d] |
|---|---|---|---|---|---|---|
| $MAA_{100}$-$EGDMA_{10}$-$DDT_{10}$ | $MAA_{100}$-$EGDMA_{8.7}$-$DDT_{9.2}$ | 97 | 13246 | 27600 | 2.08 | 0.23 |

[a] Target molar equivalent based on monofunctional monomer nominally set to 100. [b] Polymer composition was calculated from $^1$H NMR spectrum of the esterified-BCP. [c] Polymer conversion was calculated by $^1$H NMR. [d] Measured by triple-detection GPC in DMF eluent.

### 2.2.2. Potentiometric Titration of Branched Copolymer

The p$K_a$ of the BCP was determined by performing a simple titration on the BCP. The degree of protonation (α) of BCP with pH was calculated from the Henderson-Hasselbalch equation.[79] The acid-based titration curve of the BCP (**Figure 2.5A**), illustrates that BCP buffered the solution in the pH range of 10 − 3.5.

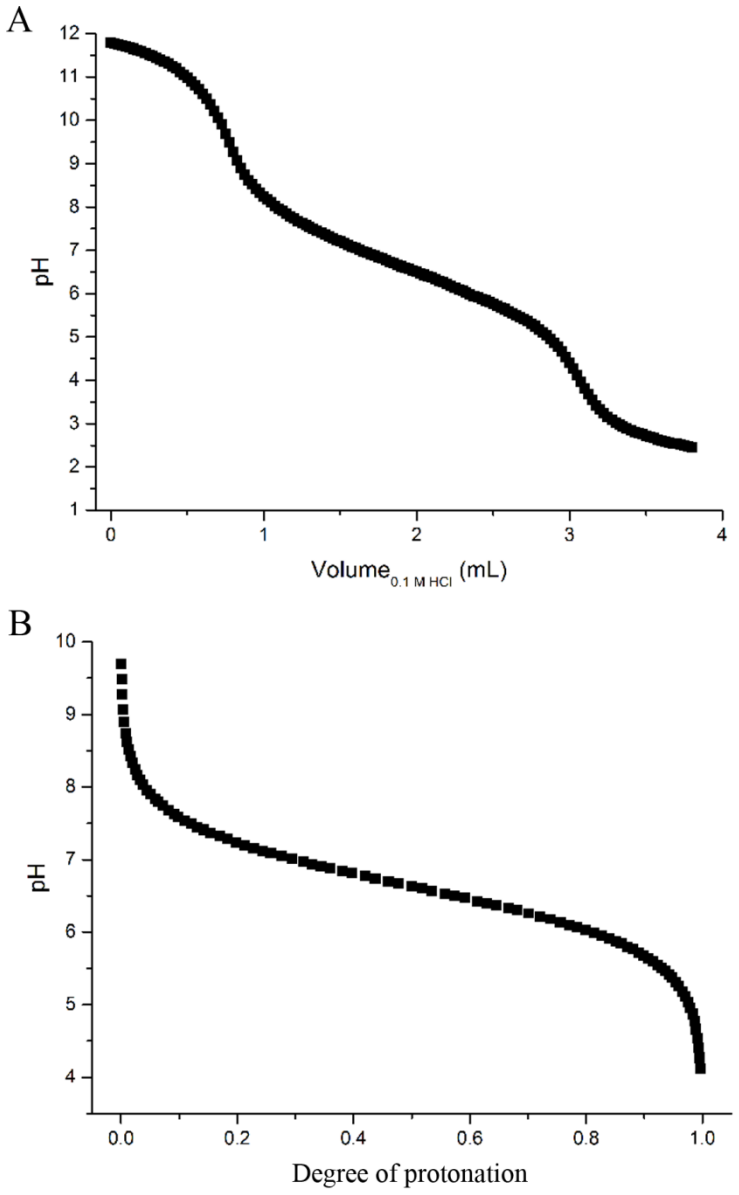


**Figure 2.5.** (A) Acid-base titration curve obtained for BCP, and (B) The degree of protonation (α) of the BCP with pH. The α of BCP; α = 0 at pH 9.70, α = 0.5 at pH 6.63, and α = 1 at pH 4.12.

The titration curve indicated a significant buffering effect of the BCP around pH 6. The α of the MAA domain in BCP increased from zero to unity as the solution pH

decreased from 9.70 to 4.12 (**Figure 2.5B**). At pH 9.70, all of the carboxylic groups of the BCP are deprotonated, and the BCP is in its anionic state. The carboxylic groups of the MAA domain are protonated upon addition of acid, and at pH 4.12, all are protonated. The p$K_a$ of the BCP was determined to be 6.63, and at this instance, 50 % of the carboxylic functional groups are protonated.

### 2.2.3. Fabrication and Characterization of Emulsion Droplets

Oil-in-water emulsions (50:50 vol%) were prepared by homogenizing dodecane in aqueous BCP solutions at pH 10, when carboxyl units is in their anionic form. Stable oil droplets were produced, which creamed after 24 hours due to the lower oil density, but did not coalesce. The emulsion droplets could be simply re-dispersed by gentle agitation. The schematic representation and the light micrograph of oil/water emulsion droplet stabilized with BCP are shown in **Figure 2.6A** and **Figure 2.6B**, respectively.

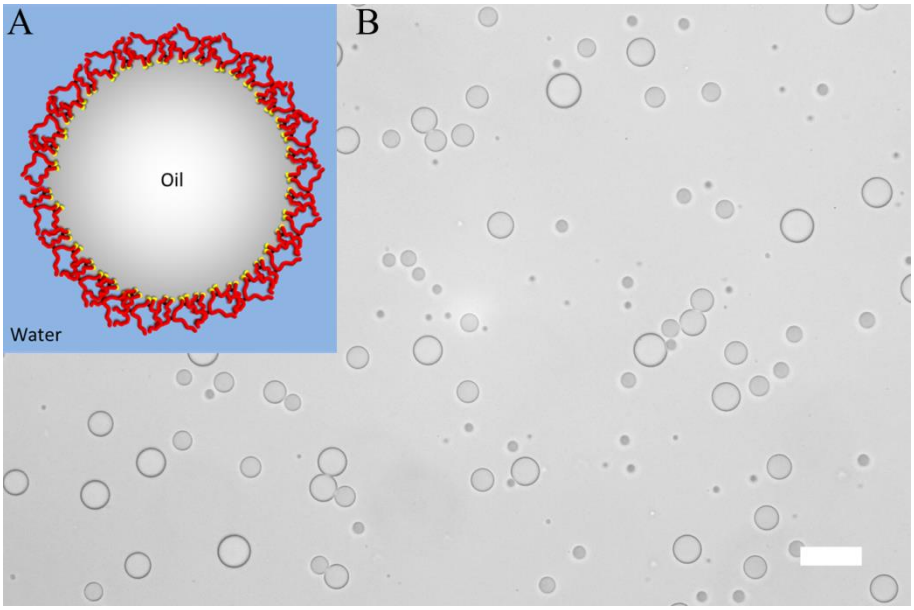


**Figure 2.6.** (A) Schematic representation of an oil/water emulsion droplet stabilized with BCP. The multiple hydrophobic chain ends of BCP, DDT (yellow), anchors at the oil phase, and the MAA domain (red) located at the aqueous phase provides electrostatic stabilization. (B) Light micrograph of oil in water emulsion droplets stabilized with BCP. Scale bar represents 20 µm.

Laser diffraction measurements revealed a monomodal population of emulsion droplets ranging from 3.3 µm to 35.0 µm, with an average droplet diameter of 13.3 µm. The emulsions showed no significant change in droplet size or size distribution for 30 days, as measured with laser diffraction, and no oil separation

(as a result of coalescence) over a five-month period was observed, proving their colloidal stability (**Figure 2.7A**). In addition, the laser diffraction chromatogram (**Figure 2.7B**) demonstrates that the emulsion droplets are stable in the diluted system because there was no significant change in droplet size over 60 minutes.

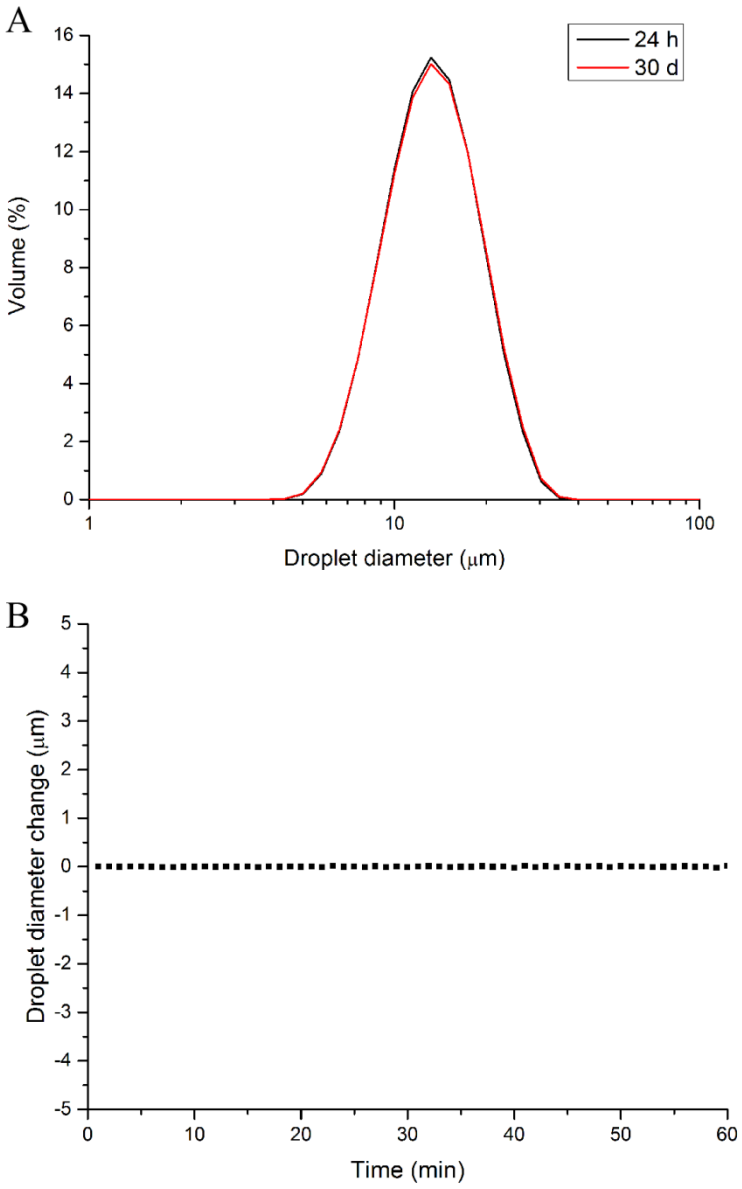


**Figure 2.7.** Laser diffraction chromatograms of (A) droplet size distribution at 24 hours and 30 days at pH 10, and (B) droplet size diameter change over time at pH 10. The laser diffraction chromatograms show no significant change in droplet size or size distribution over time.

### 2.2.4. Fabrication of Calcium Phosphate Capsules

An aliquot of the creamed emulsion was pipetted into a calcium-phosphate solution to initiate the mineralization of CaP at the surface of the oil

droplets. The protocol for the formation of the CaP capsules is illustrated in **Figure 2.8**. The main domain of the BCP, MAA, has a high density of carboxylate groups and they act as nucleating sites for CaP. The carboxylate groups, located at the surface of the droplet, chelate with calcium ions located in the aqueous phase. Phosphate ions condense with the calcium ions *via* electrostatic interaction. This increases the ionic concentration above the critical saturation point and triggers the nucleation and growth of CaP minerals.

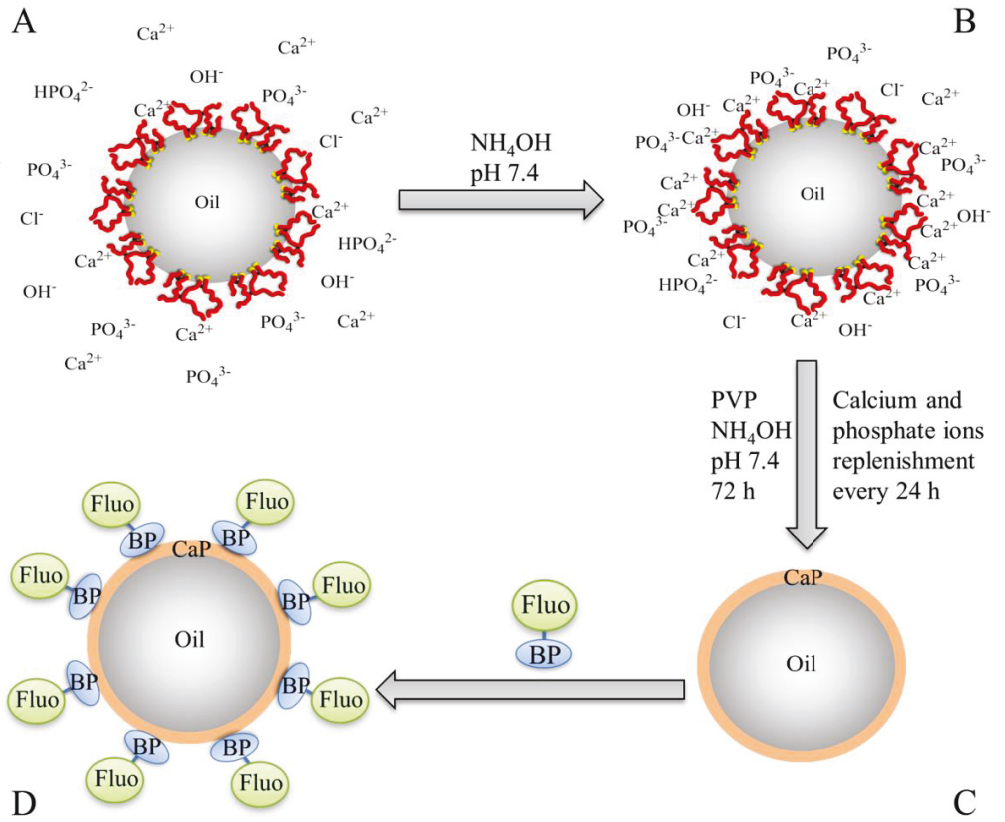


**Figure 2.8.** Schematic representation of the production of CaP capsule and the surface sorption of fluorescein−bisphosphonate conjugate on the surface of the CaP shell. (A) Oil-in-water emulsion droplet stabilized with branched copolymer (BCP) in a slightly acidic calcium-phosphate solution (BCP: red = methacrylic acid (MAA) domain, and yellow = hydrophobic dodecanethiol chain ends). The MAA domain of the BCP is located at the interface of the droplet and acts as a nucleating site for calcium phosphate (CaP) deposition. (B) The pH of the calcium-phosphate solution is raised to pH 7.4 with $NH_4OH$ to increase the number of nucleation sites for CaP, and to initiate CaP formation at the surface of the emulsion droplet. (C) The calcium phosphate solution is replenished twice (every 24 h) either by solvent replacement or addition of extra calcium and phosphate ions. The solution pH was maintained at pH 7.4 with the addition of $NH_4OH$, and poly(vinyl pyrrolidone) (PVP) was added to the water phase to reduce the aggregation of the droplets. (D) Fluorescein−bisphosphonate conjugate (Fluo−BP) is added to the CaP capsule and attaches itself to the CaP shell to yield a fluorescent capsule.

The calcium-phosphate solution has an initial pH of around 6.40. At this pH, the emulsion droplets have a calculated percentage of 37 % carboxylate anion nucleation sites at their interface for CaP. Note that for this calculation the input value for the p$K_a$ of the BCP was determined to be 6.63 (**Figure 2.5**). The pH was raised to pH 7.4 to increase the available nucleation sites from 37 % to 86 %. The reason why the pH was capped at 7.4, and not raised further to fully deprotonate all MAA sites, was to prevent the formation of CaP particles in the water phase as a competing event, and hence to allow for a 100 % CaP deposition efficiency onto the surface of the droplets. No mineralization of CaP at the surface of the emulsion droplets was noticed after 24 hours of incubation in the calcium-phosphate solution. After 48 hours of incubation, the formations of small clusters of CaP were observed at the surface of the emulsion droplets. These droplets flattened when they were dried for imaging by SEM because they possess low structural stability. Unwanted aggregation of the oil droplets was noticed after 48 hours of incubation. This is due to the compression of the electric double layer and a potential reduction in surface charge density by the chelating action of the carboxylate groups with calcium ions. Poly(vinyl pyrrolidone) (PVP, 5 wt%), a water soluble non-ionic polymer, was added into the calcium-phosphate solution to reduce the extent of this aggregation process after the initial 24 hours of incubation. In addition, PVP aids the formation of CaP at the interface of the droplets and hence, reduce the incubation period.[71] After incubating for a total period of 2 days, another aliquot of calcium and phosphate ions were added. At 60 hours of incubation period, the individual clusters of CaP, which were observed after 48 hours, had started to merge and cover the entire surface of the droplet to form a thin CaP shell. At this instance, these CaP capsules were still flexible and buckled upon drying (**Figure 2.9C**). After 72 hours of incubation, the CaP shell had grown thick, strong and rigid, providing structural stability for the CaP capsules (**Figure 2.9D** and **Figure 2.9E**). The CaP capsules have a rough surface morphology, which is depicted in **Figure 2.9F**. The CaP capsules were annealed at 600 $^{o}$C, in order to increase crystallinity of the CaP and at the same time burn off the polymer. The resulting microcapsules can be observed in **Figure 2.9G**. Most of the capsules

remained intact, especially the ones with smaller sizes, which is logical because of the correlation between wall thickness and curvature. The annealing process changed the surface morphology of the CaP shell considerably, with more pronounced morphology in comparison to the un-annealed CaP capsules (**Figure 2.9H**). This due the fact that HA crystals grow together to form a rod-like and open structure upon exposure to high temperature, which in turn changes the permeability properties of the shell. A cross-sectional view of the CaP capsule revealed a shell thickness of approximately 400 nm (**Figure 2.9I and Figure 2.9J**).

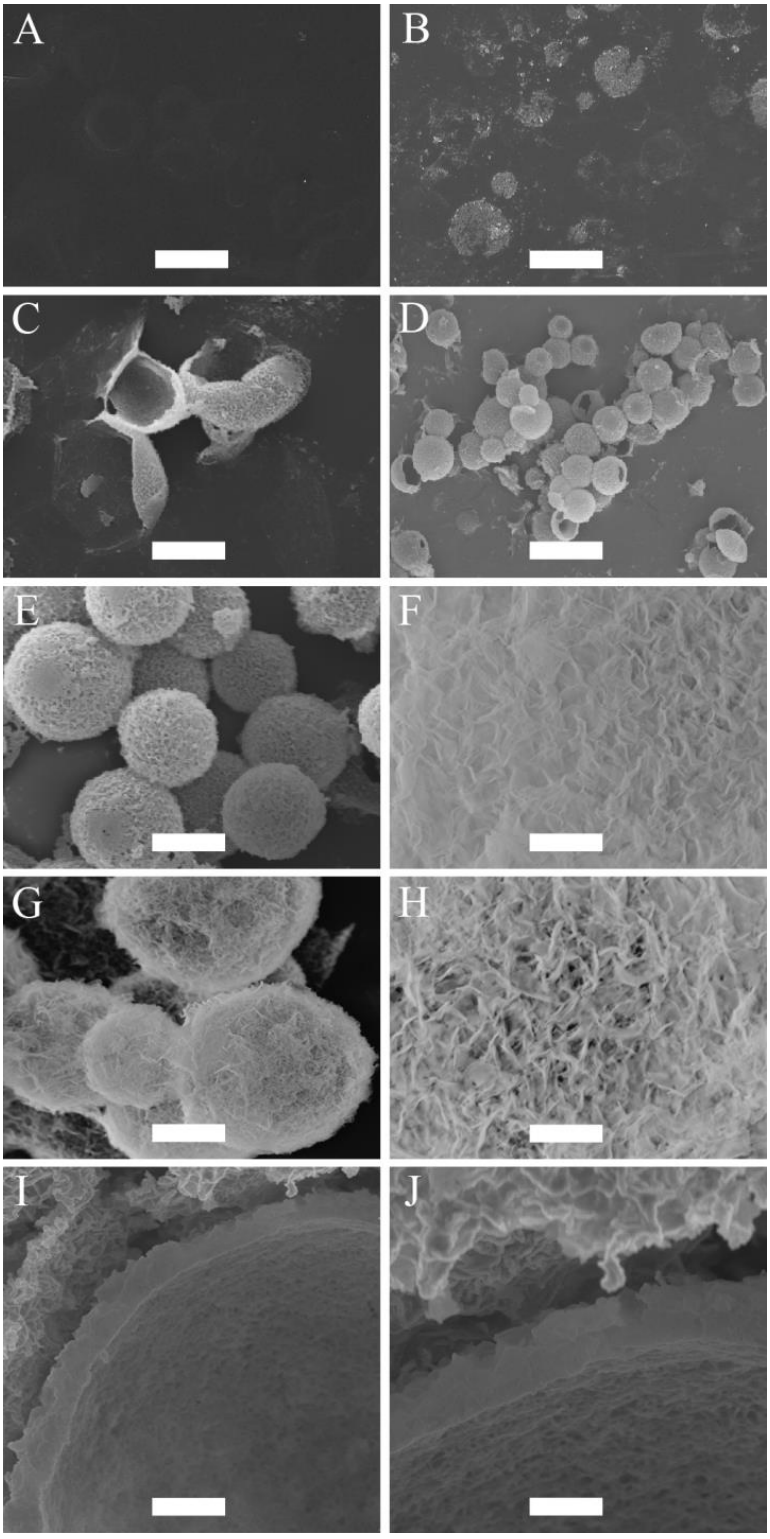


**Figure 2.9.** SEM micrographs illustrating the mineralization of CaP at the surface of oil droplets stabilized with BCP. (A) Incubation periods of 0 hours (scale bar = 37 µm), (B) 48 hours (scale bar = 16 µm), (C) 60 hours (scale bar = 7 µm), (D and E) 72 hours (scale bars = 23 µm and 7 µm, respectively), (F) surface morphology of CaP capsule (scale bar = 704 nm), (G) CaP capsules annealed at 600 $^{o}$C (scale bar = 2 µm), (H) surface morphology of CaP capsule after annealing at 600 $^{o}$C (scale bar = 648 nm), and (I and J) shell thickness of the CaP capsules before annealing (scale bars = 1 µm and 540 nm, respectively).

### 2.2.5. Characterization of the Calcium Phosphate Shell

The Fourier transform infrared (FTIR) spectra of the CaP capsules and the CaP capsules annealed at 1000 °C are shown in **Figure 2.10**. The reason for this annealing at a more elevated temperature was to confirm the potential incorporation of carbonate species within the CaP matrix. We first look at the spectrum of the CaP capsules before annealing. The appearance of various vibration modes of the P−O bond of the phosphate group confirms the existence of CaP in the shell.[72] The characteristics degenerated asymmetric stretching mode ($\nu_3$) (at 1046 $cm^{-1}$), non-generated symmetric stretching mode ($\nu_1$) (at 962 $cm^{-1}$), and degenerated bending mode ($\nu_4$) (at 562 $cm^{-1}$ and 574 $cm^{-1}$) can be found in the spectrum. However, $\nu_3$ and $\nu_4$ are not distinctly split into a triple peak, suggesting the formation of amorphous CaP.

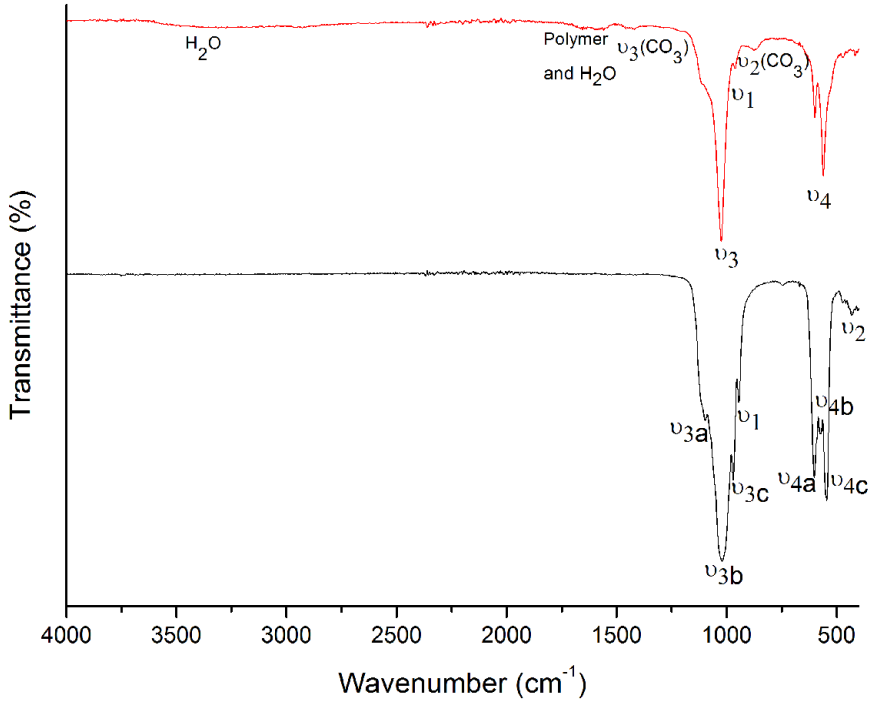


**Figure 2.10.** FTIR spectra of CaP capsules (red line), and CaP capsules annealed at 1000 °C (black line).

The broad band around 3450 $cm^{-1}$ is due to the water molecules adsorbed onto the CaP surface, whereas the other water molecule peak at around 1650 $cm^{-1}$ is overlapped by the BCP or some PVP residue (C=O bond stretch). The hydroxyl group's stretching ($\nu_s$) and librational ($\nu_L$) modes, around 3572 $cm^{-1}$ and 631 $cm^{-1}$, respectively, are not clearly seen in the CaP spectrum. This is maybe due to the

amorphous nature of the CaP or complete substitution of the OH group with $Cl^-$. The small bands at 1410 $cm^{-1}$ and 875 $cm^{-1}$ are due to $\nu_3$ ($CO_3$) and $\nu_2$ ($CO_3$), respectively. This indicates that carbonate species was incorporated into the CaP crystal structure. Carbon dioxide is reversibly soluble in water to form $H_2CO_3$ and the source of the $CO_3^{2-}$ in the mineralization process. The CaP capsules were annealed at 1000 ºC to see whether the degree of crystallinity of the amorphous CaP would increase. The splitting of the vibration bands $\nu_3$ ($\nu_{3a}$ at 1087 $cm^{-1}$, $\nu_{3b}$ at 1046 $cm^{-1}$, and $\nu_{3c}$ at 1032 $cm^{-1}$) and $\nu_4$ ($\nu_{4a}$ at 600 $cm^{-1}$, $\nu_{4b}$ at 574 $cm^{-1}$, and $\nu_{4c}$ at 564 $cm^{-1}$) into distinct triplet peaks suggests the recrystallization and stabilization of the CaP lattice. Also, the characteristic double degenerated bending mode ($\nu_2$) (at 472 $cm^{-1}$) can be clearly seen in the annealed sample. The carbonate peaks are loss when annealed at 1000 ºC because $CO_3^{2-}$ is liberated as $CO_{2(g)}$ from the CaP crystal structure at 550 – 1000 ºC.[73] This is confirmed by the mass loss between 550 − 1000 ºC from the thermogravimetric analysis (TGA) (**Figure 2.11**). On the TGA curve of the CaP capsules, there are three regions of mass losses. The mass loss of 13 % between 30 – 275 ºC is characteristic for the physisorbed water release and evaporation of dodecane residue, 10 % mass loss between 275 − 550 ºC represents the decomposition of BCP and PVP residue. The 2.6 % mass loss in the region from 550 ºC to 1000 ºC is characteristic for the $CO_{2(g)}$ release from the decomposition of carbonates from the CaP structure.

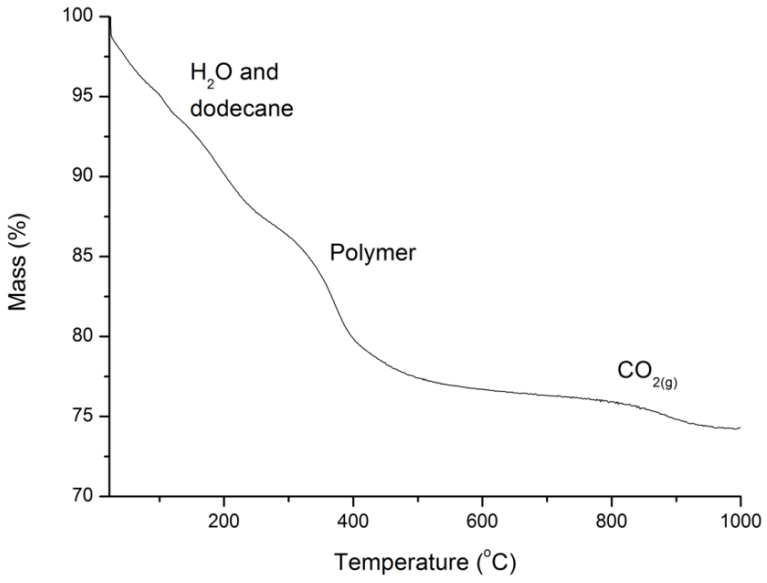


**Figure 2.11**. TGA curve of CaP capsules. The loss of masses of 13 % at 30 – 275 ºC, 10 % at 275 – 550 ºC, and 2.6 % at 550 – 1000 ºC are due to the evaporation of water and dodecane, decomposition of polymers, and the release of carbon dioxide gas, respectively.

The elemental composition of the CaP capsules was studied with an energy dispersive X-ray (EDX) spectrometer (**Figure 2.12**). The EDX spectrum of the CaP capsules comprises of calcium, phosphorous, oxygen peaks, confirming the presence of CaP. Chlorine was also detected suggesting that chlorine was incorporated in the CaP crystal structure, which originated from $CaCl_2$ as a calcium source. The carbon peak originates from the carbon coating of the CaP capsules used for the EDX analysis, and also from the BCP. The calcium-to-phosphorous (Ca/P) atomic ratio of the CaP capsules was established with an inductively coupled plasma-optical emission spectrometry (ICP-OES) to determine the type of CaP mineral phase produced in the mineralization process. The ICP-OES analysis shows the Ca/P atomic ratio is around 1.58 (**Table 2.2**). We can therefore propose that the shell of the CaP capsule is made of calcium deficient hydroxyapatite.[3]

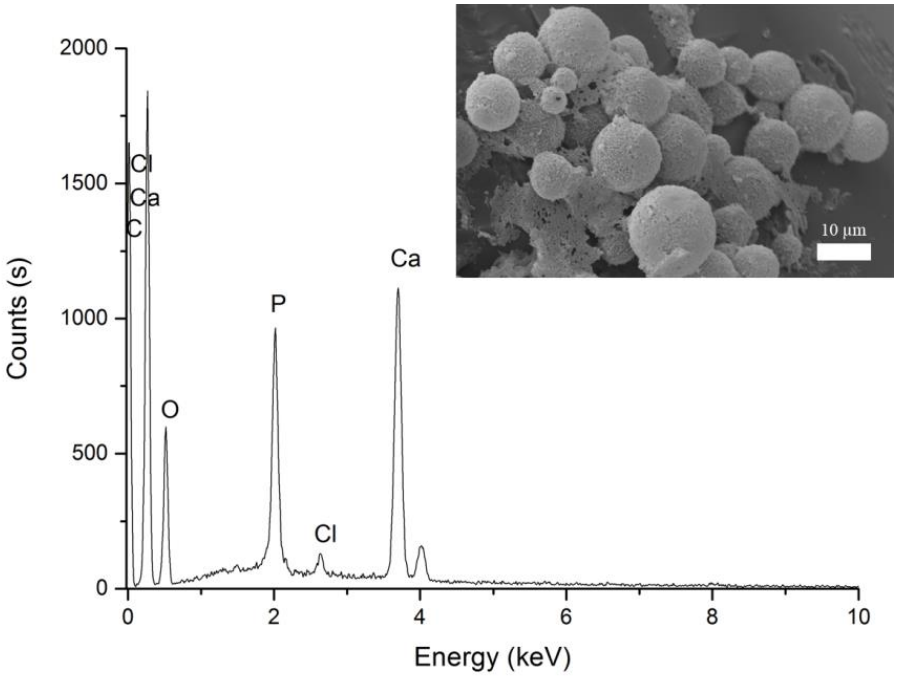


**Figure 2.12.** EDX spectrum and SEM micrograph of CaP capsules.

**Table 2.2.** ICP-OES data for CaP capsules and synthetic hydroxyapatite.

| Sample | *[Ca]* (ppm) | *[P]* (ppm) | Ca/P molar ratio |
|---|---|---|---|
| CaP capsules | 9.028 (±0.026) | 4.417 (±0.030) | 1.58 |
| Synthetic hydroxyapatite | 9.398 (±0.036) | 4.338 (±0.010) | 1.67 |

X-ray diffraction (XRD) patterns of the CaP capsules as synthesized and after annealing at 600 °C are shown in **Figure 2.13** along with an indexed simulated powder pattern of single crystal hydroxyapatite (ICSD number 22059). In both cases, patterns demonstrate very broad peaks indicative of nano-scale crystal sizes. Average size determination using Scherrer analysis was not possible due to the low intensities of the peaks. The CaP capsules sample demonstrates two broad features at around 26 ° and 32.5 ° but their intensities are too low to enable indexing of individual Bragg peak contributions. In the annealed sample features corresponding to peaks from the single crystal pattern with qualitatively correct intensity ratios can be identified suggesting crystallinity is induced by the annealing process, or amorphous material contributing to the total scattering of the sample has been removed.

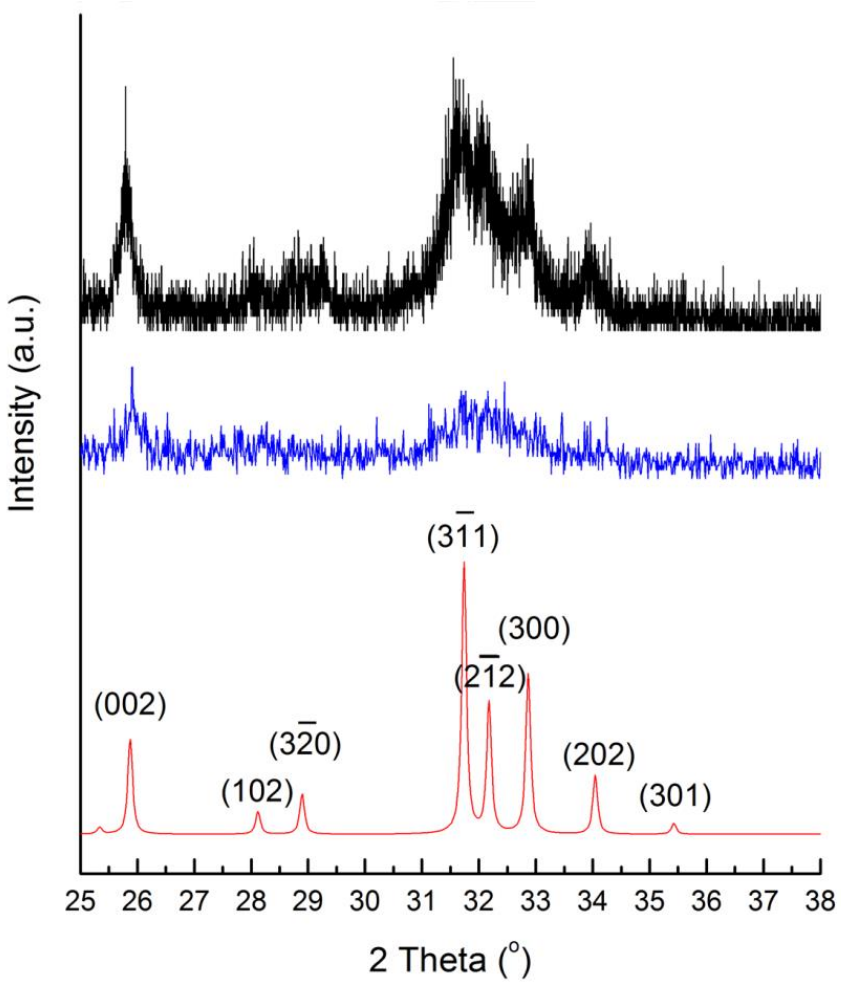


**Figure 2.13.** XRD patterns of CaP capsules as synthesized (blue line), CaP capsules annealed at 600 °C (black line), and simulated powder pattern of single crystal hydroxyapatite (red line).

### 2.2.6. Production of Fluorescent Calcium Phosphate Capsules

Our final task was to modify the CaP capsules with a fluorescent marker. Bisphosphonates (BPs) are stable synthetic analogues of inorganic pyrophosphate characterized by a non-hydrolysable P−C−P structure. BPs have been used to treat and image bone disorders, such as osteoporosis, because BPs present high affinity to adsorb onto bone mineral, and therefore prevent mineral dissolution and bone resorption, and inhibiting osteoclast activity.[74] BP was chosen as the base material to decorate the CaP capsules because the phosphonate groups have a high affinity to CaP. In addition, BPs can be modified with additional substituents adjacent to the central carbon atom to introduce a desired functionality.[74] De Rosales *et al*. have recently used this strategy to introduce metallic radionuclides and fluorophores to BPs for positron emission tomography/single photon emission computed tomography- nuclear imaging and fluorescence detection of calcium phosphate and iron oxide nanomaterials in *vivo*/*vitro*.[75–77] We now demonstrate that fluorescein−bisphosphonate conjugate (Fluo−BP) (**Figure 2.14A**) can be attached to the CaP capsule walls in order to produce fluorescent CaP capsules (**Figure 2.8D**).[77] The fluorescence properties arise from the fluorescein group, and the adsorption mode of Fluo−BP on to the CaP shell is due to the coordinate covalent interaction between the phosphonate groups in the BP and the calcium atoms in the CaP. The Fluo−BP labeled CaP capsules were imaged with confocal microscopy (**Figure 2.14B**). As a control experiment Fluo−BP was added to the dodecane droplets stabilized with BCP. No adhesion of the Fluo−BP was observed onto the surface of the emulsion droplets, which confirmed the affinity of the fluorescent labeling agent for the CaP (**Figure 2.14C**).

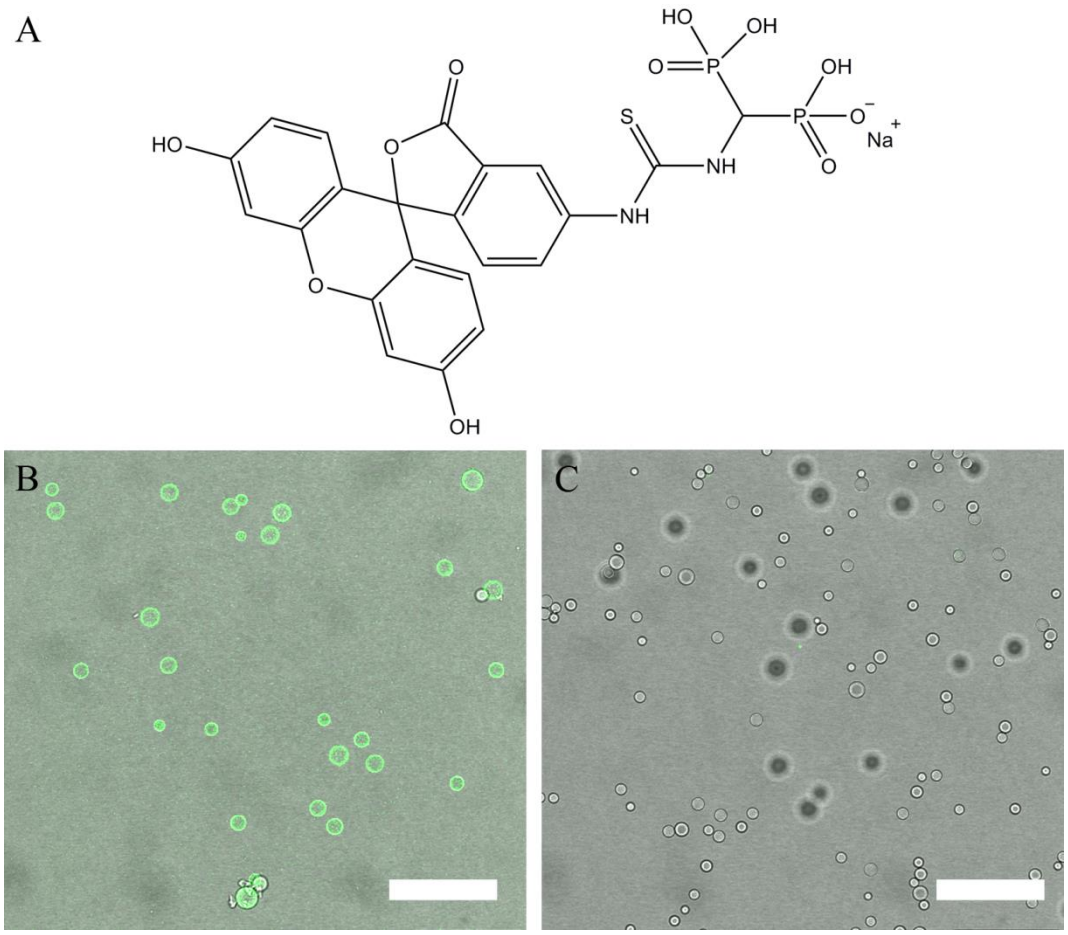


**Figure 2.14.** (A) Chemical structure of Fluo−BP. Overlay confocal micrographs of CaP capsules with Fluo−BP (B), and dodecane droplets stabilized with BCP with Fluo−BP (C). Scale bars represent 50 μm.

## 2.3. Conclusions

We have demonstrated an effective and efficient synthesis method to produce CaP microcapsules by templating oil-in-water emulsion droplets stabilized with synthetic BCP. The process is simple, requires mild conditions, high yielding, low cost, and requires short incubation time (72 hours) compared to previous work by Böker and co-workers.[65–67] The BCP provided the right architecture and functionalities to produce stable emulsion droplets, and allows the mineralization of CaP mineral at the surface of the droplet. The CaP wall was established to be calcium deficient hydroxyapatite with chlorine and carbonate species. The oil phase of the CaP capsules can act as a compartment for hydrophobic materials and can be release on demand with crushing, sonication or acidification. We successfully attached a BP conjugate containing a fluorescein fluorophore on the CaP capsules to yield fluorescent capsules. The BP moiety allows for variation in chemical structure opening up the potential to provide a specific functional group as part of the capsule wall. Interestingly the BP molecules can be recovered through capsule wall dissolution upon acidification, potentially of use for diagnostics. We foresee that the ease and versatility of our method to manufacture CaP capsules will lead to exploration of CaP capsules in a wide variety of applications, such as delivery system, micro reactors, imaging, catalysis, bioactive composites and cosmetics.

## 2.4. Experimental

### 2.4.1. Materials

Methacrylic acid (MAA, 99 %, Sigma-Aldrich), ethylene glycol dimethacrylate (EGDMA, 98%, Sigma-Aldrich), 1−dodecanethiol (DDT, ≥99 %, Sigma-Aldrich), (trimethylsilyl)diazomethane (2 M in hexanes, Sigma-Aldrich), dodecane (≥99 %, Sigma-Aldrich), calcium chloride dihydrate (Analar Normapur), ammonium dihydrogen phosphate (+99 %, Across Organics), synthetic hydroxyapatite (≥99.99 %, Sigma-Aldrich), poly(vinyl pyrrolidone) (PVP, $M_w$ = 360,000 g·mol$^{-1}$, Fluka Analytical), hydrochloric acid (37 %, Analar Normapur), sodium hydroxide pellets (Fisher chemical), ammonium hydroxide (35 %, Fisher chemical) and distilled water (Milli-Q). 2,2'−Azobis(isobutyronitrile) (AIBN) was purchased from BDH and recrystallized from methanol prior to use. Deuterated chloroform and methanol were purchased from Sigma Aldrich. All organic solvents were standard laboratory grade. Fluorescein−bisphosphonate conjugate (Fluo−BP) was synthesized according to Kapustin *et al*.[77]

### 2.4.2. Synthesis of Branched Copolymer

BCP was synthesized *via* thiol-regulated free radical polymerization.[68] A 250 mL round bottom flask was charged with MAA (10 g, 116.2 mmol), EGDMA (2.303 g, 11.6 mmol), DDT (2.351 g, 11.6 mmol) and ethanol (147 mL). The reaction mixture was degassed with nitrogen gas for 20 minutes, and subsequently immersed into a preheated oil bath at 70 ºC. The polymerization was initiated by addition of AIBN (0.147 g, 0.89 mmol) and was left stirring for 48 hours. The reaction mixture was concentrated under vacuum and the polymer was purified by precipitation in cold diethyl ether (-20 ºC). The polymer was left to dry under vacuum overnight.

The BCP was esterified and the $^1$H NMR spectrum of the esterified-BCP was used to determine the relative molar ratios of the co-monomers and chain transfer agent in BCP. BCP was esterified by firstly dissolving the BCP (50 mg) in methanol (0.2 mL). Toluene (0.2 mL) was added and agitated to obtain a homogeneous solution. (Trimethylsilyl)diazomethane (0.2 µL) was then added drop wise until a yellow color appeared and did not become colorless upon agitation. The resulting

solution was purified *via* evaporation, and left to dry in the vacuum oven overnight at 60 °C.

### 2.4.3. Characterization of Branched Copolymer

$^1$H NMR spectra of the polymers were recorded on 1 wt% branched copolymer solutions in deuterated solvents using Bruker Specrospin 400 UltrashieldTM operating at 400 MHz. Molar mass, molar mass distribution ($Đ$), and Mark-Houwink ($\alpha_\eta$) values were measured by TD-GPC using an Agilent 390-MDS Multi Detector Suite equipped with refractive index, viscometer, and UV detectors. A mobile phase of DMF with 5 mM $NH_3BF_4$ was employed with a flow rate of 1 mL·min$^{-1}$. Two PL gel Mixed-D columns and an additional guard column were used with an oven temperature of 50 °C. Specific calibration was carried out using poly(methyl methacrylate) standards.

### 2.4.4. Potentiometric Titration of Branched Copolymer

A potentiometric titration curve of BCP was generated by dissolving BCP (0.1 wt%) in a basic solution (pH ~ 11.8, adjusted with 0.5 M NaOH) to ensure complete dissolution of BCP. Changes in pH values were monitored (with an Oakton pH meter) following incremental additions of HCl (0.1 M) to the basic BCP solution. The α of BCP with pH was calculated using the Henderson-Hasselbalch equation.[79]

### 2.4.5. Emulsion Preparation and Characterization

An aqueous solution containing 3 wt% of BCP was prepared and the pH was adjusted to 10 (1 M $NH_4OH$ solution). An equal amount of dodecane was added and this biphasic mixture was homogenized at 24 000 rpm for a minute to produce an oil-in-water emulsion. The emulsion was left for 24 hours to equilibrate and the resulting emulsion formed a creamed layer (localized oil volume fraction, $\phi_{oil} = 0.64$). The size, span and stability of the emulsion were recoded using laser diffraction (Mastersizer 2000 equipped with a Hydro 2000S dispersion unit). 10 µL of creamed emulsion was added to the dispersion unit containing 100 mL of basic water (pH adjusted to 10 with 1 M $NH_4OH$ solution) with a stirring rate of 1000 rpm. The volume average droplet diameters ($D_{4/3}$) mentioned were obtained from at least 5 repeat runs ($D_{4/3} = \sum D_{i4}N_i/\sum D_{i3}N_i$). The span is a measure

of the distribution of the droplet size distribution and is expressed mathematically as (D(0.9)-D(0.1))/D(0.5), where D(0.9) is the diameter under which 90 % of the particles fall, D(0.5) is the diameter under which 50 % of the particles fall, and D(0.1) is the diameter under which 10 % of the particles fall. Light micrographs were taken using a Leica DM 2500M microscope equipped with a Nikon D5·100 digital camera.

### 2.4.6. Fabrication of Calcium Phosphate Capsules

To a slightly acidic solution containing calcium and phosphate ions (pH ~ 6.4, [calcium] = 2.5 mM, and [phosphate] = 1 mM), creamed emulsion (0.1 v/v%) was added and dispersed into the solution. The pH was adjusted to 7.4 with the addition of $NH_4OH$. After 24 hours, the old calcium-phosphate solution was renewed with a fresh calcium-phosphate solution containing PVP (pH ~ 7.4, [calcium] = 2.5 mM, [phosphate] = 1 mM, and 10 wt% PVP), and emulsion droplets were left to incubate with gentle stirring. At 48 hours, calcium-phosphate solution (100 vt% (with respect to the solution volume at 24 hours), pH ~ 6.7, [calcium] = 5 mM, and [phosphate] = 2 mM) was added to the mineralization solution at 5 $mL \cdot h^{-1}$. The pH was adjusted to pH 7.4 and left to incubate for another 24 hours. The pH of the solution was maintained at pH 7.4 throughout the mineralization process. Prior to characterization, CaP capsules were washed three times by centrifugation with distilled water to remove the PVP. Samples were dried under vacuum at 60 $^oC$ overnight.

### 2.4.7. Characterization of Calcium Phosphate Capsules

#### *2.4.7.1. SEM-EDX*

All scanning electron microscope (SEM) micrographs of the CaP capsules were obtained with a Zeiss Supra 55VP SEM with associated energy-dispersive X-ray spectroscopy (EDX). CaP capsules were gently washed twice by centrifugation with distilled water to remove the PVP, and left to dry on silicon wafer. Samples were coated with gold for imaging, or coated with carbon for EDX analysis. The imaging and analysis of CaP capsules were performed at 10 kV.

#### *2.4.7.2. FTIR*

Fourier transform infrared spectroscopy (FTIR) spectra were recorded using a Bruker Alpha-P instrument. The annealed CaP capsules sample was heated at 1000 $^{o}$C in air for 10 min with a heating rate of 10 $^{o}C \cdot min^{-1}$. The FTIR spectra of BCP and poly(vinyl pyrrolidone) (PVP) are shown in the Appendix, **Figure 2.15-Appx**.

#### *2.4.7.3. TGA*

Thermogravimetric analysis (TGA) was recorded using a Mettler Toledo TGA/DSC1 STAR$^{e}$ System instrument. The CaP capsules were heated from 30 $^{o}$C to 1000 $^{o}$C at 10 $^{o}C \cdot min^{-1}$ in a flow of dry air at 50 $mL \cdot min^{-1}$. The TG curves of BCP and PVP are shown in the Appendix, **Figure 2.16-Appx**.

#### *2.4.7.4. ICP-OES*

Inductively coupled plasma-optical emission spectrometry (ICP-OES) was used to determine the Ca/P ratio of the CaP capsules. Analysis was carried out with a Perkin Elmer 5300DV CP-OES instrument. Calibration of calcium and phosphorous were prepared from single element ICP standards at the following concentration in 0.3 % nitric acid: 0, 0.1, 0.5, 1.0, 2.5, 5.0 and 10 ppm. Samples were prepared by dissolving the CaP capsules in 0.3 % nitric acid and filtered at 200 µm. The samples were diluted until the calcium and phosphorus concentrations were within the calibration standards. The concentrations of calcium and phosphorus were determined at a wavelength of 317.933 nm and 213.617 nm, respectively. The calibration standards for calcium and phosphorous, are shown in the Appendix, **Figure 2.17-Appx**.

#### *2.4.7.5. XRD*

Powder XRD patterns were obtained using a PANalytical X'Pert Pro MPD diffractometer with monochromatic CuK$\alpha_1$ radiation. The annealed CaP capsules sample was heated at 600 $^{o}$C in air for 1 hour. The XRD patterns of BCP and PVP are shown in the Appendix, **Figure 2.18-Appx**.

#### *2.4.7.6. Production of fluorescent calcium phosphate capsules*

An aqueous solution of fluorescein−bisphosphonate conjugate (Fluo−BP) (200 µm, 0.1 wt%) was added to the CaP capsules solution and left for 1 h in the dark with stirring. CaP capsules were washed twice by centrifugation with distilled water to remove excess Fluo−BP. Confocal imaging was performed on a Zeiss SM 510 confocal microscope. A laser with a wavelength of 490 nm was used to excite Fluo−BP labeled CaP capsules.

## 2.6. Appendix

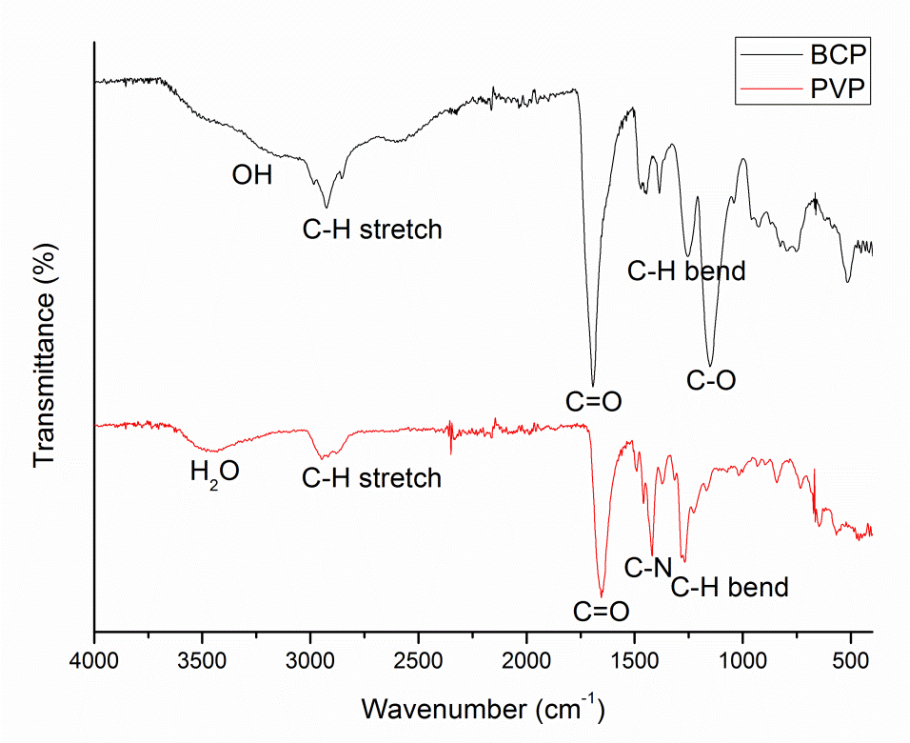


**Figure 2.15-Appx.** FTIR spectra of BCP and PVP.

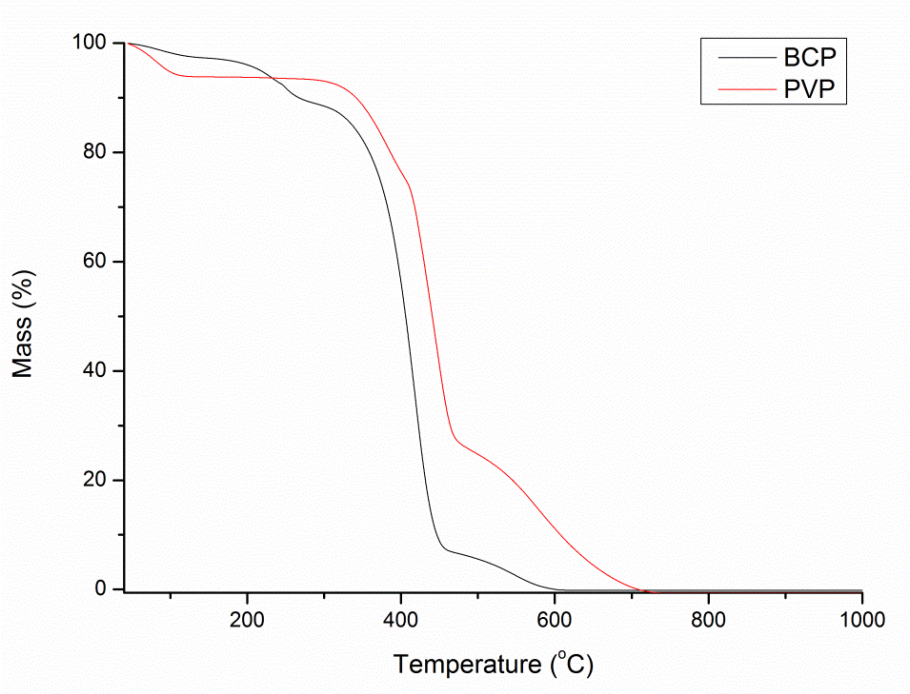


**Figure 2.16-Appx.** TG curves of BCP and PVP.

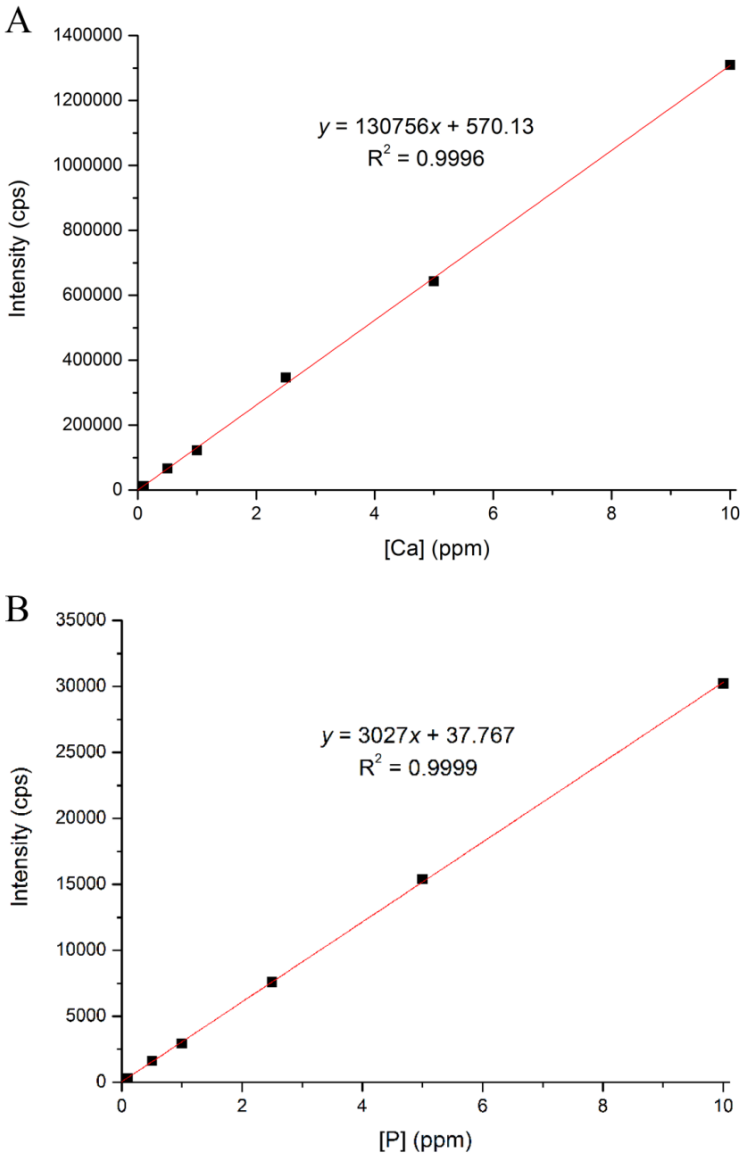


**Figure 2.17-Appx.** Calibration standards for (A) calcium and (B) phosphorous.

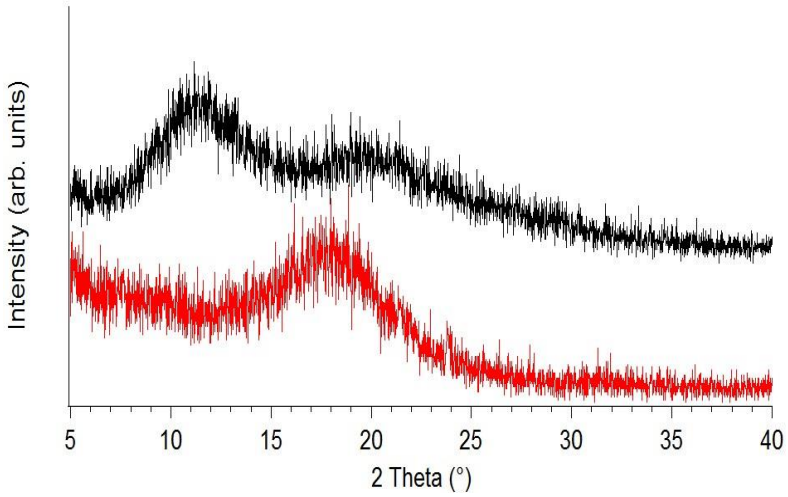


**Figure 2.18-Appx.** XRD patterns of PVP (black line), and BCP (red line).

## 2.5. References


1 A. K. Nair, A. Gautieri, S.-W. Chang and M. J. Buehler, *Nat. Commun.*, 2013, **4**, 1724.

2 K. A. Hing, *Phil. Trans. Soc. A*, 2004, **362**, 2821.

3 S. V. Dorozhkin, *Acta Biomater.*, 2010, **6**, 715.

4 M. Vallet-Regi, *Prog. Solid State Chem.*, 2004, **32**, 1.

5 S. V. Dorozhkin, *Materials*, 2009, **2**, 1975.

6 S. P. Nukavarapu, S. G. Kumbar, J. L. Brown, N. R. Krogman, A. L. Weikel, M. D. Hindenlang, L. S. Nair, H. R. Allcock and C. T. Laurencin, *Biomacromolecules*, 2008, **9**, 1818.

7 L. Xia, K. Lin, X. Jiang, Y. Xu, M. Zhang, J. Chang and Z. Zhang, *J. Mater. Chem. B*, 2013, **1**, 5403.

8 Y. Hu, H. Gao, Z. Du, Y. Liu, Y. Yang and C. Wang, *J. Mater. Chem. B*, 2015, **3**, 3848.

9 Y. Fan, K. Duan, and R. Wang, *Biomaterials,* 2005, **26**, 1623.

10 J. Li, Y. Yang and L. Huang, *J. Control. Release*, 2012, **158**, 108.

11 F. Ye, H. Guo, H. Zhang and X. He, *Acta Biomater.*, 2010, **6**, 2212.

12 F. Shao, L. Liu, K. Fan, Y. Cai and J. Yao, *J. Mater. Sci.*, 2011, **47**, 1054.

13 Y.-P. Guo, L.-H. Guo, Y. Yao, C.-Q. Ning and Y.-J. Guo, *Chem. Commun.*, 2011, **47**, 12215.

14 Y.-P. Guo, Y.-B. Yao, Y.-J. Guo and C.-Q. Ning, *Microporous Mesoporous Mater.*, 2012, **155**, 245.

15 E. V Giger, J. Puigmartí-Luis, R. Schlatter, B. Castagner, P. S. Dittrich and J.-C. Leroux, *J. Control. Release,* 2011, **150**, 87.

16 L. Wu, Y. Dou, K. Lin, W. Zhai, W. Cui and J. Chang, *Chem. Commun.*, 2011, **47**, 11674.

17 C. Zhang, C. Li, S. Huang, Z. Hou, Z. Cheng, P. Yang, C. Peng and J. Lin, *Biomaterials*, 2010, **31**, 3374.

18 S. Cazalbou, C. Combes, D. Eichert and C. Rey, *J. Mater. Chem.,* 2004, **14** 2148.

19 A. Lebugle, F. Pellé, C. Charvillat, I. Rousselot and J. Y. Chane-Ching, *Chem. Commun.*, 2006, **6**, 606.

20 S. P. Mondéjar, A. Kovtun and M. Epple, *J. Mater. Chem.*, 2007, **17**, 4153.

21 D. E. Wagner, K. M. Eisenmann, A. L. Nestor-Kalinoski and S. B. Bhaduri, *Acta Biomater.*, 2013, **9**, 8422.

22 A. Doat, F. Pellé, N. Gardant and A. Lebugle, *J. Solid State Chem.*, 2004, **177**, 1179.

23 V. Stanić, D. Janaćković, S. Dimitrijević, S. B. Tanasković, M. Mitrić, M. S. Pavlović, A. Krstić, D. Jovanović and S. Raičević, *Appl. Surf. Sci.*, 2011, **257**, 4510.

24 X. Ge, Y. Leng, C. Bao, S. L. Xu, R. Wang and F. Ren, *J. Biomed. Mater. Res. A*, 2010, **95**, 588.

25 L. Cui, L. Hu, X. Guo, Y. Zhang, Y. Wang, Q. Wei and B. Du, *J. Mol. Liq.*, 2014, **198**, 157.

26. A. Corami, S. Mignardi, and V. Ferrini, *J. Colloid Interface Sci.,* 2008, **317**, 402.

27. A. Corami, S. Mignardi, and V. Ferrini, *J. Hazard. Material.,* 2007, **146**, 164.

28 S. Saber-samandari, S. Saber-samandari, N. Nezafati and K. Yahya, *J. Environ. Manage.,* 2014, **146**, 481.

29 M. Vila, S. Sánchez-Salcedo, M. Cicuéndez, I. Izquierdo-Barba and M. Vallet-Regí, *J. Hazard. Mater.*, 2011, **192**, 71.

30 E. Boanini, M. Gazzano and A. Bigi, *Acta Biomater.*, 2010, **6**, 1882.

31 K. Ohta, H. Monma and S. Takahashi, *J. Biomed. Mater. Res.,* 2001, **55**, 409.

32. R. Freitag and F. Hilbrig, *Biotechnol. J.*, 2012, **7**, 90.

33. C. J. Morrison, P. Gagnon and S. M. Cramer, *Biotechnol. Bioeng.*, 2011, **108**, 813.

34 J. Xu, T. White, P. Li, C. He and Y.-F. Han, *J. Am. Chem. Soc.*, 2010, **132**, 13172.

35 M. Vukomanović, V. Žunič, M. Otoničar, U. Repnik, B. Turk, S. D. Škapin and D. Suvorov, *J. Mater. Chem.*, 2012, **22**, 10571.

36 K. Lin, J. Pan, Y. Chen, R. Cheng and X. Xu, *J. Hazard. Mater.*, 2009, **161**, 231.

37. K. Ganesan, A. Kovtun, S. Neumann, R. Heumann and M. Epple, *J. Mater. Chem.*, 2008, **18**, 3655.

38 M. Epple, K. Ganesan, R. Heumann, J. Klesing, A. Kovtun, S. Neumann and V. Sokolova, *J. Mater. Chem.*, 2010, **20**, 18.

39 E. I. Altinoglu, T. J. Russin, J. M. Kaiser, B. M. Barth, P. C. Eklund, M. Kester and J. H. Adair, *ACS Nano*, 2008, **2**, 2075.

40 J. Liu, F. Liu, K. Gao, J. Wu and D. Xue, *J. Mater. Chem.*, 2009, **19**, 6073.

41 X. W. Lou, L. A. Archer and Z. Yang, *Adv. Mater.*, 2008, **20**, 3987.

42 H. Fu, M. N. Rahaman, R. F. Brown and D. E. Day, *Mater. Sci. Eng. C. Mater. Biol. Appl.*, 2013, **33**, 2245.

43 H. Fu, M. N. Rahaman, D. E. Day and R. F. Brown, *J. Mater. Sci. Mater. Med.*, 2011, **22**, 579.

44 Y. Wang, A. Yao, W. Huang, D. Wang and J. Zhou, *J. Cryst. Growth*, 2011, **327**, 245.

45 Q. Wang, W. Huang, D. Wang, B. W. Darvell, D. E. Day and M. N. Rahaman, *J. Mater. Sci. Mater. Med.*, 2006, **17**, 641.

46 K. Lin, X. Liu, J. Chang and Y. Zhu, *Nanoscale*, 2011, **3**, 3052.

47 Y.-H. Yang, C.-H. Liu, Y.-H. Liang, F.-H. Lin and K. C.-W. Wu, *J. Mater. Chem. B*, 2013, **1**, 2447.

48 M.-Y. Ma, Y.-J. Zhu, L. Li and S.-W. Cao, *J. Mater. Chem.*, 2008, **18**, 2722.

49 A. Ethirajan, U. Ziener and K. Landfester, *Chem. Mater.,* 2009, **21**, 2218.

50 M. Huang and Y. Wang, *J. Mater. Chem.*, 2012, **22**, 626.

51 B. P. Bastakoti, M. Inuoe, S. Yusa, S.-H. Liao, K. C.-W. Wu, K. Nakashima and Y. Yamauchi, *Chem. Commun.*, 2012, **48**, 6532.

52 K. K. Perkin, J. L. Turner, K. L. Wooley and S. Mann, *Nano Lett.*, 2005, **5**, 1457.

53 H. J. Lee and S. C. Lee, *Polym. Bull.*, 2010, **65**, 743.

54 W. Tjandra, P. Ravi, J. Yao and K. C. Tam, *Nanotechnology*, 2006, **17**, 5988.

55 H. T. Schmidt, B. L. Gray, P. A. Wingert and A. E. Ostafin, *Chem. Mater.*, 2004, **16**, 4942.

56 Y. Fukui and K. Fujimoto, *Chem. Mater.*, 2011, **23**, 4701.

57 Q. Xu, Y. Tanaka and J. T. Czernuszka, *Biomaterials*, 2007, **28**, 2687.

58 H. T. Schmidt and A. E. Ostafin, *Adv. Mater.*, 2002, **14**, 532.

59 J. S. Sander and A. R. Studart, *Langmuir*, 2011, **27**, 3301.

60 C. Qi, Y.-J. Zhu, B.-Q. Lu, X.-Y. Zhao, J. Zhao, F. Chen and J. Wu, *Chem. Eur. J.*, 2013, **19**, 5332.

61 C. Qi, Y.-J. Zhu, B.-Q. Lu, X.-Y. Zhao, J. Zhao and F. Chen, *J. Mater. Chem.*, 2012, **22**, 22642.

62 K.-W. Wang, Y.-J. Zhu, F. Chen, G.-F. Cheng and Y.-H. Huang, *Mater. Lett.*, 2011, **65**, 2361.

63 S.-D. Jiang, Q.-Z. Yao, G.-T. Zhou and S.-Q. Fu, *J. Phys. Chem. C*, 2012, **116**, 4484.

64 M.-G. Ma and J.-F. Zhu, *Eur. J. Inorg. Chem.*, 2009, **36**, 5522.

65 G. Jutz and A. Böker, *J. Mater. Chem.*, 2010, **20**, 4299.

66 A. Schulz, B. M. Liebeck, D. John, A. Heiss, T. Subkowski and A. Böker, *J. Mater. Chem.*, 2011, **21**, 9731.

67 A. Schulz, B. Varnholt, B. M. Liebeck, M. J. Richter, K. Kreuels, T. Subkowski and A. Böker, *J. Mater. Chem. B*, 2013, **1**, 1190.

68 R. T. Woodward and J. V. M. Weaver, *Polym. Chem.*, 2011, 2, 403.

69 N. O'Brien, A. McKee, D. C. Sherrington, A. T. Slark and A. Titterton, *Polymer*, 2000, **41**, 6027.

70 P. A. Costello, I. K. Martin, A. T. Slark, D. C. Sherrington and A. Titterton, *Polymer*, 2002, **43**, 245.

71 Y. Zhang and J. Lu, *Cryst. Growth Des.*, 2008, **8**, 2101.

72 S. Koutsopoulos, *J. Biomed. Mater. Res.*, 2002, **31**, 600.

73 S. Liao, F. Watari, M. Uo, S. Ohkawa, K. Tamura, W. Wang and F. Cui, *J. Biomed. Mater. Res. B. Appl. Biomater.*, 2005, **74**, 817.

74 P. Pascaud, F. Errassifi, F. Brouillet, S. Sarda, A. Barroug, A. Legrouri and C. Rey, *J. Mater. Sci. Mater. Med.*, 2014, **25**, 2373.

75 R. Torres Martin de Rosales, R. Tavaré, R. L. Paul, M. Jauregui-Osoro, A. Protti, A. Glaria, G. Varma, I. Szanda and P. J. Blower, *Angew. Chem. Int. Ed. Engl.*, 2011, **50**, 5509.

76 L. Sandiford, A. Phinikaridou, A. Protti, L. K. Meszaros, X. Cui, Y. Yan, G. Frodsham, P. A. Williamson, N. Gaddum, R. M. Botnar, P. J. Blower, M. A. Green and R. T. M. De Rosales, *ACS Nano*, 2013, **7**, 500.

77 R. T. M. De Rosales, R. Tavaré, A. Glaria, G. Varma, A. Protti and P. J. Blower, *Bioconjug. Chem.*, 2011, **22**, 455.

78 A. N. Kapustin, M. L. L. Chatrou, I. Drozdov, Y. Zheng, S. M. Davidson, D. Soong, M. Furmanik, P. Sanchis, R. Torres Martin de Rosales, D. Alvarez-Hernandez, R. Shroff, X. Yin, K. Muller, J. N. Skepper, M. Mayr, C. P. Reutelingsperger, A. Chester, S. Bertazoo, L. J. Schurgers and C. M. Shanahan, *Circ. Res*., 2015, **116**, 1312.

79 H. N. Po and N. M. Senozan, *J. Chem. Educ*., 2001, **78**, 1499.

# Chapter 3

# Assembly of Emulsion Droplets into Fibers by Microfluidic Wet Spinning[§]

In this chapter, we show that individual emulsion droplets which are stabilized by Laponite clay discs functionalized with pH-responsive branched copolymers can be assembled into fibers using a microfluidic wet spinning process. The proton diffusion into the stream of emulsion droplets induces the reversible self-assembly process leading to the formation of a continuous supracolloidal fiber. We believe the process is versatile as we demonstrate by making stripy Janus type fibers (two and three stripes), magnetic fibers, and fibers of controlled length. This new intriguing class of soft matter material has a set of interesting features which we highlight in an application where we employ our supracolloidal emulsion fibers as a tool to in a time-controlled fashion deliver volatile compounds by means of evaporation. The release rates can be tuned as a function of ionic crosslinking degree. Moreover, we show that the dried fibers are low-weight porous materials.

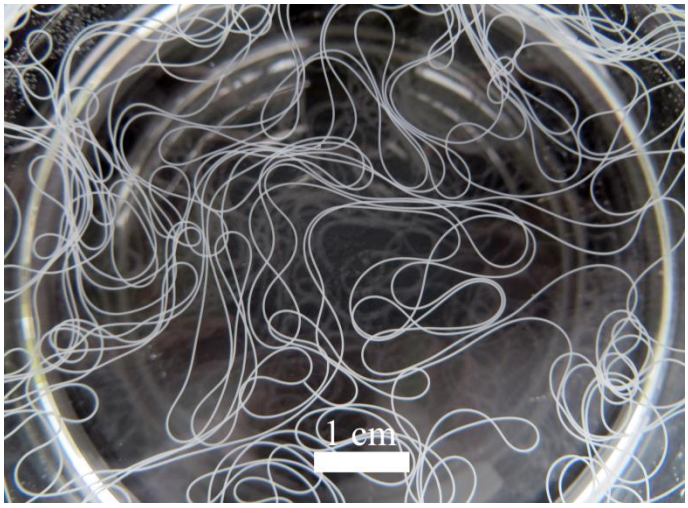


[§]Parts of the chapter were reproduced from R. V. Bell, C. C. Parkins, R. A. Young, C. M. Preuss, M. M. Stevens and S. A. F. Bon, *J. Mater. Chem. A*, 2016, **4**, 813 by permission of The Royal Society of Chemistry (Copyright 2016).

## 3.1. Introduction

Fibers are an intriguing class of materials. They can be fabricated through a spinning process in which a liquid based mixture, referred to as spinning dope, is extruded through an orifice hereby generating a jet, which can subsequently be solidified through either coagulation/precipitation and/or gelation. Nature exploits this technology to produce a plethora of natural fibers. Two extremes being spidersilk,[1] a super strong and extensible liquid-crystalline fiber, and the soft hydrogel double-strings of toad eggs, as spawn by the common toad (*Bufo bufo*). The production of manmade fibers using dry and wet spinning techniques – both starting from a liquid mixture – goes back to the 19$^{th}$ century. An early example is the development of Rayon fibers initiated by the discovery of Schweizer in 1857, who found that cellulose could be dissolved in and re-precipitated from an aqueous solution of ammonia and copper (II) hydroxide (coined Schweizer's reagent (dry or wet)).[2] Examples of wet-spun high performance fibers include ultrahigh molecular weight poly(ethylene) fibers (commercially known as Dyneema),[3] and polyaramid fibers (commercially branded as Kevlar or Ameka/Twaron) are shown in **Figure 3.1**.[4,5] These high performance fibers have been used in aviation and automotive components, protective clothing, vehicle and personal armor in military and law enforcement, nets and ropes for commercial fishing, and renewable energy.[6,7]

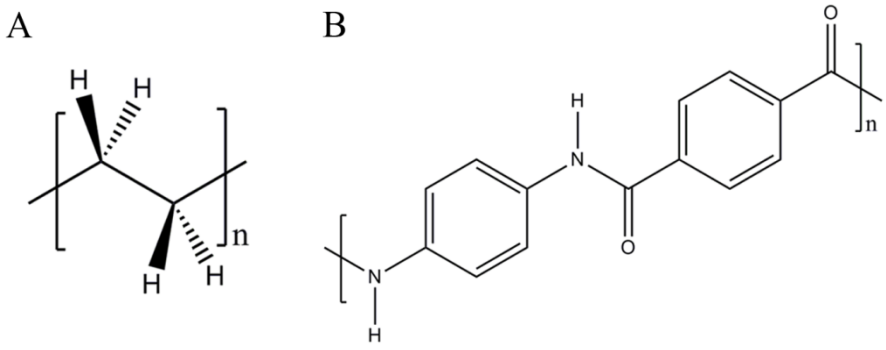


**Figure 3.1.** The chemical structure of high performance fibers ultrahigh molecular weight poly(ethylene) (A), and polyaramid (B). Ultrahigh molecular weight poly(ethylene) is a linear polymer with a molar mass > 3.1 million g·mol$^{-1}$. The wear and impact resistance of the polymer arises from the extremely long molecular chains (formation of multiple van der Waals interactions) and its semi-crystalline solid state conformation. Polyaramid owes its outstanding high strength to numerous inter-chain bonds, such as intermolecular hydrogen bonds between carbonyl and NH groups, and aromatic stacking interactions.[8,9]

An emerging trend is the development of soft, often hydrogel-based, fibers wet spun into water.[10,11] In lab-based environments microfluidics is used as a versatile technology platform to fabricate a wide range of soft matter fibers aiming for applications in tissue engineering, such as the fabrication of micro- and nanoscale scaffolds or cell encapsulation,[12–15] or conductors.[16] The advantage is taken of the fact that microfluidic systems are characterized by the low Reynolds number flow regime, which dictates that all fluid flow in the channels is laminar.[17,18] Application of coaxial flow of fluids in the microchannels, where the inner continuous flow of the fiber precursor solution or dispersion is sheathed by a second liquid phase, allows for easy fiber formation (**Figure 3.2**). The fiber precursor solution undergoes either physical or chemical change, for instance precipitation by solvent exchange,[19] crosslinking with $Ca^{2+}$,[20] or by photopolymerization,[21] to produce a continuous solid fiber. A great variety of microfluidically spun fibers with diverse shapes, dimensions, and encapsulates have been reported, including solid/porous fibers,[19] tubular,[22,21] hybrid fibers,[20,23] Janus fibers,[24] spatially controlled fibers,[25–27] flat fibers with grooves,[28] crimped fibers,[29] and nano fibers.[30]

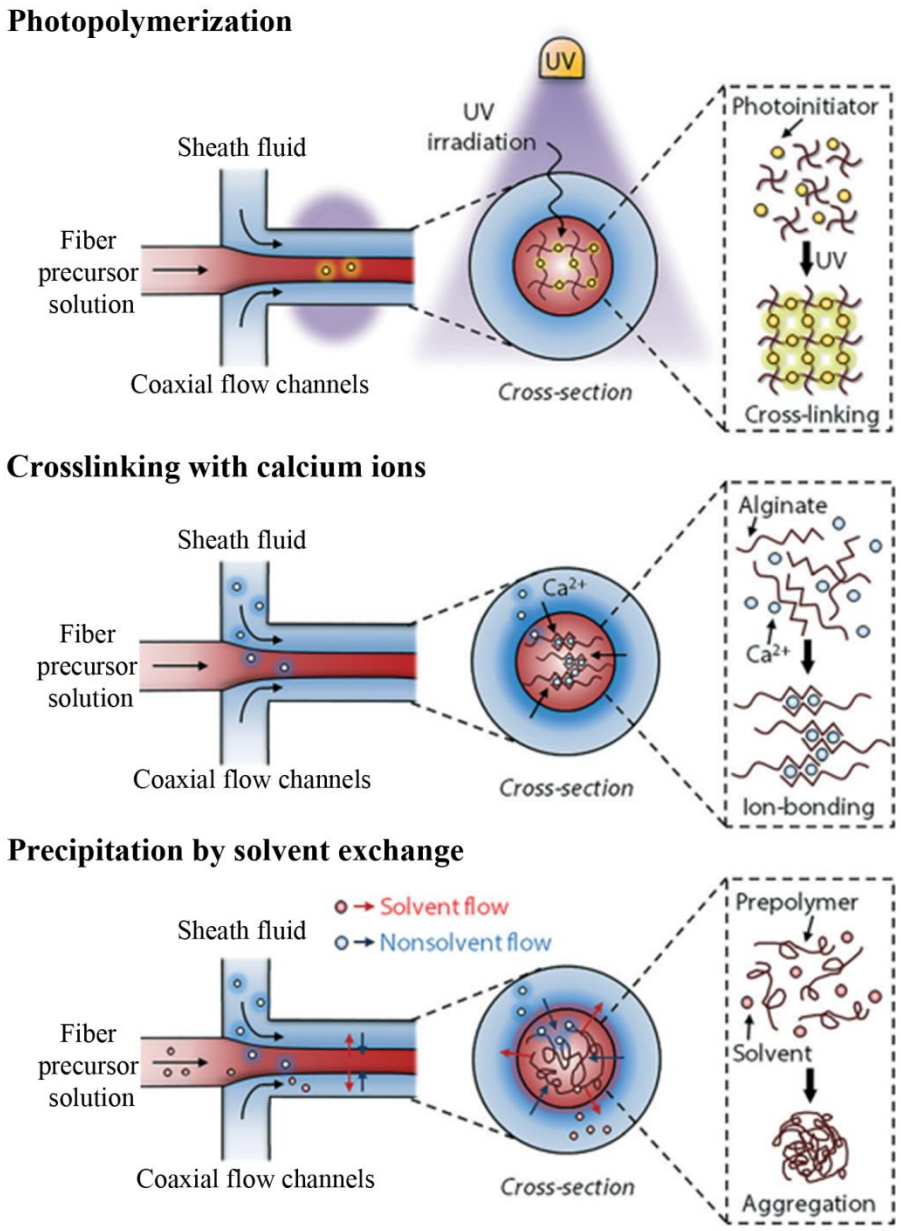


**Figure 3.2.** The general fiber fabrication by microfluidics. A schematic diagram illustrating the coaxial flow channels containing the inner fiber precursor solution sheathed with an outer fluid in a continuous flow. The cross-sections show the principles underlying the fiber formation by various methods.[10] Adapted from Reference 10. Copyright (2014) with permission of The Royal Society of Chemistry.

An example that drew our particular interest was recently reported by Qin and co-workers who combined a droplet microfluidic technique with a wet-spinning process to produce a hybrid calcium alginate microfibers containing spatially arranged single emulsion droplets, which they referred to as biomimetic bamboo-like hybrid microfibers.[20] We asked ourselves whether it would be possible to fabricate fibers which were made through assembly of emulsion droplets, so-

called HIPE (High Internal Phase Emulsion) fibers. We took inspiration from the work of Weaver and co-workers who reported a class of synthetic biphasic soft material called 'Engineered emulsions', where highly stable emulsion droplets are organized into macroscopic supracolloidal structures by shape templating and molding.[31] The emulsion droplets are stabilized with pH-responsive branched copolymers ($PEGMA_5/MAA_{95}$-$EGDMA_{10}$-$DDT_{10}$) to generate highly stable emulsion droplets and to provide surface functionality on the droplets. The assembly process of the emulsion droplets is driven by the controllable formation of multiple hydrogen bonds between the branched copolymers by changing the pH of the solution to acidic conditions (**Figure 3.3**). The macroscopic supracolloidal structures can be reversibly assembled and disassembled owing to the pH-dependence of the non-covalent hydrogen bonding.

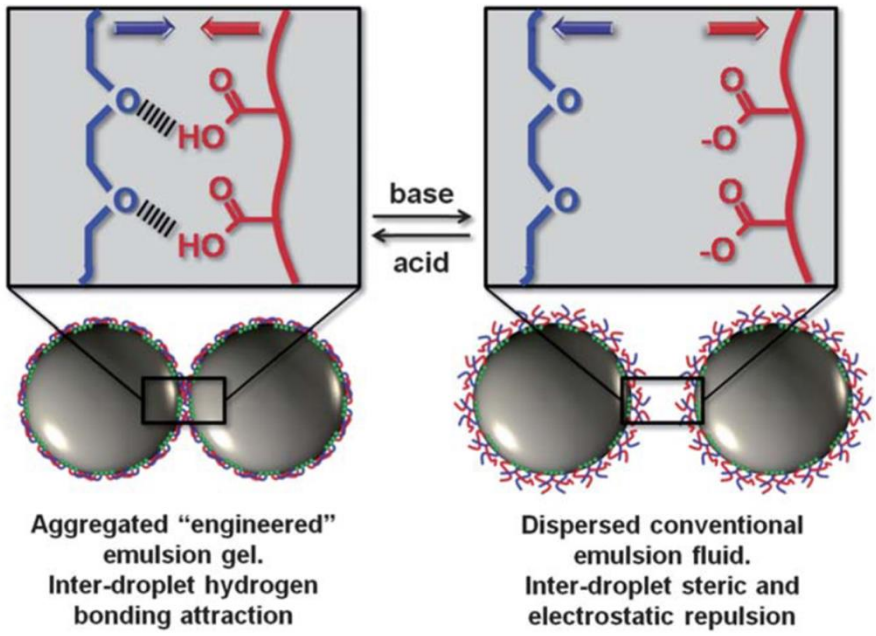


**Figure 3.3.** Schematic representation of the reversible transition from fluid emulsion dispersion to gelled emulsion. The formation of inter-droplet hydrogen bonds between ethylene glycol (blue) and methacrylic acid (red) residues on the emulsion droplet surfaces are dependent on the pH of the aqueous solution.[32] Reproduced from Reference 32. Copyright (2011) with permission of The Royal Society of Chemistry.

Herein we will show the fabrication of fibers from emulsion droplets. We use flow-focusing microfluidic set-up whereby a generated jet of emulsion droplets stabilized by amphiphilic pH-responsive branched copolymers (pH-BCP) and reinforced by Laponite clay discs is exposed to an external surrounding liquid

flow of lower pH. Proton diffusion into the stream of emulsion droplets induces the self-assembly process leading to the formation of a continuous supracolloidal fiber. We demonstrate that the fiber can disintegrate back into individual emulsion droplets upon increase in pH value. We discuss control of fiber composition hereby using two and three combined streams of emulsion droplets to generate Janus fibers, and using ferrofluid to produce magnetic fibers. We show control of fiber length by employing air bubbles as a mean to produce short fibers of discrete length. Looking towards applications, we demonstrate the use of our supracolloidal emulsion droplet fibers as a material to control the delivery of volatile compounds through evaporation, and we show that the dried fibers are a nanocomposite highly porous and light material.

## 3.2. Results and Discussion

### 3.2.1. Synthesis and Characterization of pH-Responsive Branched Copolymer

An amphiphilic pH-responsive branched copolymer based on poly(ethylene glycol) methyl ether methacrylate (PEGMA) and methacrylic acid (MAA) with hydrophobic dodecane functionalized chain ends was synthesized by thiol-regulated free radical polymerization as previously reported by Weaver and co-workers.[31] The chemical structure and the schematic illustration of the pH-BCP architecture are shown in **Figure 3.4A** and **Figure 3.4B**. PEGMA and MAA functionalities were chosen to provide steric and electrostatic stabilization for the emulsion droplets under neutral or basic solution, as well as to provide the ability to form multiple hydrogen bonds between these two domains under acidic conditions, enabling emulsion droplets to assemble. The molar ratio of EG : MAA in the pH-BCP was chosen to equal 1 : 1 as hydrogen bonding between these moieties occurs in 1 : 1 stoichiometry.[32] The chain transfer agent, 1−dodecanethiol (DDT), was particularly selected to provide hydrophobic chain ends in the polymer. The branched architecture of the pH-BCP was generated by the addition of the branching agent, ethylene glycol dimethacrylate (EGDMA). The branched architecture of the polymer ensures multiple potential points of attachment to the surface of an emulsion droplet, compared to its linear analogue, hereby improving adhesion and plausibly enhancing the colloidal stability of the droplet.

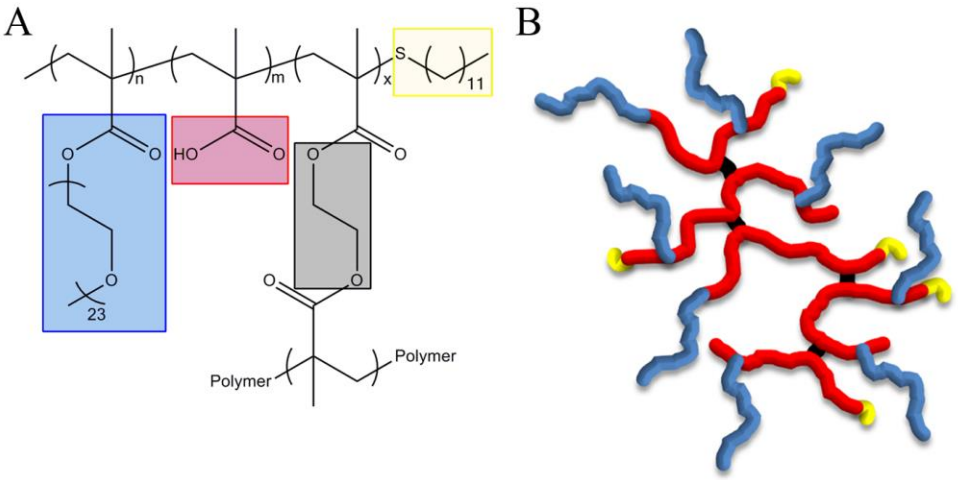


**Figure 3.4.** (A) Chemical structure of the pH-BCP. (B) Schematic illustration of the pH-BCP architecture. The blue color represents PEGMA domain, the red color represents MAA domain, the black color represents the branching unit, EGDMA, and the yellow color represents the hydrophobic chain ends, DDT.

The carboxylic groups of the pH-BCP were esterified to determine the comonomer ratios of the pH-BCP using trimethylsilyl diazomethane. The $^{1}$H NMR of the esterified pH-BCP was used to calculate the relative molar ratios of the co-monomers and chain transfer agent in the pH-BCP with the help of the extra peak arising from the new methyl group on the ester (peak 'k'). The $^{1}$H NMR spectra of the pH-BCP and the esterified pH-BCP are shown in **Figure 3.5A and Figure 3.5B**, respectively. The target and actual compositions of the pH-BCP can be seen in **Table 3.1**.

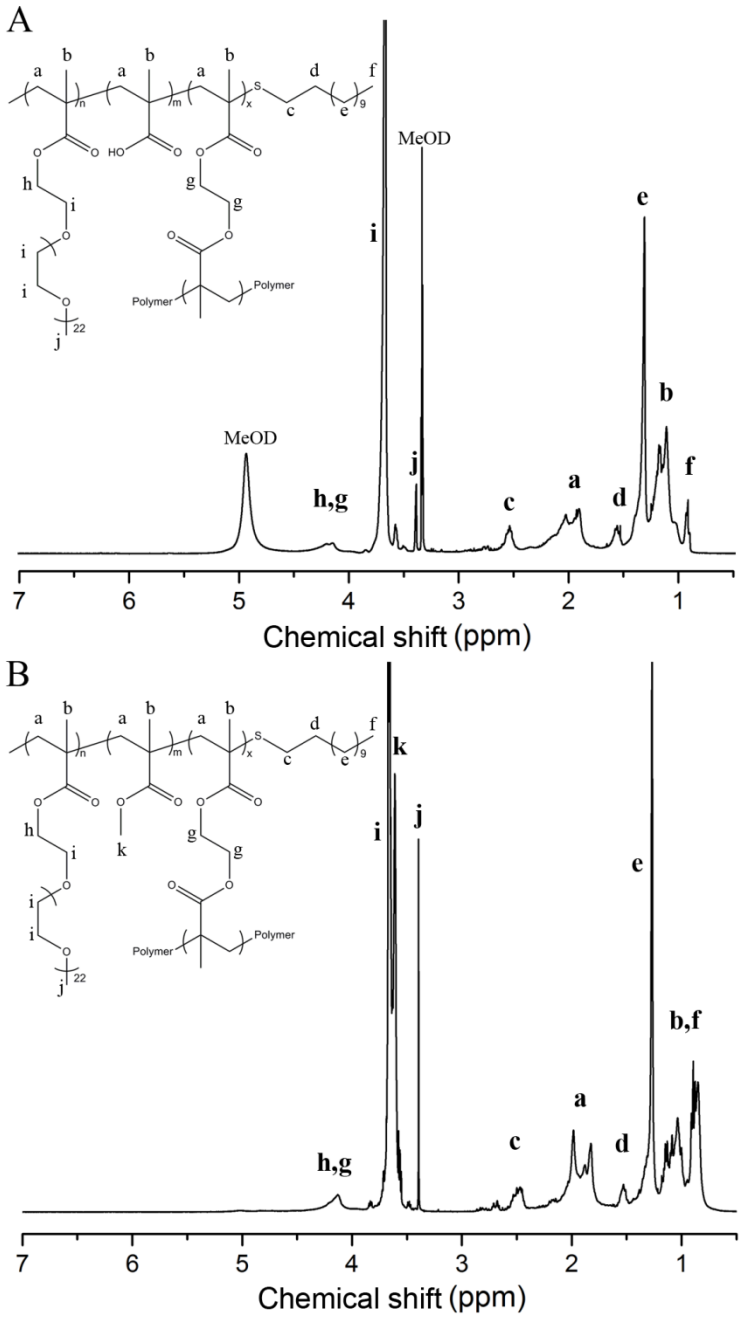


**Figure 3.5.** $^{1}$H NMR spectra of (A) pH-BCP in $CD_3OD$, and (B) esterified pH-BCP in $CDCl_3$. The appearance of peak 'k' (methyl from the ester group) confirms esterification of the pH-BCP.

Triple-detection gel permeation chromatography (TD-GPC) analysis in a DMF eluent was used to analyze the molecular parameters of the pH-BCP. The molecular parameters of the pH-BCP are shown in **Figure 3.6** and **Table 3.1**. The number-average molecular weights ($M_n$) and weight-average molecular weights ($M_w$) values of the pH-BCP were similar with previous studies by Weaver and coworkers.[31] The polydispersity ($Đ$) of the pH-BCP ($Đ = 1.84$) has a broad distribution, which is indicative of a free radical polymerization process. The

Mark-Houwink ($\alpha_\eta$) value of 0.30 represents a relatively compact conformation, which is expected for polymers with branched architecture.[32–34]

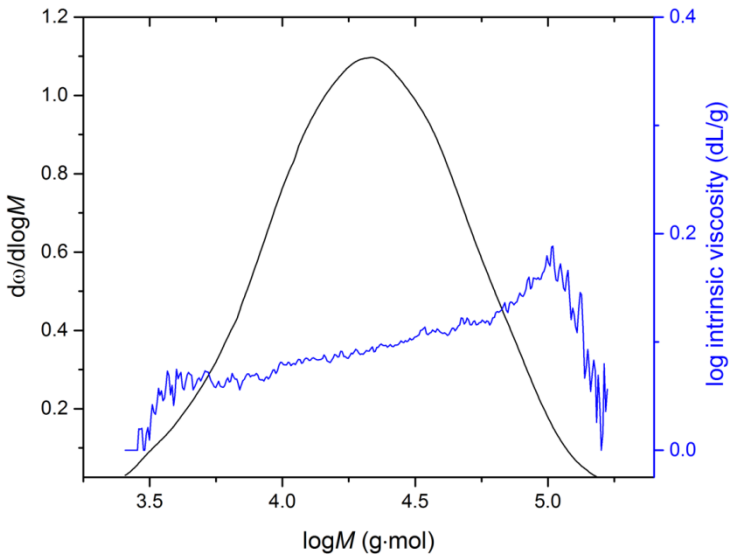


**Figure 3.6.** The TD-GPC chromatograms of the pH-BCP. Molar mass distribution of pH-BCP (black line), and molar mass vs. intrinsic viscosity plot of pH-BCP (blue line).

**Table 3.1.** Composition and molecular parameters of the pH-BCP.

| Target polymer composition[a] | Actual polymer composition[b] | Conversion (%)[c] | $M_n$ (g·mol$^{-1}$)[d] | $M_w$ (g·mol$^{-1}$)[d] | $Đ^d$ | $\alpha_\eta{}^d$ |
|---|---|---|---|---|---|---|
| $PEGMA_5$/ $MAA_{95}$-$EGDMA_{10}$-$DDT_{10}$ | $PEGMA_{4.4}$/ $MAA_{95.6}$-$EGDMA_{7.5}$-$DDT_{10.7}$ | 98 | 15274 | 28163 | 1.84 | 0.30 |

[a] Target molar equivalent based on monofunctional monomer nominally set to 100. [b] Polymer composition was calculated from $^1$H NMR spectrum of the esterified pH-BCP. [c] Polymer conversion was calculated by $^1$H NMR. [d] Measured by triple-detection GPC in DMF eluent.

### 3.2.2. Potentiometric Titration of pH-Responsive Branched Copolymer

The p$K_a$ of the pH-BCP was determined by performing a simple titration on the polymer (**Figure 3.6A**). The pH-BCP buffered the solution in the pH range of 10 – 3.5. The α of the pH-BCP with pH was calculated from the Henderson-Hasselbalch equation.[35] At pH 9.68, all of the carboxylic groups of the pH-BCP are deprotonated. The carboxylic groups of the MAA domain are all protonated at

pH 3.88. The p$K_a$ of the pH-BCP was determined to be 6.46, and at this instance, 50 % of the carboxylic functional groups are protonated (**Figure 3.7B**).

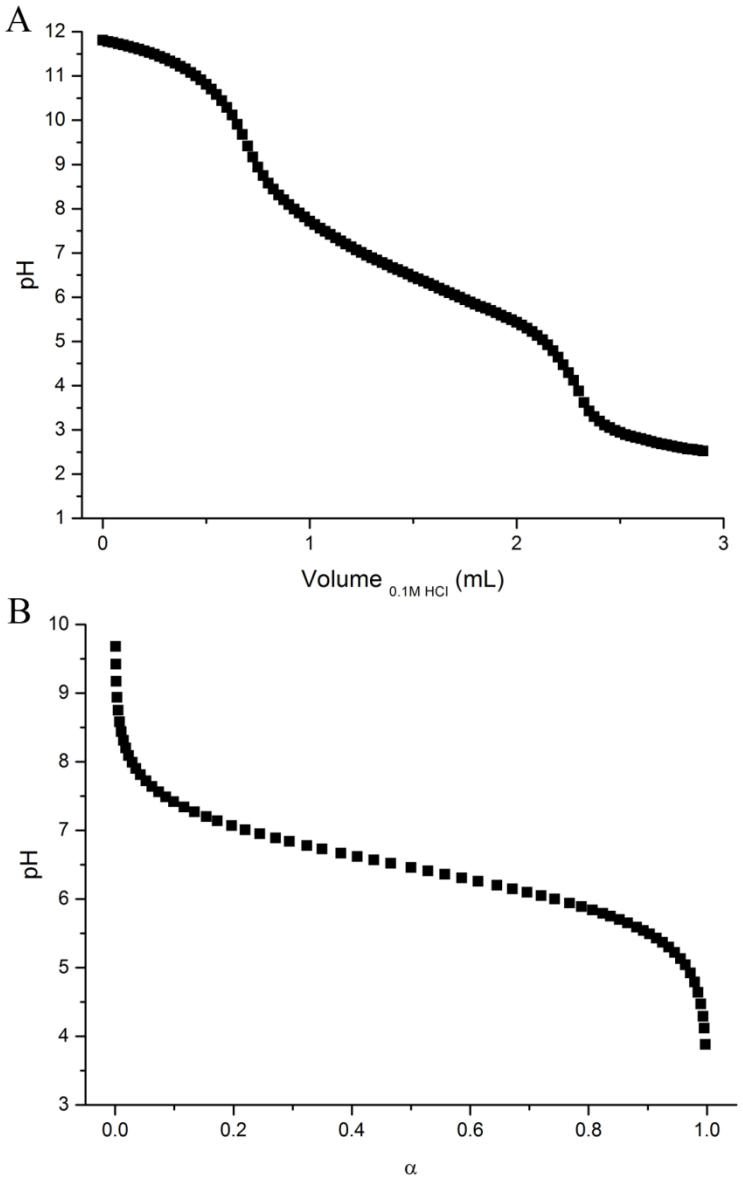


**Figure 3.7.** (A) Acid-base titration curve obtained for pH-BCP, and (B) degree of protonation of pH-BCP with pH. The α of pH-BCP; α = 0 at pH 9.68, α = 0.5 at pH 6.46, and α = 1 at pH 3.88.

### 3.2.3. Preliminary Fiber Fabrication with pH-BCP as Stabilizer for Emulsion Droplets

Initially, we ran a series of fiber fabrications using the pH-BCP as the sole stabilizer for the emulsion droplets, which resulted in very weak and fragmented fibers as shown **Figure 3.8**. Furthermore, fibers were prone to breaking when moved.

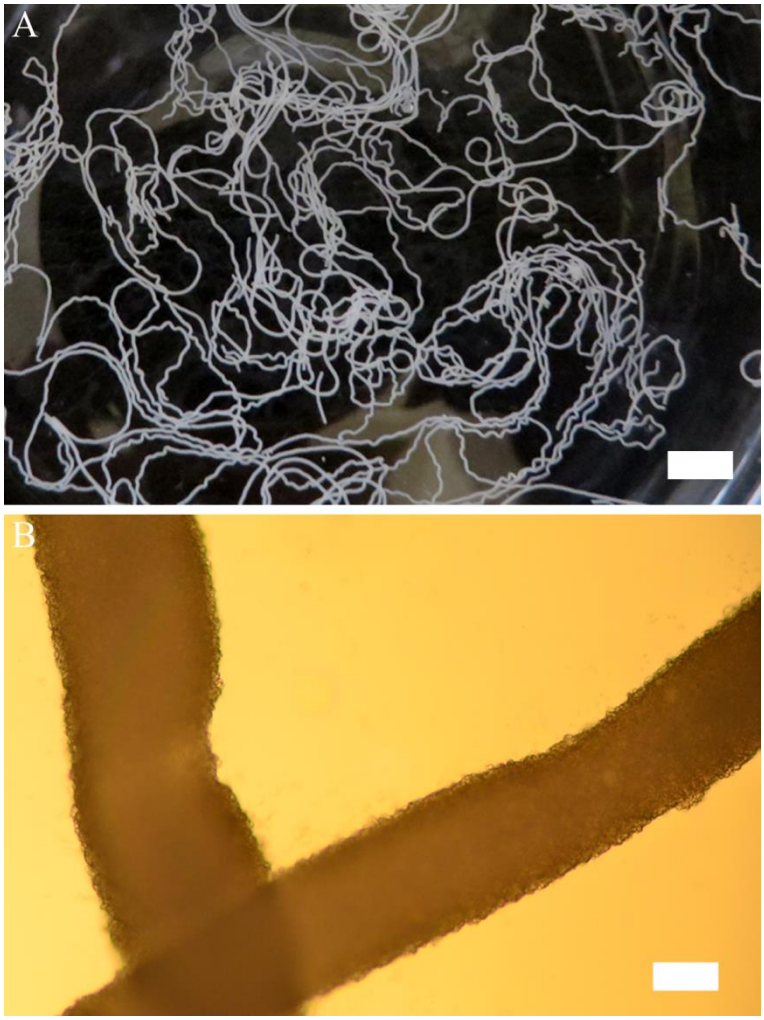


**Figure 3.8.** Photograph (A) and light micrograph (B) of fibers using the pH-BCP as the sole stabilizer for the emulsion droplets. The fibers fabricated were very weak and resulted in fragmentation of fibers. Scale bars represent 0.4 cm and 100 µm, respectively.

To overcome this issue, we employed Laponite clay platelets to reinforce *(i)* the stability of the emulsion droplets rendering the system towards a Pickering stabilization,[36] hereby increasing the adhesion interaction of the now pH-BCP Laponite composite, and *(ii)* the interaction between the individual emulsion droplets, hereby enhancing the mechanical properties of the assembled supracolloidal fiber.

Laponite is commercially available synthetic smectite clay which has a similar structure and composition to the natural clay mineral hectorite.[37] Laponite is a 2:1 phyllosilicate with a unit crystal structure consisting of sheets of octahedrally coordinated magnesium oxide located between two parallel sheets of tetrahedrally coordinated silica (**Figure 3.9A**).[37]

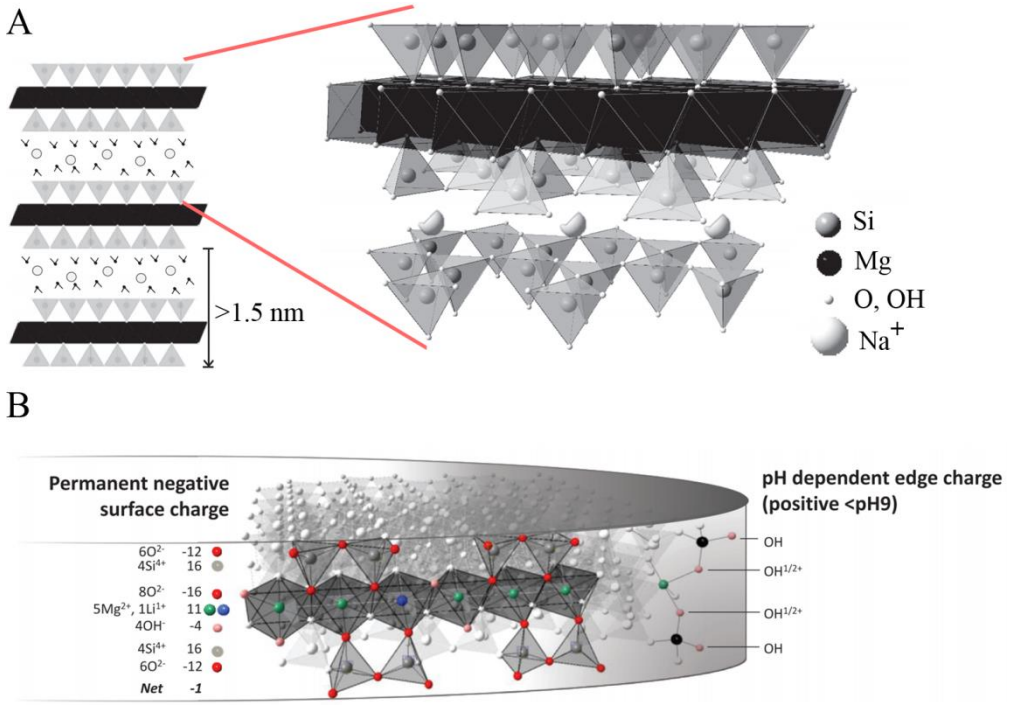


**Figure 3.9.** (A) Smectites crystals (synthetic hectorite Laponite) are constituted of tetrahedrally coordinated silica sandwiching an octahedrally coordinated magnesium oxide located. The charge deficiencies in the layered platelets are balanced by exchangeable cations, which accommodate on or between the faces of the platelets. (B) Single Laponite platelet possesses a permanent negative surface charge due to isomorphic substitution in the crystal structure, and a pH dependent positive rim.[37] Modified and redrawn from Reference 37. Copyright (2013) with permission from John Wiley and Sons.

It has a chemical composition of $Na^{+}_{0.7}$ $[(Si_8Mg_{5.5}Li_{0.3})O_{20}(OH)_4]^{-0.7}$,[38] and can be described as anisotropic platelets with a particle diameter of approximately 25 nm − 30 nm and a thickness of 0.92 nm.[39,40] In its dry state (fine white powder with a density of 2.53 $g \cdot cm^{-3}$), these platelets are arranged into stacks and are held together electrostatically by interlayer cations. The reason for this is that $Mg^{2+}$ in the octahedral sheets can be partially substituted by $Li^{+}$ forming a net negative charge on the faces of the platelets. This negative charge is balanced with cations (predominantly $Na^{+}$, and including as much as 15 % water) that accommodate on or between the faces of the platelets.[41,42] When dispersed in water, the stacks of platelets are completely delaminated to individual charged platelets to form a colloidal dispersion. The release of interlayer $Na^{+}$ leads to a negative charge on the faces of the platelets.[43] The rims of the platelets have oxygen atoms (Si−OH and Mg−OH), which, are pH dependent, may be protonated to form a positive charge (**Figure 3.9B**).[43] The colloidal dispersion is mainly stabilized by

electrostatic repulsion between the negative charged faces (face-face) or the positive rims (rim-rim).

### 3.2.4. Functionalization of Laponite with pH-Responsive Branched Copolymer

To produce the pH-BCP Laponite Pickering composite, the clay discs was hydrated with water to form an aqueous dispersion. A physical transition was observed from a free flowing aqueous solution to a gel after a few minutes of mixing. This physical transition arises from the delamination of the layered Laponite platelets to individual charged platelets (negative faces and positive rims). The Laponite platelets in the dispersion started to interact with each other and form a gel, owing to the electrostatic interaction between the negative faces and the positive rims of the platelets.[44] In addition, van der Waals attractions exist between these platelets owing to the high concentration of Laponite in the system.[45] Afterwards, a basic aqueous pH-BCP solution (pH 10) was added to the Laponite gel. Upon addition of the polymer solution, the gel instantaneously collapsed and formed a viscous liquid, indicating that there was an interaction between the Laponite platelets and the pH-BCP. The viscous liquid exhibited a pH value of ~ 9.8, which arises from the buffering effect of Laponite. At this pH value, the carboxylic groups of the pH-BCP are completely deprotonated creating a negatively charged state polymer. The p$K_a$ of the pH-BCP was determined to be 6.46 by titration (**Figure 3.6**). The negatively charged pH-BCP is more likely to be repelled by the negative charged faces of the platelets and, thus, adsorbs onto the positive rim of the platelets. Furthermore, the ethylene glycol moieties in our branched copolymer can undergo hydrogen bond interactions with the rim (functional groups: Si−OH and Mg−OH). A pH-BCP functionalized Laponite platelet (pH-BCP-Laponite) is illustrated in **Figure 3.10**.

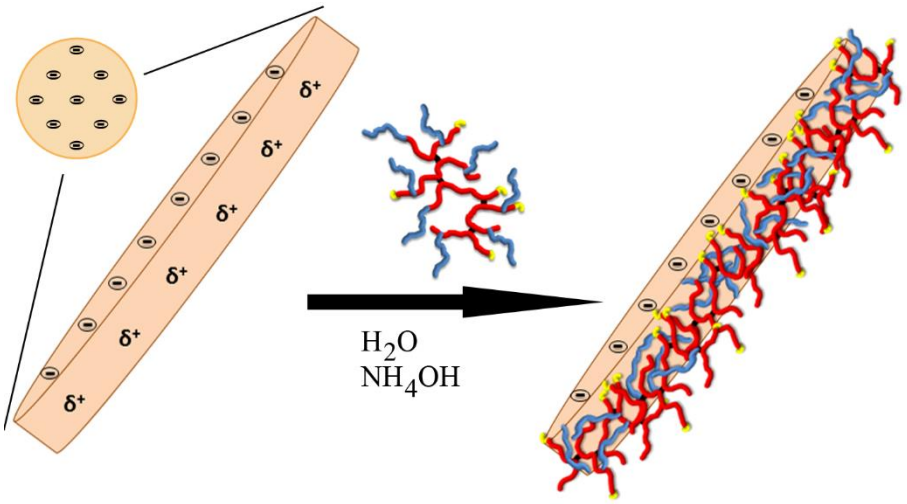


**Figure 3.10.** Schematic representation of the functionalization of Laponite platelet with pH-BCP. Unfunctionalized Laponite platelet with a positive rim and negative faces (left hand side). Top view of the unfunctionalized Laponite platelet (top left hand side). Laponite platelet functionalized with pH-BCP (pH-BCP-Laponite) (right hand side). The pH-BCP (Blue = PEGMA domain, red = MAA domain, black = branching unit, EGDMA, and yellow = hydrophobic chain ends, DDT) adsorb on the positive rim of the platelet by electrostatic interaction and hydrogen bonding.

### 3.2.5. Fabrication and Characterization of Pickering Emulsion

Oil-in-water emulsions (50:50 vol%) stabilized with pH-BCP-Laponite were prepared by homogenizing the oil phase (dodecane) in basic aqueous pH-BCP-Laponite solution (pH ~ 9.8). The pH-BCP-Laponite stabilizes the emulsion droplets by *(i)* Pickering stabilization from the Laponite platelets, *(ii)* the amphiphilic pH-BCP located at the positive rim of the platelets that offers electrostatic stabilization from the MAA domain at neutral and basic conditions, and *(iii)* steric stabilization by the PEGMA domain. The multiple hydrophobic chain ends provide strong oil-droplet surface adsorption (**Figure 3.11**).

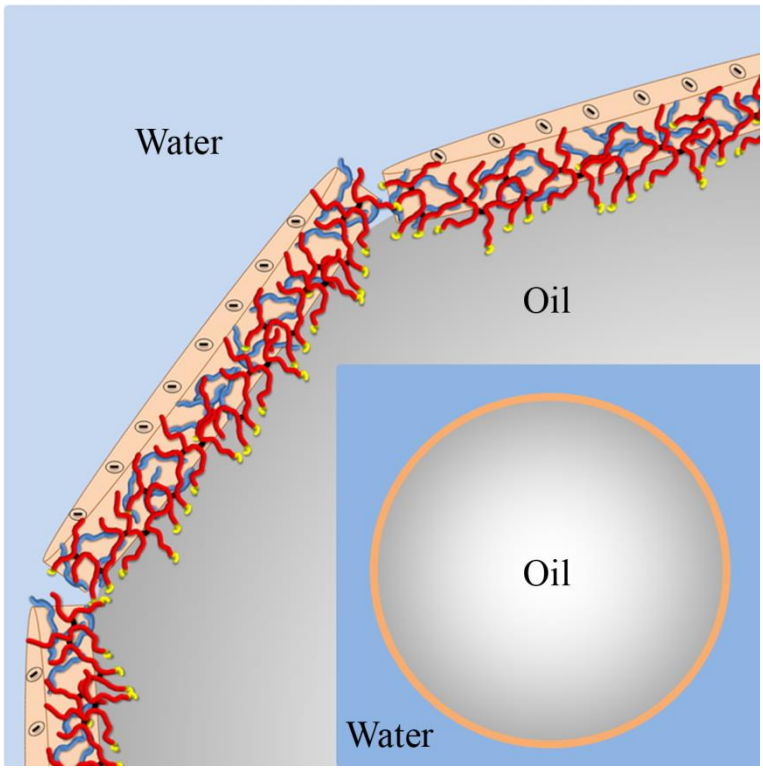


**Figure 3.11.** Schematic illustration of the Pickering oil-in-water emulsion droplet stabilized with the pH-BCP-Laponite. The pH-BCP-Laponite acts as a Pickering stabilizer with additional electrostatic and steric stabilizations arising from the pH-BCP adsorbed on the positive rim of the Laponite platelet.

The emulsions were left for 48 hours. In the meantime, the emulsion droplets creamed owing to lower oil density, and to reach an emulsion volume fraction value of 0.81 (High Internal Phase Emulsion, HIPE). The creamed emulsion droplets did not coalesce, and no oil separation was observed over 12 weeks. The emulsion droplets can be simply re-dispersed by gentle agitation in neutral or basic aqueous solution. Laser diffraction measurement on the emulsion in basic aqueous solution (pH 11) revealed a monomodal population of emulsion droplets ranging from 3.1 μm to 33.9 μm, with an average droplet diameter of 12.4 μm. (**Figure 3.12A**). Light micrograph of Pickering oil-in-water emulsion droplets stabilized with pH-BCP-Laponite is shown in **Figure 3.12B**.

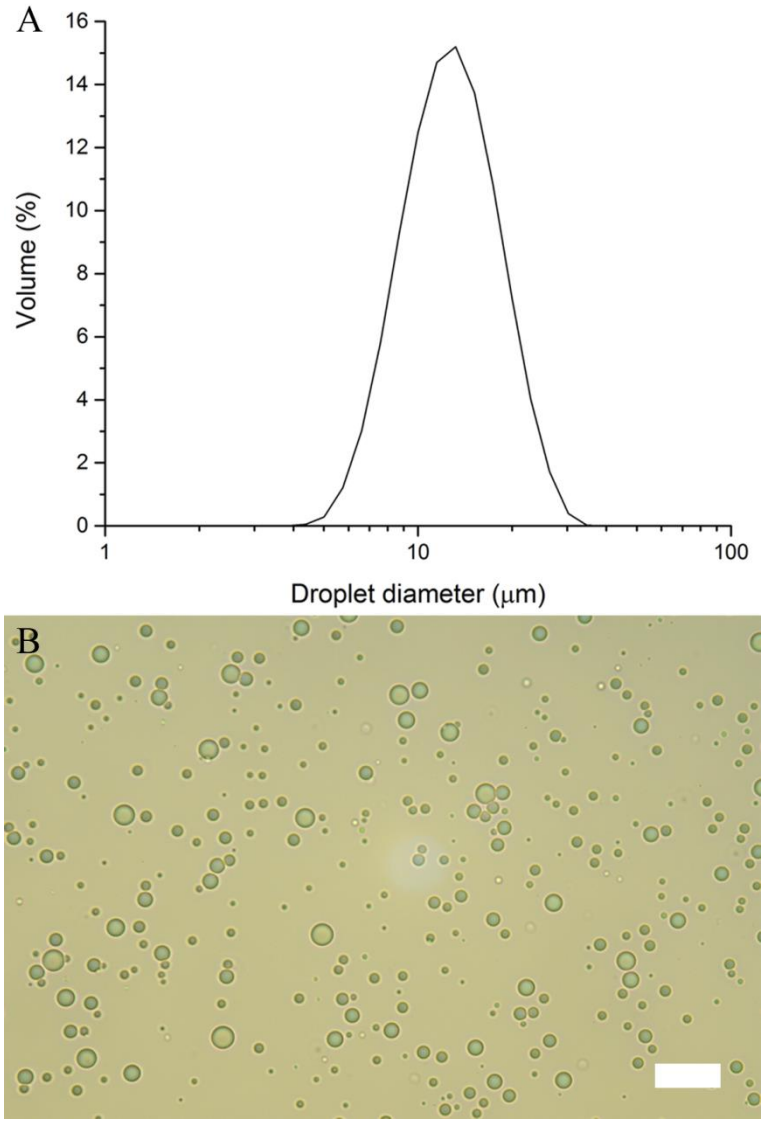


**Figure 3.12.** (A) Laser diffraction chromatogram of emulsion droplets stabilized with pH-BCP-Laponite at pH 11. (B) Light micrograph of Pickering oil-in-water emulsion droplets stabilized with pH-BCP-Laponite in basic aqueous solution (pH 11). Scale bar represents 25 μm.

### 3.2.6. Fabrication of High Internal Phase Emulsion (HIPE) Fibers with pH-BCP-Laponite as Stabilizer for Emulsion Droplets

The HIPE fibers were spun by employing a double coaxial laminar flow microfluidic device composed of two pulled inner capillaries (injection and collection inner capillaries) and one regular glass capillary (outer capillary) (**Figure 3.13**). The two inner capillaries were aligned within the outer capillary to produce a flow-focusing junction where the HIPE fiber is fabricated through assembly of the emulsion droplets. The injection inner capillary contained the

concentrated emulsion, and the outer capillary contained the sheath fluid, (acidic water at pH 3). Both the emulsion and sheath fluid were kept at continuous flow.

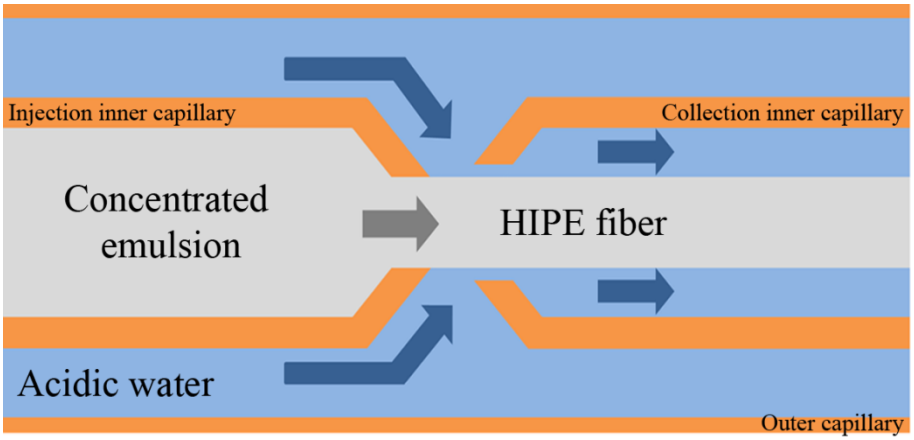


**Figure 3.13.** Schematic representation of the fabrication of microfluidically spun HIPE fiber. The diagram shows coaxial flow channels in the microfluidic device, where the inner and outer capillaries contain concentrated emulsion and acidic water, respectively, in a continuous flow. A continuous HIPE fiber is produced upon exposure of the emulsion to the acidic water. The acidic conditions allow the formation of multiple hydrogen bonds between emulsion droplets, initiating them to assemble into a macroscopic supracolloidal fiber.

Upon contact with the acidic water, the emulsion droplets lose their electrostatic repulsive interaction as now the carboxylic acid groups become protonated. Upon collision with one another they are 'locked' through a combination of van der Waals interactions and hydrogen bonding, hereby producing a uniform fiber composed of emulsion droplets in a continuous manner (**Figure 3.14**).

**Figure 3.14.** HIPE fiber fabricated with acidic water as sheath fluid. Scale bar represents 1 cm. Several fragmented fibers arise from blockage of capillaries and viscosity mismatch of the concentrated emulsion and sheath fluid.

An interesting feature of the produced fiber is that the assembly process is reversible. Addition of a base results in disintegration of the HIPE fiber into individual emulsion droplets (**Figure 3.15 and Movie 3.1**).

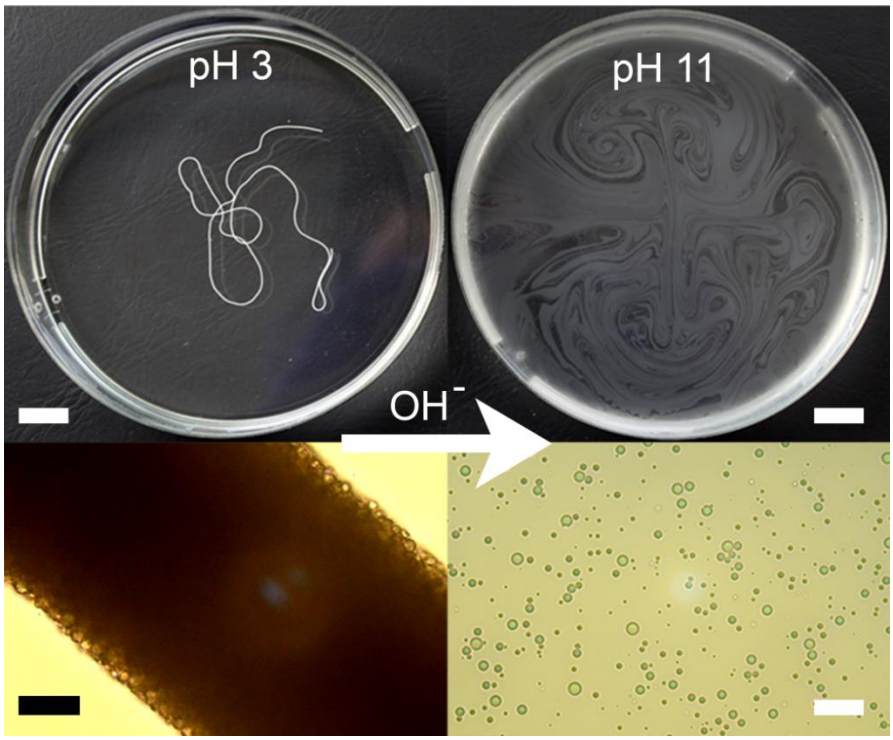


**Figure 3.15.** Photograph of a HIPE fiber in acidic aqueous solution (top left), and disintegration into individual dispersed emulsion droplets upon addition of base (top right). Scale bars represent 1 cm. Light micrographs of the HIPE fiber in acidic condition (bottom left) and disintegrated HIPE fiber in basic condition (bottom right). Scale bars represent 50 μm and 25 μm, respectively.

The fabrication of the HIPE fibers by microfluidics raised some challenges initially. First, the capillary was prone to clogging, which lead to limitation on the length of the HIPE fiber that can be created. Furthermore, the HIPE fibers were in their 'stressed' state when they are initially exposed to acidic environment. The 'stressed' state HIPE fiber tends to break when moved. The HIPE fibers attain their 'relaxed' state with time and, therefore, the fibers were not moved for 30 minutes after exposure to acidic aqueous solution. These issues were overcome by addition of poly(vinyl alcohol) (PVA) to the sheath fluid, as PVA acts as a lubricant for the fiber extrusion, and matches the viscosity of the sheath fluid with the concentrated emulsion. Thus, the HIPE fiber can be subjected to movement even in its 'stressed' state when PVA is present in the system. The addition of PVA in the sheath fluid allows for fabrication of uniform continuous HIPE fiber with ease (**Figure 3.16**).

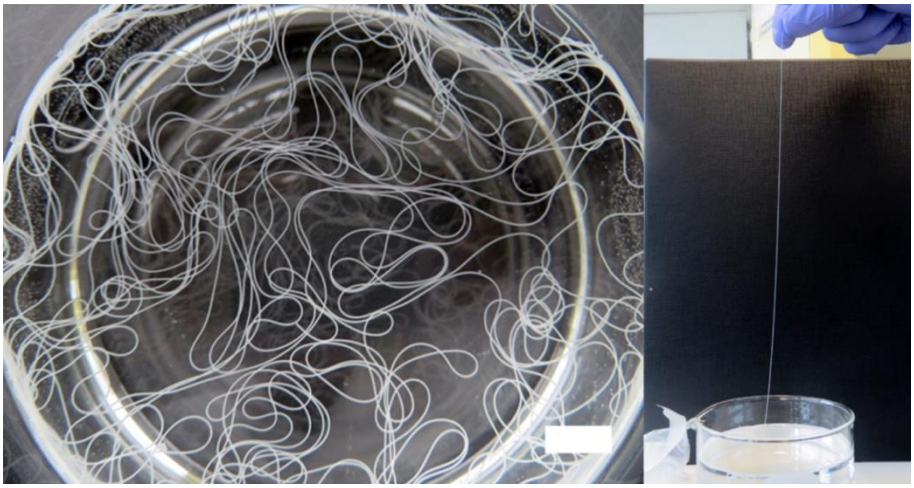

**Figure 3.16.** Photograph of continuous long HIPE fibers fabricated with acidic water containing poly(vinyl alcohol) as sheath fluid. Scale bar represents 1 cm.

HIPE fibers with desired lengths can be generated by separating the concentrated emulsion into defined segments in the injection inner capillary with air bubbles prior exposure to the sheath fluid (**Figure 3.17**).

**Figure 3.17.** Photograph of HIPE fibers with uniform length. The HIPE fibers with uniform length were fabricated by utilizing air bubbles as a cutting mechanism. Scale bar represents 0.5 cm.

Interestingly, under the experimental flow conditions we applied, the following simple relationship holds:

$$\frac{F_e}{F_t} = \left(\frac{d_f}{d_{ic}}\right)^2 \tag{3.1}$$

In which $F_e$ is the volumetric flow rate of the emulsion, $F_t$ is the combined flow rates of both the emulsion and the outer sheath fluid, $d_f$ is the diameter of the fiber and $d_{ic}$ is the inner diameter of the collection channel. It shows that there is essentially no liquid exchange and that the fiber is composed of 81 vol% oil droplets.

The incorporation of PVA in the sheath fluid prevents the HIPE fiber to fully disintegrate into individual dispersed emulsion droplets when base is added. Also, permanently cross-linking the HIPE fiber (fabricated with sheath fluid containing PVA) with calcium ions completely stops the disintegration process of the HIPE fiber under basic conditions.

### 3.2.7. Fabrication of Asymmetric Fibers and Magnetic-Responsive Fibers

The HIPE fibers can serve as a carrier for oils and hydrophobic dissolved/dispersed ingredients with various cross-sectional segments, which can be achieved easily by incorporating hydrophobic materials in the oil phase of the emulsion droplets prior to the emulsification process. In order to demonstrate this design concept, we produced a variety of fibers of different colors (employing dyes) (**Figure 3.18**).

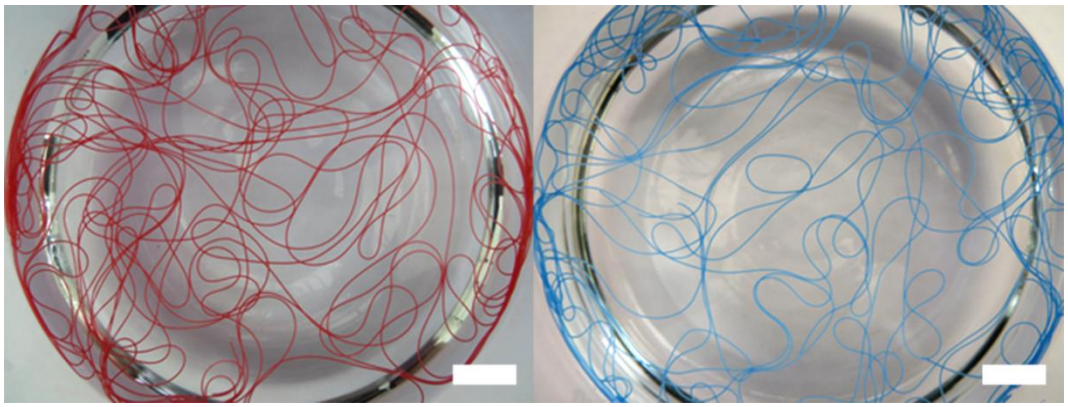

**Figure 3.18.** Photographs of HIPE fibers loaded with hydrophobic materials. Red and blue HIPE fibers loaded with hydrophobic red and blue dyes, respectively. Scale bars represent 1 cm.

Asymmetric fibers were also fabricated by providing the injection inner capillary with multiple inlets containing a continuous flow of emulsions loaded with different dyes. These Janus (red and blue segments) and 'toothpaste' (white, red, and blue segments) asymmetric fibers are depicted in **Figure 3.19A** and **Figure 3.19B**, respectively. The width of each section in the HIPE fiber can be easily changed by varying the flow rate of the concentrated emulsions.

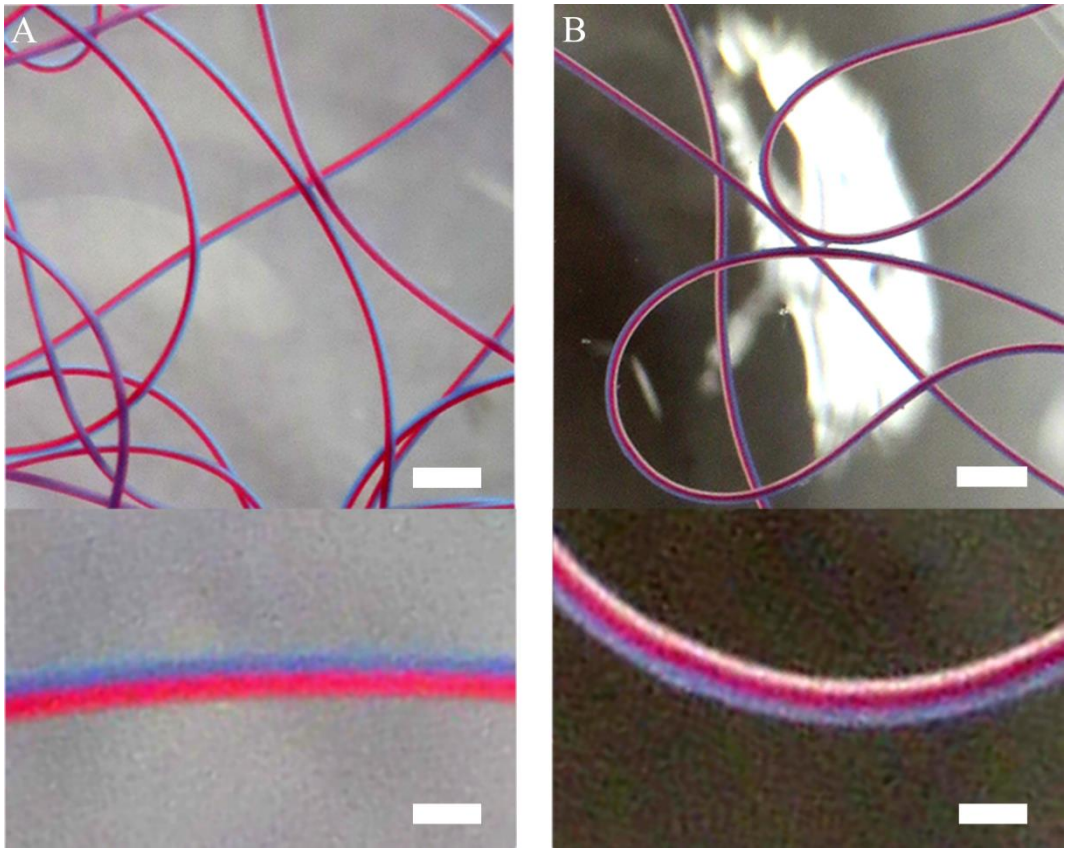


**Figure 3.19.** (A) Photograph of asymmetric Janus HIPE fiber. Scale bars represent 0.1 cm (top) and 300 µm (bottom). (B) Photograph of asymmetric HIPE fiber consisting of three different sections 'toothpaste'. Scale bars represent 0.1 cm (top) and 300 µm (bottom).

HIPE fibers with magnetic response were also fabricated by addition of ferrofluid in the oil phase of the emulsion (**Figure 3.20A, and Movie 3.2**). As seen in **Figure 3.20B**, the magnetic HIPE fiber (fiber with a slight yellow color) is attracted to by an external magnet, whereas the non-magnetic HIPE fiber (white color fiber) is not subjected to the magnetic forces of the magnet.

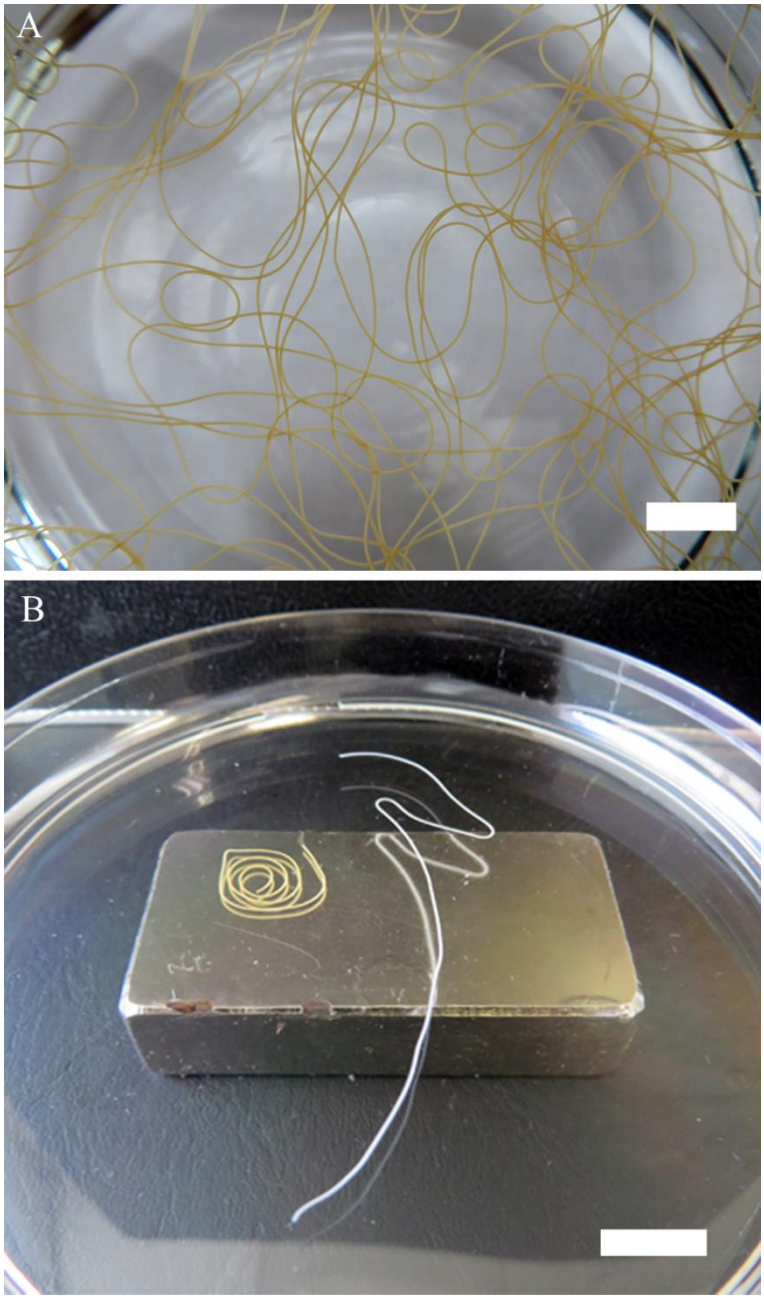


**Figure 3.20.** (A) Photograph of magnetic HIPE fibers. Scale bar represent 1 cm. (B) Photograph of magnetic HIPE fiber attracted by an external magnet (fiber with a slight yellow color - left hand side), and no magnetic response with the non-magnetic HIPE fiber (white color fiber - right hand side). Scale bar represents 1 cm.

### 3.2.8. Fabrication of Fibers Nanocomposite Mesh

The solid and liquid contents of the HIPE fiber were calculated by monitoring the mass loss at 30 – 1000 ºC with thermogravimetric analysis (**Figure 3.21**). The fibers consists of 98.32 % liquid (dodecane and water) and 1.68 % solid, with a mass percent ratio of 0.70 : 1 of polymer (pH-BCP and PVA) to Laponite.

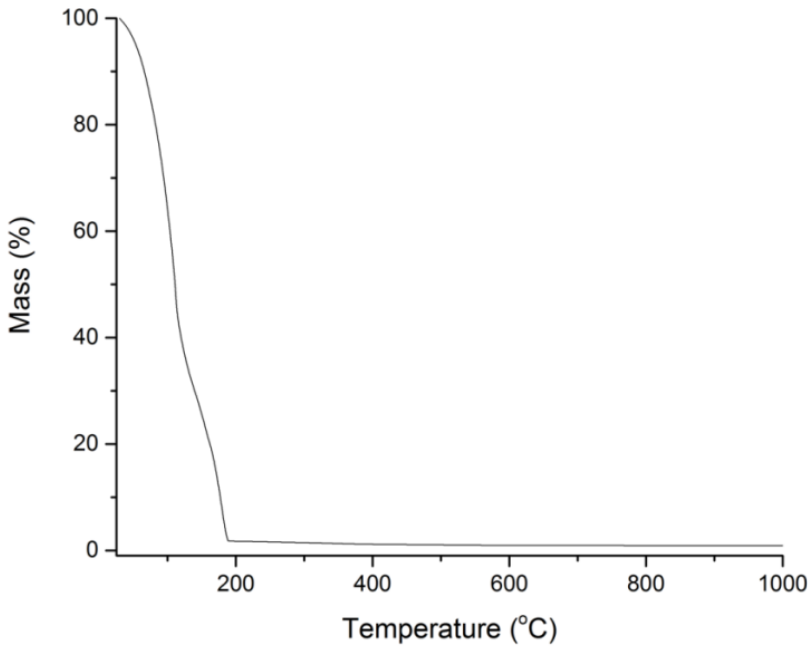


**Figure 3.21.** Thermogravimetric (TG) curve of the HIPE fiber. There are two regions of mass losses on the TG curve of the HIPE fiber. The mass loss of 98.32 % between 30 – 220 °C is due to the evaporation of dodecane and water. Therefore, the solid content of the HIPE fiber is 1.68 %, which is a combination of Laponite and polymer. The mass loss of 0.69 % between 220 °C – 550 °C represents decomposition of the polymer (pH-BCP and poly(vinyl alcohol)). This means there is 0.99 % Laponite and 0.69 % polymer in the HIPE fiber (polymer 0.70 : 1 Laponite).

The emulsion droplets in the fibers are held together by a continuous honeycomb clay-polymer network. When the HIPE fibers were air dried, hereby removing the water and dodecane through evaporation, the nano composite structure was retained with the fibers staying intact. There was a decrease of 22.2 % ± 3.2 % in volume of the fiber when dried, and a decreased in length and diameter of 60 % ± 2.84 % and 60.7 % ± 3.25 %, respectively. Therefore, the fiber dries isotropically, as $0.6^3 = 0.22$. The HIPE fiber became more rigid upon drying but remarkably could be bent multiple times without breakage (**Movie 3.3**). The surface morphology and internal structure of the dried fiber were observed by focused ion beam scanning electron microscopy (FIB/SEM) (**Figure 3.22**). The surface morphology was rough and dotted with pores throughout the surface of the fiber (**Figure 3.22A**), the diameters of the pores being within the dimensions of the original emulsion droplets. The internal structure of the HIPE fiber was exposed through ablation of the surface regions of the HIPE fiber with the ion beam. A highly interconnected honeycomb macroporous structure was observed (**Figure 3.22B**).

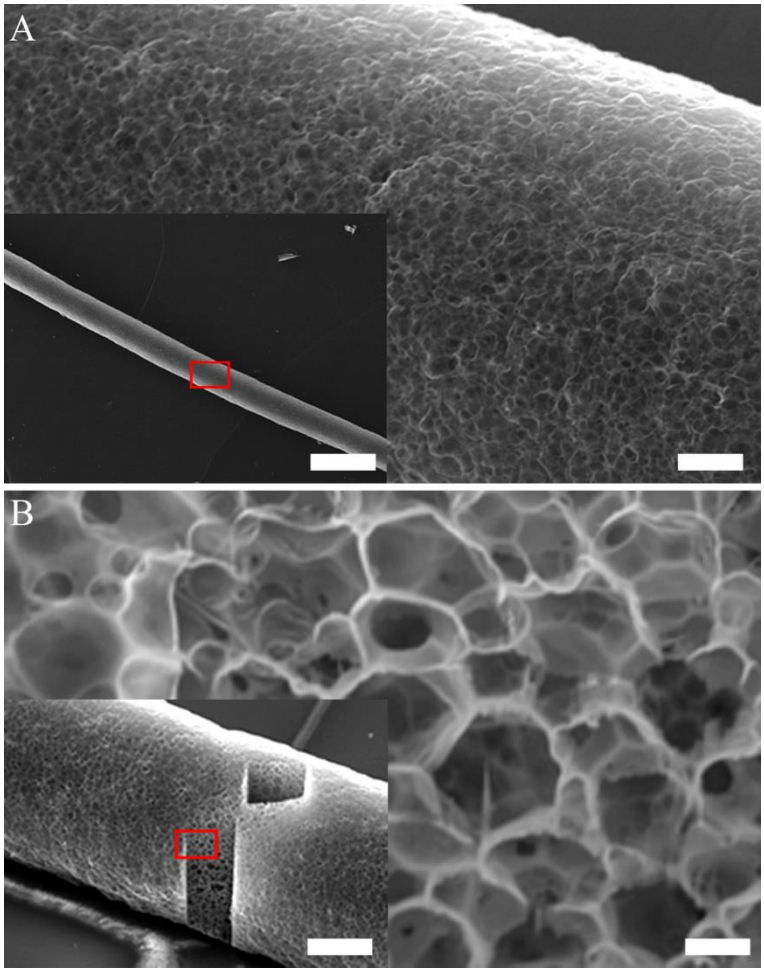


**Figure 3.22.** FIB/SEM micrographs of the dried HIPE fiber. (A) Surface morphology of the dried HIPE fiber. The scale bars represent 325 µm (left hand side), 20 µm (right hand side). (B) The ablation of surface material to reveal the internal structure of the dried HIPE fiber. The internal structure of the dried HIPE fiber shows a highly interconnected macroporous structure with micron sized almost spherical voids that are interconnected *via* numerous smaller pores. The scale bars represent 50 µm (left hand side) and 2.5 µm (right hand side).

The internal pores are micron sized almost spherical voids originating from the emulsion droplets (templates) and are interconnected *via* numerous smaller pores originating from the interstitial spaces due to packing. Owing to the highly porous structure of the dried HIPE fiber, a very light weight material was generated. The structural density of the nanocomposite mesh was determined with pycnometry at a value of 2.04 $g \cdot cm^{-3}$ ±0.02 $g \cdot cm^{-3}$, which aligns with the TGA data stating a mass ratio of Laponite clay ($d = 2.65\ g \cdot cm^{-3}$) and polymer ($d \approx 1.2\ g \cdot cm^{-3}$) of 1:0.7. The measured bulk density of the fiber is 0.044 $g \cdot cm^{-3}$, in agreement with the calculated value using the TGA and pycnometry data of (0.0168 ● 2.04 / 0.78) = 0.044 $g \cdot cm^{-3}$, which makes our fiber only approximately 36 times heavier than

air. Magnetic responsiveness was retained when the magnetically responsive HIPE fibers were dried (**Movie 3.4**).

### 3.2.9. Release Study of the Liquid Phases of the HIPE Fiber

Our HIPE fibers can be potentially used to deliver oils, for example fragrances or insect repellants. For this purpose, we investigated the evaporation of the liquid phases of a series of HIPE fibers at ambient temperature with time, which were ionically crosslinked with different amounts of calcium ions (**Figure 3.23A)**. The evaporation profiles show two distinct stages. The first stage (from 0 to ~ 120 minutes), represents the evaporation of mostly water from the HIPE fiber. Extrapolation of the stage 2 data to time = 0 s would state that the all the fibers contain approximately 45 % dodecane, in contrast with the earlier stated 76 wt% (= 81 vol%). The reasons for this are that the fibers are collected/stored in an acidic water bath and are non-drained and, therefore, contain roughly an additional 30 wt% of water. The second stage (~ 120 to ~ 8000 minutes), refers to the slow evaporation of the oil phase from the HIPE fiber. It is clear that the extent of $Ca^{2+}$ cross-linking has a marked effect on the evaporation rate of the dodecane. The fibers were post-annealed at 220 °C for 30 minutes to remove remaining traces of water and oil from the HIPE fiber. The mass difference in the HIPE fiber after annealing is caused by the incorporation of calcium chloride into the fiber.

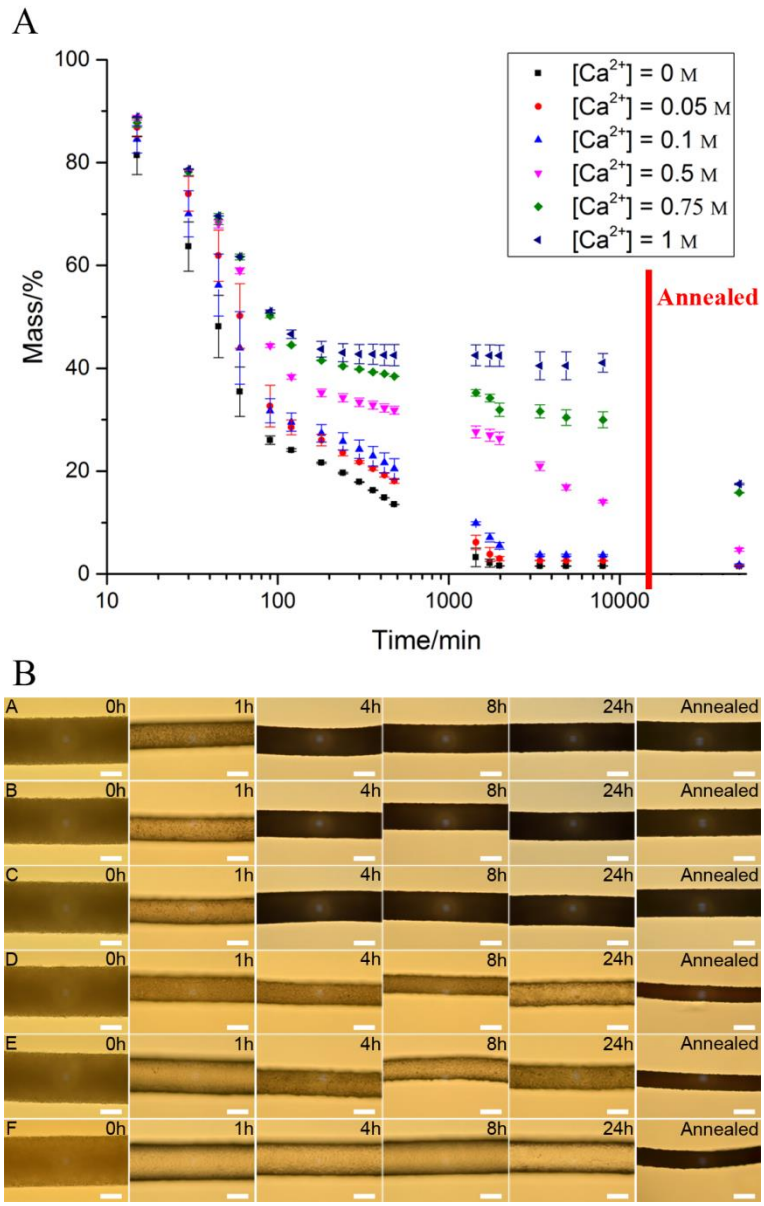


**Figure 3.23.** (A) The evaporation of the liquid phases of the HIPE fiber at ambient temperature with time (crosslinked at different calcium concentrations). The mass of the HIPE fiber was recorded over time and annealed at 220 °C to determine the final mass of the dried HIPE fiber. (B) The light micrographs of the HIPE fibers (crosslinked at different calcium concentrations) at different points of time and after annealing (annealed at 220 °C for 30 minutes) ($[Ca^{2+}]$ = 0 M (A), 0.05 M (B), 0.1 M (C), 0.5 M (D), 0.75 M (E), and 1 M (F)). Scale bars represent 100 µm.

The light micrographs of the HIPE fibers (crosslinked at different calcium concentrations) at different points of time and after annealing are shown in **Figure 3.23B**, demonstrating the same effect. The clearer contrast (transition from light to dark) is the result of the higher refractive index difference due to presence of air inside the fiber.

### 3.2.10. The Fabrication of Solid pH-BCP-Laponite Fiber

The pores of the HIPE fiber can be removed by simply soaking the HIPE fiber in ethanol prior to drying. By doing so, the oil phase of the emulsion (dodecane) diffuses from the HIPE fiber to the ethanol solution as dodecane is miscible with ethanol. The rapid diffusion process causes the voids in the fiber to collapse and form a solid Laponite-pH-BCP fiber. This fiber is more flexible and can sustain some strain compared to analogue porous dried HIPE fiber (**Figure 3.24**).

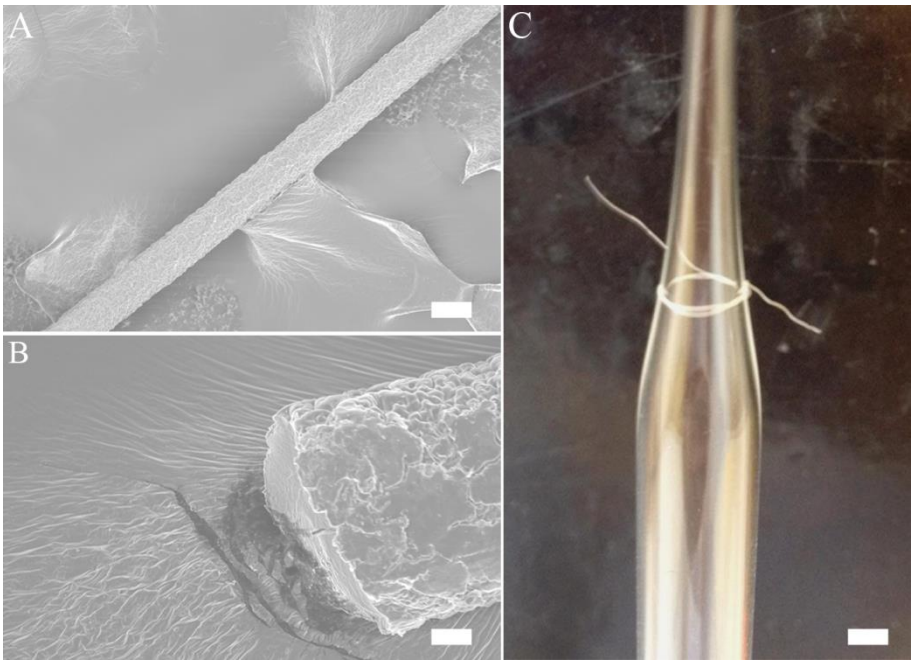


**Figure 3.24.** Scanning electron micrographs and photograph of solid pH-BCP-Laponite fiber. (A) Surface morphology of the solid pH-BCP-Laponite fiber. Scale bar represents 51 µm. (B) Non porous internal structure of the solid pH-BCP-Laponite fiber. Scale bar represents 10 µm. (C) The solid Laponite-pH-BCP fiber tied around a glass capillary with multiple loops. Scale bar represents 2.7 mm.

## 3.3. Conclusions

We have shown that soft matter fibers can be made through assembly of emulsion droplets with a potential application as evaporative dispensers. The essential step was to lock the droplets together with a nanocomposite mesh of Laponite clay and hyperbranched copolymer, which possess the capability to undergo secondary interactions (ionic and hydrogen bond interactions). We believe that the use of liquid flow to direct the assembly of colloidal components – in this case droplets – illustrate an innovative pathway to generate supracolloidal structures away from random equilibrium based assembly processes. It opens up an exciting opportunity in the design process of colloidal formulations for a variety of application areas.

## 3.4. Experimental

### 3.4.1. Materials

Poly(ethylene glycol) methyl ether methacrylate (PEGMA, $M_n$ = 1100 g·mol$^{-1}$, Sigma-Aldrich), methacrylic acid (MAA, 99 %, Sigma-Aldrich), ethylene glycol dimethacylate (EGDMA, 98 %, Sigma-Aldrich), 1−dodecanethiol (DDT, ≥98 %, Sigma-Aldrich) and (trimethylsilyl)diazomethane (2 M in hexane, Sigma-Aldrich). 2,2'−Azobis(isobutyronirile) (AIBN, BDH) was recrystallized from methanol prior to use. Deuterated chloroform and methanol were purchased from Sigma-Aldrich. All organic solvents were standard laboratory grade. Laponite RD (BYK), dodecane (≥99 %, Sigma-Aldrich), oil blue N (96 %, Sigma-Aldrich), oil red O (Sigma-Aldrich), ferrofluid (Reference code: EFH1, Ferrotec), D-(+)-Gluconic acid δ-lactone (≥99 %, Sigma-Aldrich), mowiol 8-88 (poly(vinyl alcohol), (PVA, $M_w$ ~ 67,000 g·mol$^{-1}$, Sigma-Aldrich), calcium chloride dihydrate (Analar normapur), ammonium hydroxide (35 %, Fisher chemical), hydrochloric acid (37 %, Analar Normapur), and sodium hydroxide pellets (Fisher chemical).

### 3.4.2. Synthesis of pH-Responsive Branched Copolymer

The pH-responsive branched copolymer (pH-BCP) was synthesized *via* thiol-regulated free radical polymerization. A round bottom flask was charged with PEGMA (3 g, 2.73 mmol), MAA (4.456 g, 51.80 mmol), EGDMA (1.080 g, 5.45 mmol), DDT (1.102 g, 5.45 mmol) and ethanol (96 mL). The reaction mixture was degassed with nitrogen gas for 20 minutes, and subsequently immersed into a preheated oil bath of 70 ºC. The polymerization was initiated by addition of AIBN (0.096 g, 0.59 mmol) and was left stirring for 48 h. The reaction mixture was concentrated under vacuum and the polymer was purified by precipitation in cold diethyl ether (-20 ºC). The polymer was left to dry under vacuum overnight.

The pH-BCP was esterified and the $^1$H NMR spectrum of the esterified-BCP was used to determine the relative molar ratios of the co-monomers and chain transfer agent in pH-BCP. The pH-BCP was esterified by firstly dissolving the pH-BCP (50 mg) in methanol (0.2 mL). Toluene (0.2 mL) was added and agitated to obtain a homogeneous solution. (Trimethylsilyl)diazomethane (~ 0.2 mL) was then added drop wise until a yellow color appeared and did not become colorless upon

agitation. The resulting solution was purified *via* evaporation, and left to dry in the vacuum oven overnight at 60 $^{o}$C.

### 3.4.3. Characterization of pH-Responsive Branched Copolymer

$^{1}$H NMR spectra of the polymers were recorded on 1 wt% branched copolymer solutions in deuterated solvents using Bruker Specrospin 400 UltrashieldTM operating at 400 MHz. Molar mass, molar mass distribution ($Đ$), and Mark-Houwink ($\alpha_{\eta}$) values were measured by TD-GPC using an Agilent 390-MDS Multi Detector Suite equipped with refractive index, viscometer, and UV detectors. A mobile phase of DMF with 5 mM $NH_3BF_4$ was employed with a flow rate of 1 mL·min$^{-1}$. Two PL gel Mixed-D columns and an additional guard column were used with an oven temperature of 50 $^{o}$C. Specific calibration was carried out using poly(methyl methacrylate) standards.

### 3.4.4. Potentiometric Titration of pH-Responsive Branched Copolymer

A potentiometric titration curve of pH-BCP was generated by dissolving BCP (0.1 wt%) in a basic solution of pH ~ 11.8 using NaOH (0.5 M) to ensure complete dissolution of polymer. Changes in pH values were monitored (with an Oakton pH meter) following incremental additions of HCl (0.1 M) to the basic pH-BCP solution. The α of pH-BCP with pH was calculated using the Henderson-Hasselbalch equation.[35]

### 3.4.5. Fabrication and Characterization of Emulsions

Laponite functionalized with pH-BCP (pH-BCP-Laponite) was prepared by initially preparing an aqueous Laponite dispersion (6.67 w/v%). A physical transition was observed from a flowing aqueous solution to a gel after a few minutes of vigorous mixing. A basic aqueous solution containing 8 w/v% of pH-BCP (the pH was adjusted to 10 with 1 M $NH_4OH$ solution) was added to the Laponite gel with vigorous stirring, and left to stir for 30 minutes to produce a viscous pH-BCP-Laponite aqueous solution (Laponite = 5 w/v%, pH-BCP = 2 w/v%, and pH ~ 9.8). An equal amount of dodecane was added to the viscous pH-BCP-Laponite aqueous solution to give a biphasic mixture. For colored creamed emulsions, oil red O or oil blue N dyes were added to dodecane (0.1 w/v%). Ferro fluid (1 v/v%) was added to dodecane to give magnetic

response. This biphasic mixture was homogenized at 24 000 rpm for two minutes to produce an oil-in-water emulsion. The emulsion was left for 48 hours to equilibrate and the resulting emulsion formed a creamed layer. Similar method and conditions were applied for fabricating emulsion that was solely stabilized with pH-BCP but Laponite was not added in the system. The size and span of the emulsion were recoded using laser diffraction (Mastersizer 2000 equipped with a Hydro 2000S dispersion unit). 10 μL of creamed emulsion was added to the dispersion unit containing 100 mL of basic water (pH adjusted to 11 with 1 M NaOH solution) with a stirring rate of 1000 rpm. The volume average droplet diameters ($D_{4/3}$) mentioned were obtained from at least 5 repeat runs ($D_{4/3} = \sum D_{i4}N_i/\sum D_{i3}N_i$). The span is a measure of the distribution of the droplet size distribution and is expressed mathematically as (D(0.9)-D(0.1))/D(0.5), where D(0.9) is the diameter under which 90 % of the particles fall, D(0.5) is the diameter under which 50 % of the particles fall and D(0.1) is the diameter under which 10 % of the particles fall. Light micrographs were taken using a Leica DM 2500M microscope equipped with a Nikon D5·100 digital camera.

### 3.4.6. Fabrication of Microfluidic Device and HIPE Fibers

A glass capillary with an inner and outer diameter of 1.16 mm and 2.0 mm, respectively, forms the outer capillary of the device, and contains the sheath fluid. Within the outer capillary, two capillaries (injection and collection inner capillaries) with inner and outer diameters of 0.58 mm and 1.0 mm, respectively, were tapered with a laser puller to allow flow focusing of the concentrated emulsion. The injection inner capillary and collection inner capillary has a diameter of ~110 μm and ~120 μm, respectively. The inner capillaries were aligned to produce a flow-focused junction where the HIPE fibers are fabricated. The optimum flow rates for the HIPE fiber fabrications were 0.1 $mL \cdot min^{-1}$ for the sheath fluid and 0.02 $mL \cdot min^{-1}$ for the concentrated emulsion. Harvard Apparatus PHD 2000 Infusion was used as the pumping system. The sheath fluid was acidified by adding gluconic acid δ-lactone (3 w/v%). All HIPE fibers were collected in an acidic aqueous solution reservoir (pH 3, adjusted by addition of 1 M HCl). HIPE fiber was disintegrated in basic aqueous solution (pH 11, adjusted by addition of 1 M NaOH). The fabrication of HIPE fiber was optimized

by adding poly(vinyl alcohol) in the acidic sheath fluid (3 w/v%). HIPE fiber was permanently cross-linked with calcium ion by incubating the HIPE fiber in acidic aqueous solution containing calcium ions for 1 hour (pH 3, adjusted by addition of 1 M HCl, $[Ca^{2+}]$ = 1 M).

### 3.4.7. Fabrication of Various Types of HIPE Fiber by Microfluidics

HIPE fibers with uniform length and asymmetric fibers were fabricated by having multiply inlets to the injection inner capillary. The **Table 3.2** shows the flow parameters to fabricate these various HIPE fibers. The photograph and light micrograph of the microfluidics devices are shown in **Figure 3.25-Appx**.

**Table 3.2.** The flow parameters to fabricate various HIPE fibers.

| | **Outer capillary** | **Injection inner capillary** | | |
|---|---|---|---|---|
| | | **Inlet 1** | **Inlet 2** | **Inlet 3** |
| **HIPE fiber with uniform length** (1 cm) | 0.1 mL·min$^{-1}$ *Acidic PVA solution* | 0.02 mL·min$^{-1}$ *Unloaded concentrated emulsion* | 0.002 mL·min$^{-1}$ *Air* | |
| **Janus** | 0.1 mL·min$^{-1}$ *Acidic PVA solution* | 0.01 mL·min$^{-1}$ *Red concentrated emulsion* | 0.01 mL·min$^{-1}$ *Blue concentrated emulsion* | |
| **'Toothpaste'** | 0.1 mL·min$^{-1}$ *Acidic PVA solution* | 0.007 mL·min$^{-1}$ *Red concentrated emulsion* | 0.007 mL·min$^{-1}$ *Blue concentrated emulsion* | 0.007 mL·min$^{-1}$ *Unloaded concentrated emulsion* |

### 3.4.8. Thermogravimetric Analysis of HIPE Fiber

Thermogravimetric analysis was recorded using a Mettler Toledo TGA/DSC1 STAR$^e$ System instrument. The HIPE fiber was heated from 30 $^oC$ to 1000 $^oC$ at10 $^oC \cdot min^{-1}$ in a flow of dry air at 50 $mL \cdot min^{-1}$

### 3.4.9. Imaging of the Dried HIPE Fiber by Focused Ion Beam Scanning Electron Microscopy

The surface morphology and internal structure images of the dried HIPE fiber were obtained using a JEOL 4500 focused ion beam scanning electron microscope. The dried HIPE fiber was coated with carbon prior to imaging. The imaging was performed at 20 kV.

### 3.4.10. Determination of Density of the Dried Nanocomposite Mesh

Density of the sample was measured using a Micrometric AccuPyc II 1340 gas displacement pycnometer with Helium gas. The gas tank's pressure regulator, the purge fill pressure, and cyclic filling pressure were set at 22 psig, 19.5 psig, and 19.5 psig respectively. Before measuring the material's density, the machine was calibrated with a supplied standard of known volume. A 1 $cm^3$ crucible was used with the sample filling two thirds of it. Prior to the measurement of the sample, the crucible with sample was purged with Helium gas at 19.5 psig for 30 minutes to remove any adsorbed gases from the air.

### 3.4.11. Release Study of the Oil Phases of the HIPE Fiber

The evaporation of the liquid phases of the HIPE fiber at ambient temperature was investigated by initially incubating the HIPE fiber (total length = 216 cm) in acidic aqueous solution containing different calcium ion concentrations ($[Ca^{2+}]$ = 0 M, 0.05 M, 0.1 M, 0.5 M, 0.75 M, and 1 M) overnight. The HIPE fibers were collected on a pan. The mass loss of the HIPE fiber was measured over time with a five decimal places weighing balance, Mettler Toledo.

### 3.4.12. The Fabrication of Solid pH-BCP-Laponite Fiber

The solid Laponite-pH-BCP was fabricated by firstly incubating the HIPE fiber in acidic aqueous solution containing calcium ions ($[Ca^{2+}]$ = 1 M) for 3 hours. The

cross-linked HIPE fiber is then soaked in ethanol for 30 minutes, and air dried. All scanning electron micrographs were obtained with a Zeiss Supra55VP scanning electron microscope. Samples were coated with gold for imaging. The imaging was performed at 10 kV.

## 3.5. Appendix

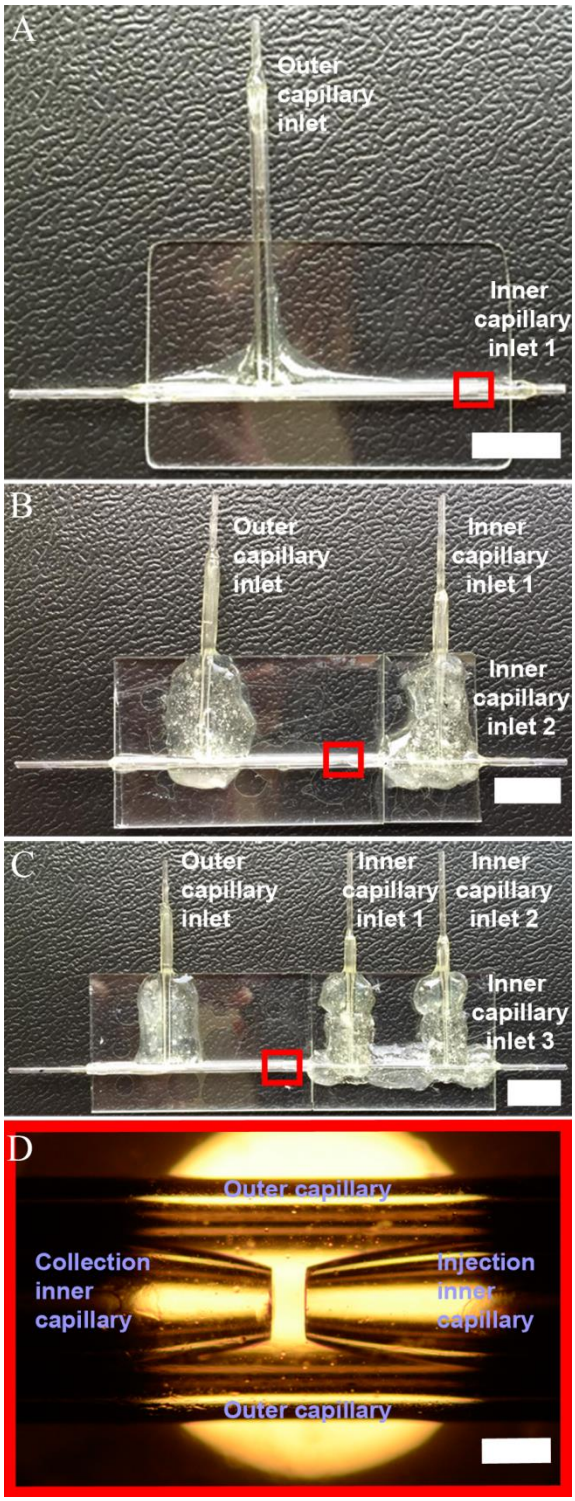


**Figure 3.25-Appx.** Photograph of microfluidics devices with one (A) two (B) and three (C) inlets to the injection inner capillary. Scale bars represent 1 cm. (D) The two inner capillaries (injection and collection inner capillaries) are aligned within the outer capillary to produce a flow-focusing junction. Scale bar represents 100 μm.

## 3.6. References


1 F. Vollrath and D. P. Knight, *Nature*, 2001, **410**, 541.

2 G. B. Kauffman, *J. Chem. Educ.*, 1984, **61**, 1095.

3 C. E. Meihuizen, A. J. Pennings, A. Zwijnenburg (Stamicarbon, B. V.), *US4137394*, **1979**.

4 S. L. Kwoleck (Du Pont), *US3819587*, **1967**.

5 L. Vollbracht, T. J. Veerman (Akzo N. V.), *US4308374*, **1981**.

6 http://www.dsm.com/products/dyneema/en_GB/industries.html, (accessed 12/10/2015).

7 http://www.dupont.co.uk/products-and-services/fabrics-fibers-nonwovens/fibers/brands/kevlar.html, (accessed 12/10/2015).

8 J. M. Kelly, *J. Macromol. Sci. Part C Polym. Rev.*, 2002, **42**, 355.

9 M. Jass and S. Ghosh, *J. Fibre Text. Res.*, 2002, **27**, 290.

10 Y. Jun, E. Kang, S. Chae and S.-H. Lee, *Lab Chip*, 2014, **14**, 2145.

11 M. A. Daniele, D. A. Boyd, A. A. Adams and F. S. Ligler, *Adv. Healthc. Mater.*, 2015, **4**, 11.

12 H. Onoe, T. Okitsu, A. Itou, M. Kato-Negishi, R. Gojo, D. Kiriya, K. Sato, S. Miura, S. Iwanaga, K. Kuribayashi-Shigetomi, Y. T. Matsunaga, Y. Shimoyama and S. Takeuchi, *Nat. Mater.*, 2013, **12**, 584.

13 Y. Jun, M. J. Kim, Y. H. Hwang, E. A. Jeon, A. R. Kang, S. H. Lee and D. Y. Lee, *Biomaterials*, 2013, **34**, 8122.

14 M. Yamada, R. Utoh, K. Ohashi, K. Tatsumi, M. Yamato, T. Okano and M. Seki, *Biomaterials*, 2012, **33**, 8304.

15 C. M. Hwang, Y. Park, J. Y. Park, K. Lee, K. Sun, A. Khademhosseini and S. H. Lee, *Biomed. Microdevices*, 2009, **11**, 739.

16 J. Puigmartí-Luis, D. Schaffhauser, B. R. Burg and P. S. Dittrich, *Adv. Mater.*, 2010, **22**, 2255.

17 D. J. Beebe, G. A. Mensing and G. M. Walker, *Annu. Rev. Biomed. Eng.*, 2002, **4**, 261.

18 H. A. Stone, A. D. Stroock and A. Ajdari, *Annu. Rev. Fluid Mech.*, 2004, **36**, 381.

19 C. M. Hwang, A. Khademhosseini, Y. Park, K. Sun and S. -H. Lee, *Langmuir*, 2008, **24**, 6845.

20 Y. Yu, H. Wen, J. Ma, S. Lykkemark, H. Xu and J. Qin, *Adv. Mater.*, 2014, **26**, 2494.

21 W. Jeong, J. Kim, S. Kim, S. Lee, G. Mensing and D. J. Beebe, *Lab Chip*, 2004, **4**, 576.

22 C.-H. Choi, H. Yi, S. Hwang, D. A. Weitz and C.-S. Lee, *Lab Chip*, 2011, **11**, 1477.

23 E. Um, J. K. Nunes, T. Pico and H. A. Stone, *J. Mater. Chem. B*, 2014, **2**, 7866.

24 J.-H. Jung, C.-H. Choi, S. Chung, Y.-M. Chung and C.-S. Lee, *Lab Chip*, 2009, **9**, 2596.

25 S. Cho, T. S. Shim and S.-M. Yang, *Lab Chip*, 2012, **12**, 3676.

26 E. Kang, G. S. Jeong, Y. Y. Choi, K. H. Lee, A. Khademhosseini and S.-H. Lee, *Nat. Mater.*, 2011, *10,* 877.

27 L. Leng, A. McAllister, B. Zhang, M. Radisic and A. Günther, *Adv. Mater.*, 2012, **24**, 3650.

28 E. Kang, Y. Y. Choi, S. -K. Chae, J. H. Moon, J. Y. Chang and S. -H. Lee, *Adv. Mater.*, 2012, **24**, 4271.

29 J. K. Nunes, H. Constantin and H. A. Stone, *Soft Matter*, 2013, **9**, 4227.

30 S. -K. Chae, E. Kang, A. Khademhosseini and S. -H. Lee, *Adv. Mater.*, 2013, **25**, 3071.

31 J. V. M. Weaver, S. P. Rannard and A. I. Cooper, *Angew. Chem. Int. Ed.*, 2009, **48**, 2131.

32 R. T. Woodward and J. V. M. Weaver, *Polym. Chem.*, 2011, **2**, 403.

33 N. O'Brien, A. McKee, D. C. Sherrington, A. T. Slark and A. Titterton, *Polymer*, **2000**, 41, 6027.

34 P. A. Costello, I. K. Martin, A. T. Slark, D. C. Sherrington and A. Titterton, *Polymer*, **2002**, 43, 245.

35 H. N. Po and N. M. Senozan, *J. Chem. Educ.*, 2001, **78**, 1499.

36 T. Ngai and S. A. F. Bon, *Particle-Stabilized Emulsions and Colloids*, The Royal Society Of Chemistry, 2015.

37 J. I. Dawson and R. O. C. Oreffo, *Adv. Mater.*, 2013, **25**, 4069.

38 L. Rosta and H. R. von Gunten, *J. Colloid Interface Sci.*, 1990, **134**, 397.

39 R. G. Avery and J. D. F. Ramsay, *J. Colloid Interface Sci.*, 1986, **109**, 448.

40 E. Balnois, S. Durand-Vidal and P. Levitz, *Langmuir*, 2003, **19**, 6633.

41 B. Ruzicka and E. Zaccarelli, *Soft Matter*, 2011, **7**, 1268.

42 M. M. Lezhnina, T. Grewe, H. Stoehr and U. Kynast, *Angew. Chem. Int. Ed.*, 2012, **51**, 10652.

43 S. L. Tawari, D. L. Koch and C. Cohen, *J. Colloid Interface Sci.*, 2001, **240**, 54.

44 H. Z. Cummins, *J. Non. Cryst. Solids*, 2007, **353**, 3891.

45 A. Mourchid, A. Delville, J. Lambard, E. Lécolier and P. Levitz, *Langmuir*, 1995, **11**, 1942.

# Chapter 4

# Enzymatic Catalyzed Time-Controlled Release of Emulsion Droplets from Soft Matter Fibers[§]

In Chapter 3, we demonstrated that individual emulsion droplets, which are stabilized by Laponite clay discs functionalized with pH-responsive branched copolymers, can be assembled into supracolloidal fibers using a microfluidic wet spinning process. In this chapter, we employ these fibers as a storage material for emulsion droplets, where emulsion droplets are 'locked' in the fiber structure under acidic condition, and are released from the fiber upon basification of the system. The fiber is coated with a flexible composite film clay/polymer, which acts as a physical barrier between the emulsion droplets in the fiber structure and the exterior medium, and only permits the escape of emulsion droplets at the endpoints of the fiber. The release of emulsion droplets from the fiber can be time-controlled by programming the transient acidic pH states of the system by combining a fast acidic promoter with a feedback-driven biocatalytically controlled slow generation of base in a close system. These fibers show autonomous dynamics and self-regulation properties. Fabrication and release profiles of other supracolloidal structures, such as 'matchstick' fiber and 'cake', have been demonstrated to suggest the versatility of the material.

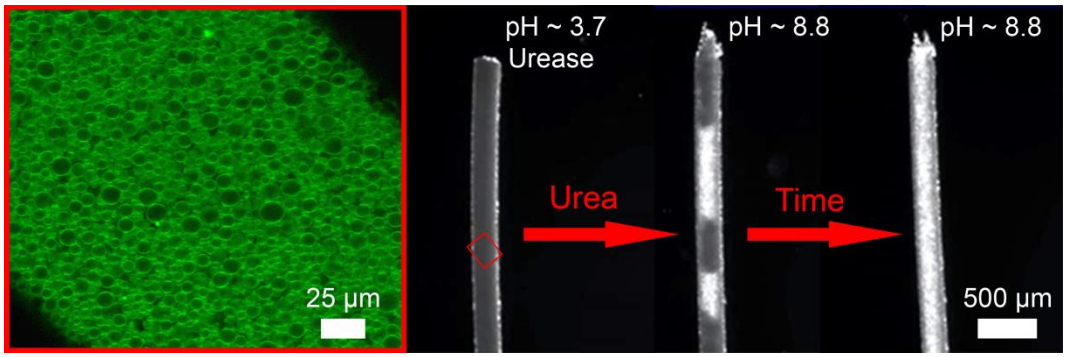


[§]Parts of this chapter are in preparation for publication. R. V. Bell, T. Heuser, R. W. Jaggers, C. M. Preuss, M. M. Stevens, A. Walther and S. A. F. Bon.

## 4.1. Introduction

Materials that have the ability to store, protect, and release actives in a controlled manner are showing a great deal of attention in numerous applications, such as in sensors, catalysis, ultrafiltration, and drug/molecule delivery systems.[1] Generally, these materials comprise of stimuli-responsive polymeric constituents, which are capable of receiving an external signal, like temperature, pH, or light stimuli, in order to experience conformation and chemical changes. These changes are accompanied by variations in the physical and chemical properties of the polymer that can be fine-tuned depending on requirements of the system. Materials that possess stimuli-responsiveness for controlled release, such as micelles,[2–5] vesicles,[6–8] layer by layer capsules,[9–11] core-shell microcapsules,[11–14] and hydrogels,[15–17] have been reported.

Emulsions are important materials since they allow the dispersion of an immiscible liquid in another continuous liquid phase, which have proven to be fundamental in many modern products and formulations.[18] Furthermore, emulsions are desirable in applications where large release of playloads are required because emulsions have a high loading capacity, high loading efficiency, and are capable to protect an encapsulated material from degradations during storage. Stimuli-responsive emulsions can be fabricated if the surfactants and particles that are employed−to kinetically stabilized emulsions−have ability to change their properties in response to external stimuli. Stimuli-responsive emulsions that response to pH,[19–21] $CO_2$,[22] or light,[23,24] have been reported. These emulsions can demulsify on demand due to the change of the wettability properties of the surfactants at the droplet interface upon exposure to external stimuli. In addition, stimuli-responsive emulsions that have the capability to assemble into supracolloidal structures and disassemble to individual disperse emulsion droplets in response to external stimuli have been reported.[25–29] Despite the development in the area of stimuli-responsive emulsions, it has remained a challenge to advance their properties from classical, passive responsiveness to a system that shows autonomous dynamics and self-regulating properties. Heuser *et al.* have reported autonomously self-regulating dynamic hydrogels with programmed lifetimes in a closed system.[30] The hydrogels are made of pH-

responsive dipeptides (Fmoc−Leu−Gly−OH) that are able to assemble to twisted ribbon-type nanofibrils and form hydrogels at low pH values, and disassemble at basic condition as a result of the formation of electrostatic repulsion between the dipeptides.[31] The programmed lifetimes of the hydrogels were achieved by combining a fast acidic activator (acidic buffer, fast promoter) with a slow urease-catalyzed hydrolysis of urea for feedback-driven generation of ammonia (ammonia, active deactivator) (**Figure 4.1**). The transient acidic pH states were programmed over orders of magnitude in time by varying the concentration of urease and urea, and the pH value and ionic strength of the acidic buffer in the system. Other self-regulating hydrogels with autonomous behavior in closed systems include kinetically controlled biocatalytic assembly of peptide nanofibers,[32] and energy-dissipating self-assembly of gelator with the use of chemical fuel,[33] have been reported.

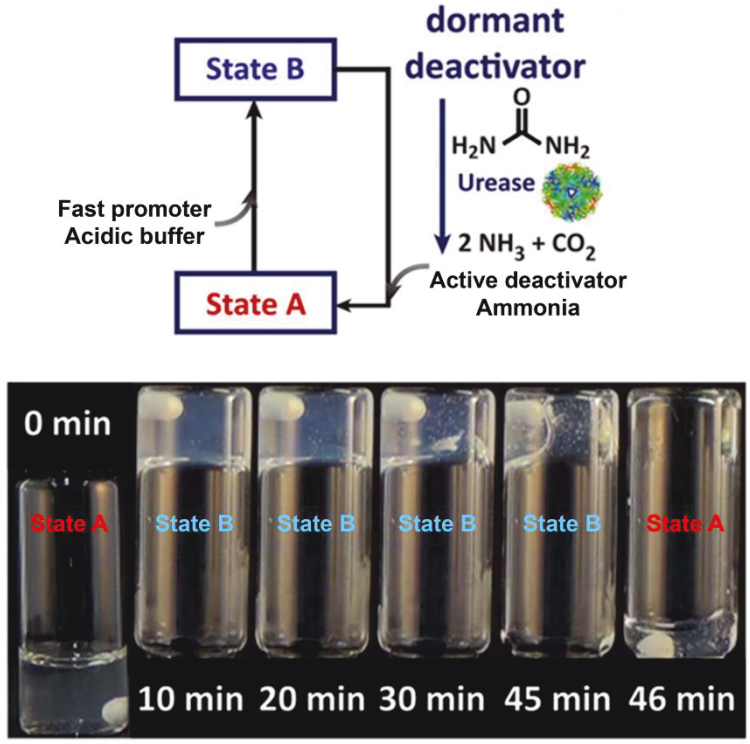


**Figure 4.1.** Enzyme-catalytic control of time-domain of pH-responsive dipeptide hydrogelators in a closed system. The programmed lifetimes of the hydrogels is achieved by combining a fast acidic activator (fast promoter) with urease-catalyzed hydrolysis of urea for slow feedback-driven generation of ammonia (active deactivator).[30] Adapted from Reference 30. Copyright (2015) with permission of John Wiley and Sons.

We recently showed that emulsion droplets stabilized with Laponite discs functionalized with branched copolymers can be microfluidically spun into supracolloidal fibers (Chapter 3).[34] The assembly of emulsion droplets into fibers arises from the ability of the branched copolymers to form reversible hydrogen bonds with a pH stimulus. Upon exposure to acidic environment, emulsion droplets assemble into fiber due to formation of inter/intra molecular hydrogen bonds between ethylene glycol and methacrylic acid residues in the polymer. Furthermore, the laminar fluid flow provided by the microfluidics process allows for easy fiber formation. The fibers can serve as storage for oils and hydrophobic cargos. Fibers with magnetic response, and asymmetric fibers with multiple cross-sectional segments, such as Janus (two segments) and 'toothpaste' (three segments), were fabricated by simple addition of hydrophobic materials to the oil phase of the emulsions.

Herein, we demonstrate Pickering emulsion droplets assembled into supracolloidal fibers by microfluidic wet spinning. These fibers can act as a storage material for emulsions, where emulsion droplets are locked in the fiber structure in acidic conditions, and are released from the fiber upon basification of the system. Emulsion droplets are only permitted to escape at the endpoints of the fiber as the fiber is coated with an inorganic-organic composite film. These self-regulating fibers display autonomous dynamics, and the release of emulsion droplets can be time-controlled by programming the transient acidic pH states of the system through the combination of a fast acidic promoter with a feedback-driven slow urease-catalyzed hydrolysis of urea for controlled generation of ammonia in a close system.

## 4.2. Results and Discussion

### 4.2.1. Fabrication and Characterization of Pickering Emulsion

Refer to Chapter 3 for a full detailed discussion for 'Synthesis and Characterization of pH-Responsive Branched Copolymer' (pH-BCP) (Chapter 3.2.1), 'Functionalization of Laponite with pH-Responsive Branched Copolymer' (Chapter 3.2.4), and 'Fabrication and Characterization of Pickering Emulsion' (Chapter 3.2.5).

A stable Pickering oil-in-water emulsion was produced with an average droplet diameter of 12.4 μm by homogenizing the oil phase (dodecane) in a basic aqueous solution containing Laponite discs functionalized with pH-responsive branched copolymers (pH-BCP-Laponite) (pH ~ 9.8, 50:50 vol%). The pH-BCP-Laponite stabilizes the emulsion droplets by *(i)* Pickering stabilization from the Laponite disc, *(ii)* the amphiphilic pH-BCP located at the positive rim of the disc that offers electrostatic stabilization from the methacrylic acid (MAA) domain at neutral and basic conditions, and *(iii)* steric stabilization by the poly(ethylene glycol) methyl ether methacrylate (PEGMA) domain. The multiple hydrophobic chain ends, 1−dodecanethiol (DDT), arising from the branched architecture of the polymer, provide strong oil-droplet surface adsorption (**Figure 4.2A**). The light micrograph of the Pickering oil-in-water emulsion is shown in **Figure 4.2B**.

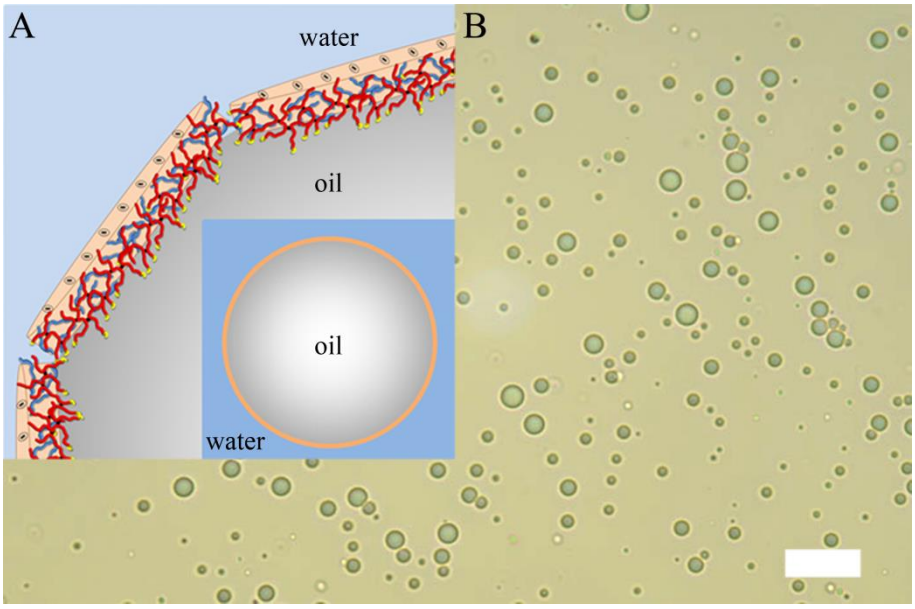


**Figure 4.2.** (A) Schematic illustration of the Pickering oil-in-water emulsion droplet stabilized with the pH-BCP-Laponite. The pH-BCP-Laponite acts as a Pickering stabilizer with additional electrostatic and steric stabilizations arising from the pH-BCP adsorbed on the Laponite disc. The pH-BCP-Laponite (Blue = PEGMA domain, red = MAA domain, black = branching unit, EGDMA, and yellow = hydrophobic chain ends, DDT) adsorb on the positive rim of the disc by electrostatic interaction and hydrogen bonding. (B) Light micrograph of Pickering oil-in-water emulsion droplets stabilized with pH-BCP-Laponite in basic aqueous solution (pH 11). Scale bar represents 25 μm.

### 4.2.2. Fabrication of Microfluidically Spun Fiber Made Out of Emulsion Droplets

The fibers were spun by employing a double coaxial laminar flow microfluidic device composed of two pulled inner capillaries (injection and collection inner capillaries) and one regular glass capillary (outer capillary) (**Figure 4.3**). The two inner capillaries were aligned within the outer capillary to produce a flow-focusing junction, where the fibers were fabricated through assembly of the emulsion droplets. The injection inner capillary contained the concentrated emulsion, and the outer capillary contained the sheath fluid, (poly(vinyl alcohol) (PVA) acidic solution at pH 3). Both the emulsion and sheath fluid were kept at continuous flow.

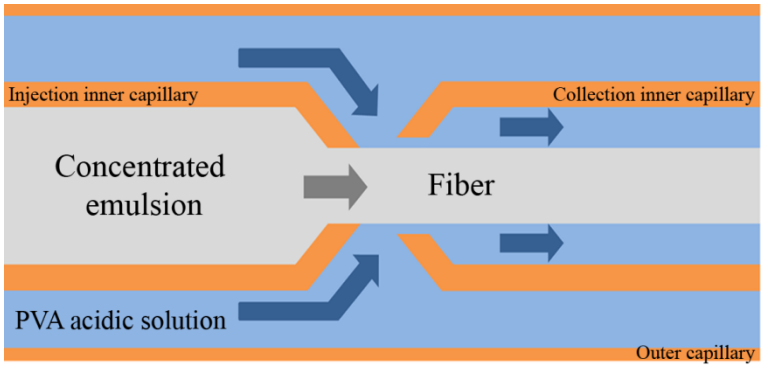


**Figure 4.3.** Schematic representation of the fabrication of microfluidically spun fiber made out of emulsion droplets. The diagram shows coaxial flow channels in the microfluidic device, where the inner and outer capillaries contain concentrated emulsion and poly(vinyl alcohol) (PVA) acidic solution, respectively, in a continuous flow. A continuous fiber is produced upon exposure of the emulsion to the PVA acidic solution. The acidic conditions allow the formation of multiple hydrogen bonds between emulsion droplets, initiating them to assemble into a macroscopic supracolloidal fiber.

Upon contact with the PVA acidic solution, the emulsion droplets lose their electrostatic repulsive interaction owing to the protonation of the carboxylic acid groups. The emulsion droplets are 'locked' in the fiber structure upon collision through a combination of van der Waals interactions, and hydrogen bonding between ethylene glycol and MAA residues in the branched copolymers. Hereby, producing a uniform fiber composed of emulsion droplets in a continuous manner (**Figure 4.4**).

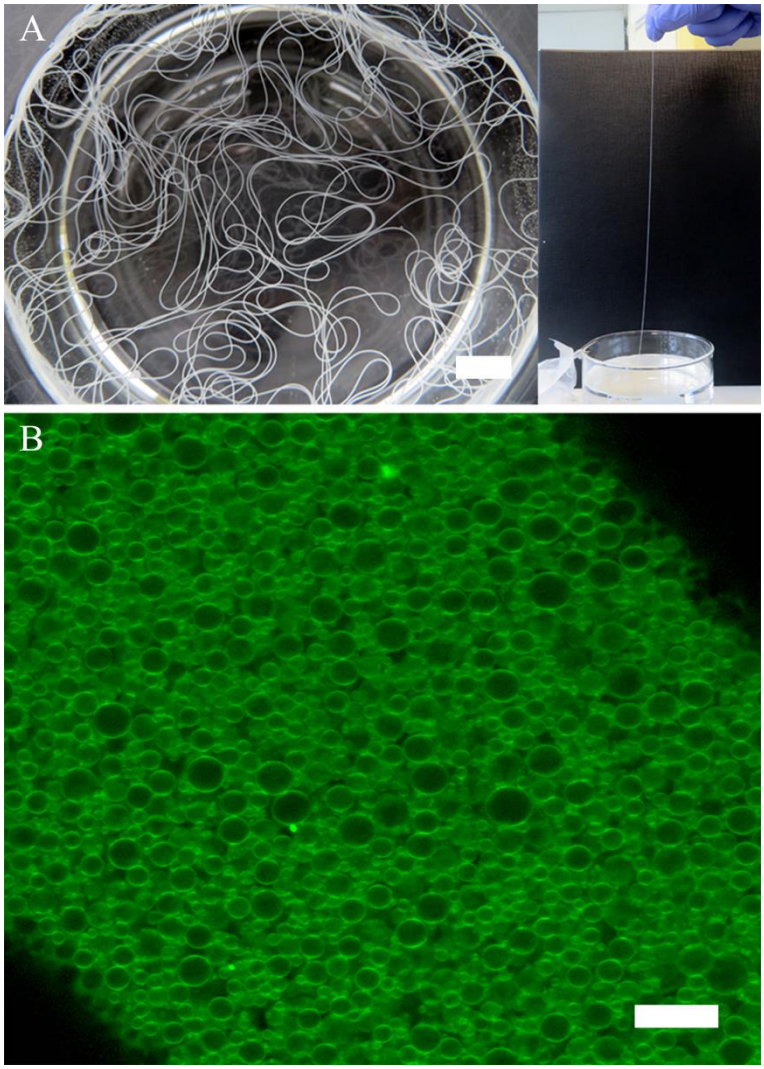


**Figure 4.4.** (A) Photograph of continuous long microfluidically spun fibers. Scale bar represents 1 cm. (B) Confocal micrograph of the fiber comprising of emulsion droplets loaded with a florescent dye. Scale bar represents 25 μm.

We discovered that the fibers fabricated did not fully disintegrate upon pH increase. Upon closer inspection of the fiber fragments, it became apparent that the fiber was coated with a stable pH-resistant coherent film. The formation of the film on the fiber was a spontaneous process, and was mainly due to the present of PVA in the sheath fluid and Laponite clay in the concentrated emulsion solution. PVA is a hydrophilic uncharged polymer which contains a large amount of hydroxyl groups. These hydroxyl groups form multiple hydrogen bonds to the oxygen of the $SiO_4$ tetrahedrons on the basal plane of the Laponite disc, and the vacant hydroxyl group of Si−OH and pH-BCP on the rims of the Laponite discs. Laponite clay and PVA have been utilized to fabricate polymer/clay composite films by layer-by-layer process.[35–37]

Furthermore, we discovered that when we manually cut the isolated supracolloidal fibers into fragments and exposed them to an aqueous solution of high pH (pH 10 – 11), emulsion droplets were released solely from the two ends of the fiber structure (**Figure 4.5A, Figure 4.5B, and Figure 4.5C**). The composite polymer/clay film that coats the fiber acts as a physical barrier between the emulsion droplets in the fiber structure and the exterior medium. Manually cutting the fiber creates areas where the composite film is not present, and, thus, creating exit points. Upon basification of the system, emulsion droplets in the fiber structure disassemble into individual emulsion droplets allowing them to escape individually from the ends of the fiber in a fluidic manner. After the release, a supracolloidal emptied tube was left behind (**Figure 4.5D**).

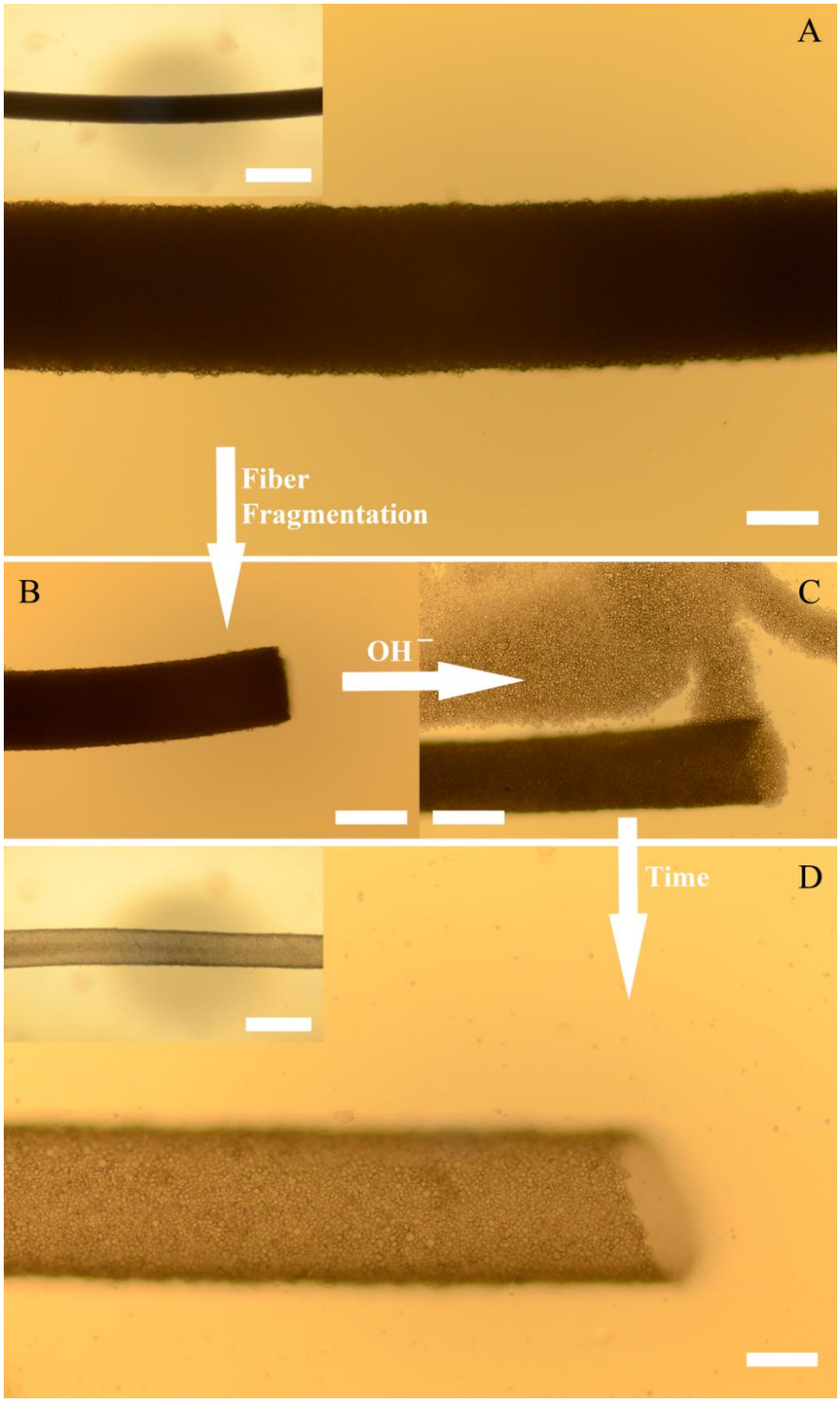


**Figure 4.5.** Light micrographs of the fiber before release, during release, and after release. (A) Fiber under acidic condition (pH 3). Scale bars represent 100 µm and 500 µm in the large and small light micrographs, respectively. (B) Fragmentation of the fiber by manually cutting the fiber with a scissor. No release of emulsion droplets from the fiber under acidic condition (pH 3). Scale bar represents 200 µm. (C) Emulsion droplets are released only at the end point of fiber upon basification of the medium (pH 10 − 11). Scale bar represents 200 µm. (D) An empty supracolloidal tube is left behind after the release. Scale bars represent 100 µm and 500 µm in the large and small light micrographs, respectively.

The tubular material is a thin flexible composite film (PVA-Laponite-pH-BCP composite film) embedded with emulsion droplets throughout the film (**Figure 4.6**).

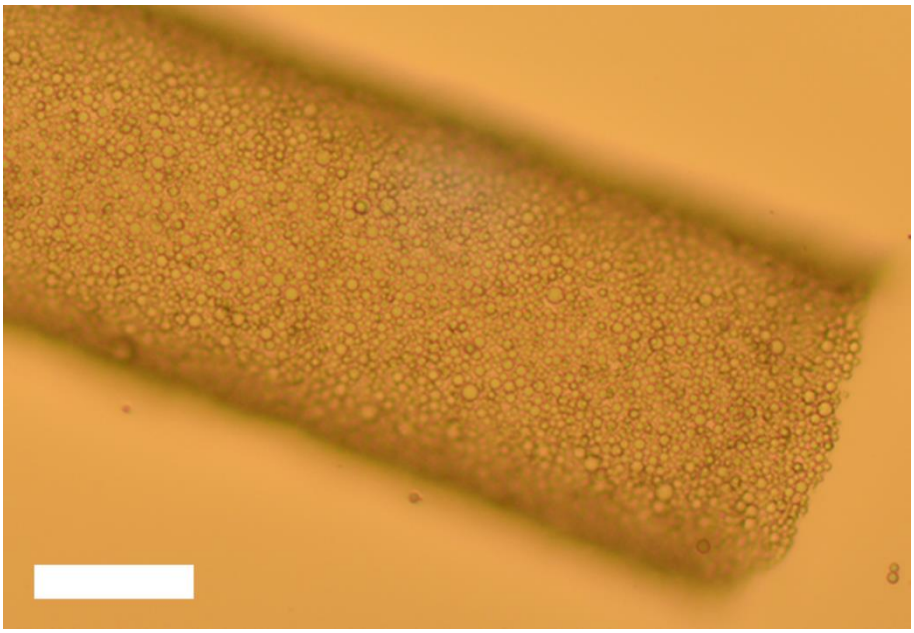

**Figure 4.6.** Light micrograph of the supracolloidal composite polymer/clay tube embedded with emulsion droplets. Scale bar represents 100 μm.

The release of emulsion droplets from the fiber can be arrested by changing the pH value of the medium back to ~3, or by permanently cross-linking the emulsion droplets inside the fiber with calcium ions. Interestingly, when we manually cut the fiber into fragments and dip them into an acidic or neutral solution containing PVA (3 w/v%) and subsequently transferring them to a basic aqueous solution, no release was observed (**Figure 4.7**). This essentially meant that PVA had the ability to repair ('self-heal') and reseal the exit points of the fiber fragments. This is because the free pH-BCP-Laponite discs present on surface the fiber will always interact and form a film if sufficient amount of PVA is present in the exterior medium.

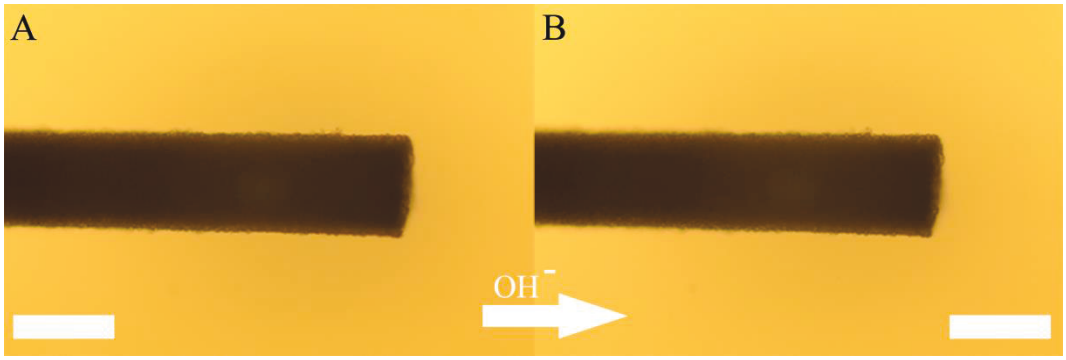


**Figure 4.7.** Light micrograph of the fragmented fiber dipped in acidic or neutral solution containing PVA (3 w/v%) to reseal the exit point of the fiber. (A) Resealed fiber under acidic condition (pH 3). (B) Resealed fiber under basic condition (pH 10 − 11). No release of emulsion droplets from the resealed fiber upon basification of the medium. Scale bars represent 200 µm.

### 4.2.3. Fabrication and Release Profile of 'Matchstick' Fibers

Apart from cutting the fibers manually, fibers can also be cut by utilizing air bubbles. Fibers with desired lengths were generated by separating the concentrated emulsion into defined segments in the injection inner capillary with air bubbles prior to exposure to the sheath fluid (**Figure 4.8**).

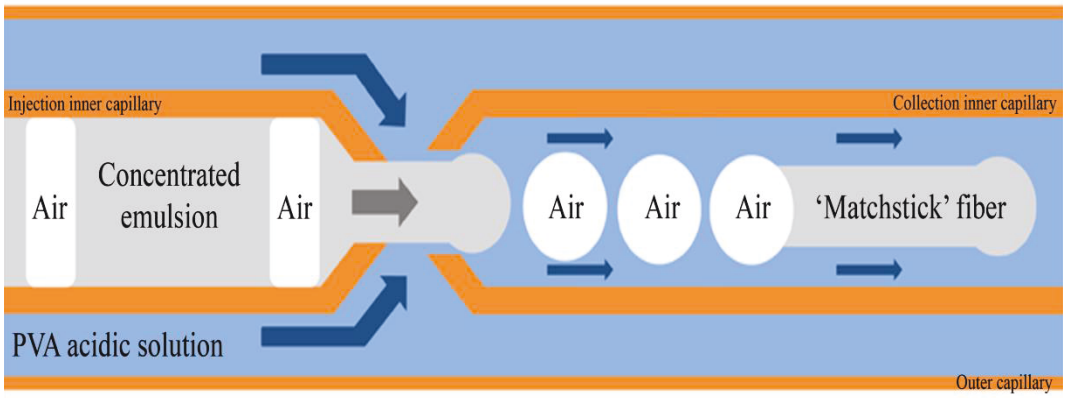


**Figure 4.8.** Schematic representation of the fabrication of 'matchstick' fibers. The diagram shows coaxial flow channels in the microfluidic device, where the inner and outer capillaries contain concentrated emulsion and poly(vinyl alcohol) (PVA) acidic solution, respectively, in a continuous flow. Fibers ('matchstick' fiber) with desired lengths are generated by separating the concentrated emulsion into defined segments in the injection inner capillary with air bubbles prior to exposure to the sheath fluid. A spherical air bubble is temporally fixed on the 'tail' of the 'matchstick' fiber upon exposure to the sheath fluid. The air bubble prevents the formation of the composite film on the 'tail' of the 'matchstick', creating an exit point for emulsion droplets to escape upon basification of the medium.

The advantage of this process compared to cutting the fiber manually is the production of numerous fibers with uniform length in a short period time (**Figure 4.9**).

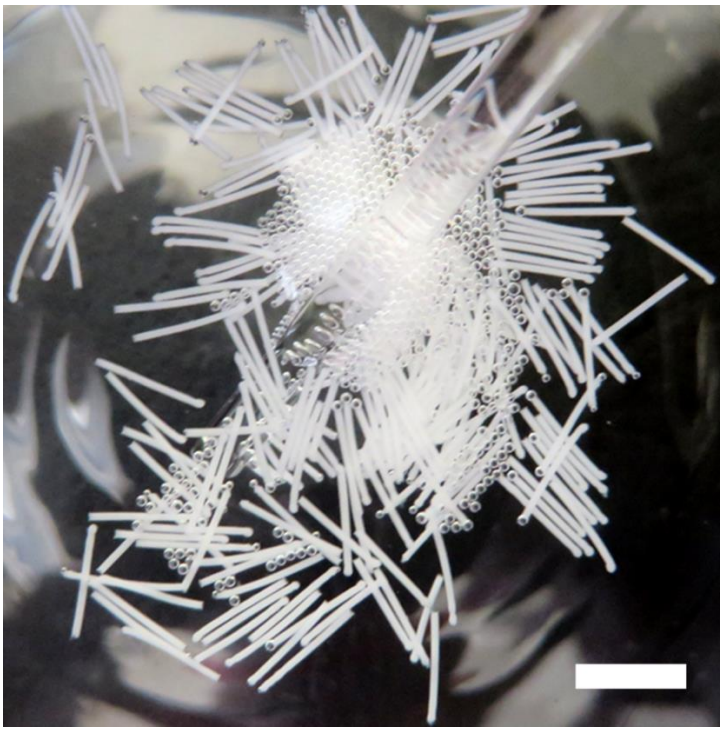

**Figure 4.9.** Photograph of 'matchstick' fibers with uniform length. The 'matchstick' fibers were fabricated by 'air bubble cutting' process. Scale bar represents 0.5 cm.

The 'air bubble cutting' process created fibers which resemble the shape of a matchstick. These uniform fibers have a 'head' at one end and a 'tail' on the other end of the fiber (**Figure 4.10**).

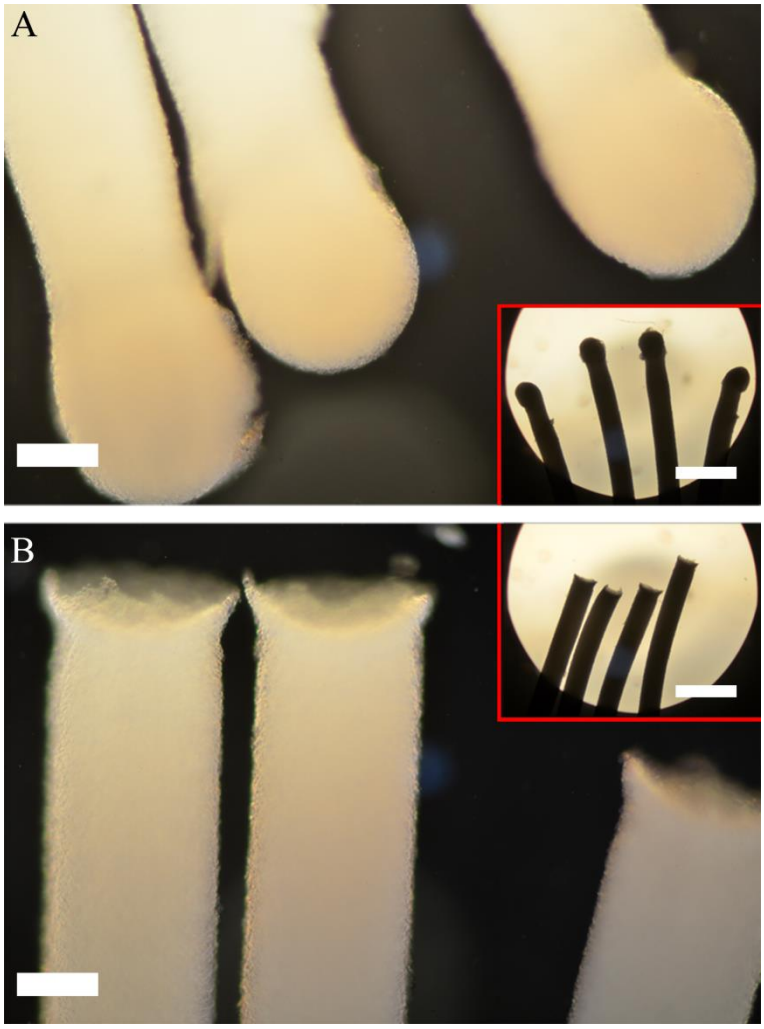


**Figure 4.10.** Dark (base images) and bright (overlay images) fields light micrographs of the 'head' (A) and 'tail' (B) of 'matchstick' fibers. Scale bars represent 100 µm and 500 µm on the base and overlay light micrographs, respectively.

The 'head' of the 'matchstick' fiber is created when the concentrated emulsion is initially exposed to the sheath fluid. The round shape of the 'head' forms due to the minimization of the surface energy between the concentrated emulsion and the sheath fluid. On the other hand, the end of the 'tail' of the 'matchstick' fiber has an arc shape (**Figure 4.10B**). This originates from the 'bubble cutting' process, where a spherical air bubble is temporally fixed at the end of the 'tail' upon exposure to the sheath fluid. Moreover, the temporally fixed bubble on the 'tail' prevents the formation of the composite clay/polymer film at the end of the 'tail', and therefore, creates an exit point for emulsion droplets to escape upon basification of the medium. Emulsion droplets are only released from the end of the 'tail' of the 'matchstick' fiber upon basification of the solution (pH 10 − 11) as shown in **Figure 4.11** and **Movie 4.1**.

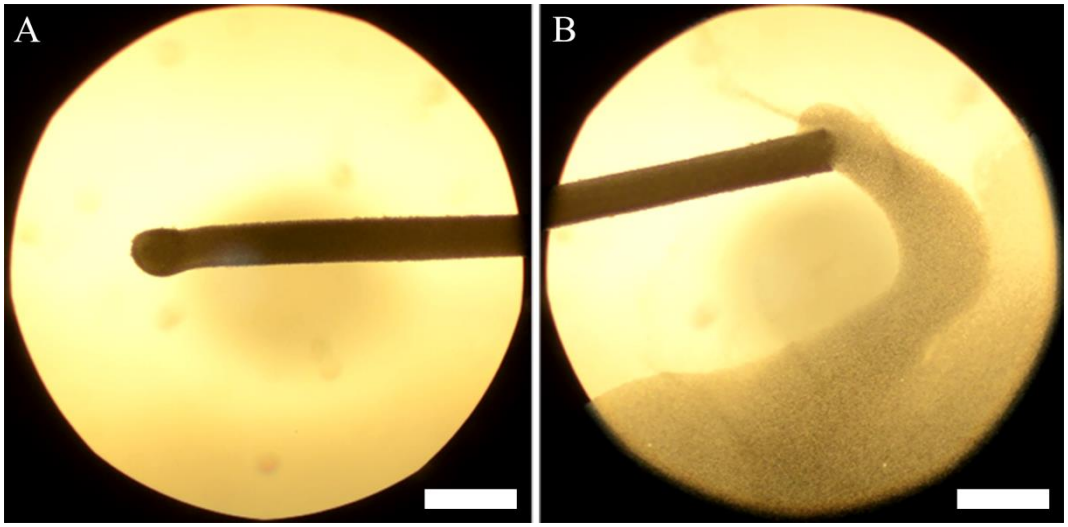


**Figure 4.11.** Still images taken from **Movie 4.1** showing no release of emulsion droplets from 'head' and the main body (A) and release only occurs from the end of the 'tail' (B) of the 'matchstick' fiber upon basification of the system. Scale bars represent 500 µm.

### 4.2.4. Enzymatic Catalyzed Feedback-Driven of Time-Controlled Release of Emulsion Droplets from Fibers

Now that we have established that these supracolloidal fibers can act as storage materials for emulsions, where emulsion droplets are locked in the fiber structure in acidic media, and are released only from both ends of the fiber upon basification of the system. We can add complexity to the system in a way that allows for time-controlled release of emulsion droplets from the fiber by programming the transient acidic pH states *via* the combination of a fast acidic promoter (acidic buffer) with a slow urease-catalyzed feedback-driven generation of ammonia.

The time-controlled release of emulsion droplets from the fiber is illustrated in **Figure 4.12**. A fiber with a specific length was manually cut and submerged into an acidic solution containing an enzyme−urease. The solution was acidified with an acidic buffer to give a solution pH value of ~ 3.7 (to give a final concentration of 20 mM of acetic acid/sodium acetate buffer at 9:1 volume ratio). The fiber did not show any release of emulsion droplets at this pH value. At pH ~ 3.7, all of the carboxylic groups in the pH-BCP are all protonated, and, therefore, there is a 100 % hydrogen bonding between the EG : MAA residues in the polymer. The p$K_a$ of the pH-BCP was determined to be 6.46 by titration (Chapter 3.2.2). The hydrogen bonds formed between the residues 'lock'

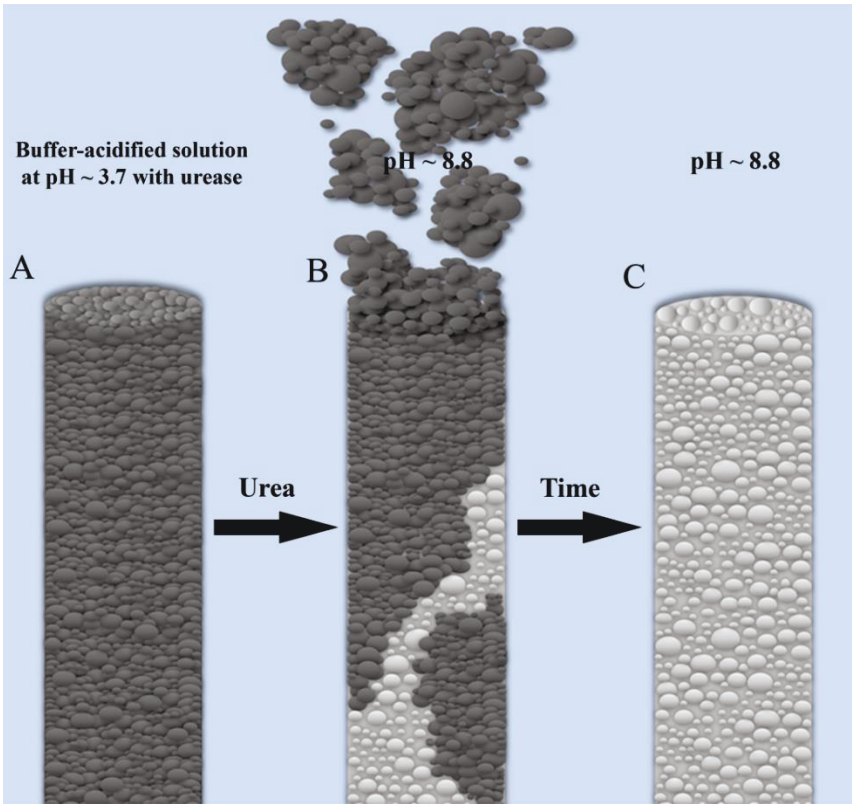


**Figure 4.12.** Schematic representation of the enzymatic catalyzed feedback-driven of the time-controlled release of emulsion droplets from a fiber. (A) Pickering emulsion droplets assembled into fibers by microfluidic wet spinning coated with a composite film. The fiber is in a buffer-acidified solution containing an enzyme (urease) at pH ~ 3.7. (B) Urea is added to initiate the release of emulsion droplets from the fiber. Ammonium hydroxide is produced by the urease-catalyzed conversion of urea into ammonia and carbon dioxide. Base generation lifts the pH value to ~ 8.8, and permits the release of emulsion droplets from the fiber. (C) A composite polymer/clay film embedded with emulsion droplets hollow tube is left after the release.

the emulsion droplets in the fiber structure and prevents any release of emulsion droplets from the fiber. The release of emulsion droplets from the fiber was initiated with the addition of urea to the acidic solution containing urease (to give a final concentration of 60 mM of urea). The urease present in the acidic solution is an enzyme that catalyzes the hydrolysis of urea into ammonia and carbon dioxide, and the ammonia produced then reacts with water to form ammonium hydroxide.[30,38] The homogeneous generation of base offers a negative pH feedback and increases the pH value without any external interference (closed system), which leads to release of emulsion droplets from the fiber. Another advantage of this approach is the catalytic nature of the process, in which the rate of base generation can be fine-tune through the enzyme concentration in the system (**Figure 4.13**).

**Figure 4.13** shows the pH profile of the buffer-acidified solution with time at different urease concentrations.

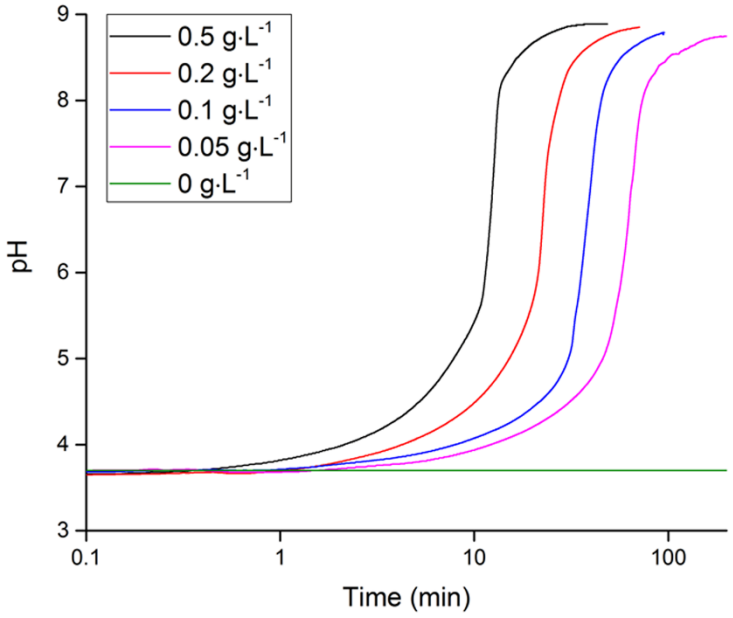


**Figure 4.13.** The pH profile of the buffer-acidified solution with time at different urease concentrations. The urea was added at 0 minute (Final solution concentration = 20 mM of acetic acid/sodium acetate buffer at 9:1 volume ratio and 60 mM urea).

Fidaleo and Lavecchia reported that the activity of urease is dependent on the pH of the media.[38] Urease has a bell-shaped curve enzymatic activity, where low enzyme activity are seen at low and high pH values (pH < 4 and pH > 9), and an optimum enzyme activity at pH ~ 7. At pH ~ 3.7 (initial pH value of the solution), urease has a low catalytic activity and slow generation of base, and therefore, creates a plateau at low pH values (**Figure 4.13**). The elongation of the plateau at low pH values was observed with the decrease of urease concentration as fewer enzymes are present for the generation of base. At pH > 4, increase in pH value occurs immediately as urease is in the pH window of higher catalytic activity. Eventually, all the curves for the different enzyme concentrations level off at pH ~ 8.8 as urease leaves the high activity zone and becomes inactive again. In addition, an ammonia buffer gives a pH value of ~ 9. As the pH value increases with time, due to the slow enzymatic generation of base, the carboxylic groups of the pH-BCP are gradually deprotonated. The de-protonation of the carboxylic groups destabilizes the hydrogen bonding between the EG and MAA residues of the polymer. Eventually, the combination of *(i)* the loss of multiple hydrogen

bonds between the residues, *(ii)* the newly gain of electrostatic stabilization from the carboxylate group, and *(iii)* the density difference between the oil phase of the emulsion and the medium, allow emulsion droplets to be release from the fiber. The composite polymer/clay film that coats the fiber acts as a physical barrier between the emulsion droplets in the fiber and the exterior medium. Manually cutting the fiber created areas where the composite film was not present. These newly formed areas become the only exit points for emulsion droplets to escape from upon basification of the system.

The inhibition and release profiles of the fibers were video recorded and analyzed with a video camera (**Movie 4.2 and Movie 4.3**). Still images of the inhibition and release profiles of the fiber are shown in **Figure 4.14.** The inhibition stage is the total time where there was no release of emulsion droplets from the fiber after the addition of urea into the system. On the other hand, the release stage is the total time required to fully empty the fiber of emulsion droplets.

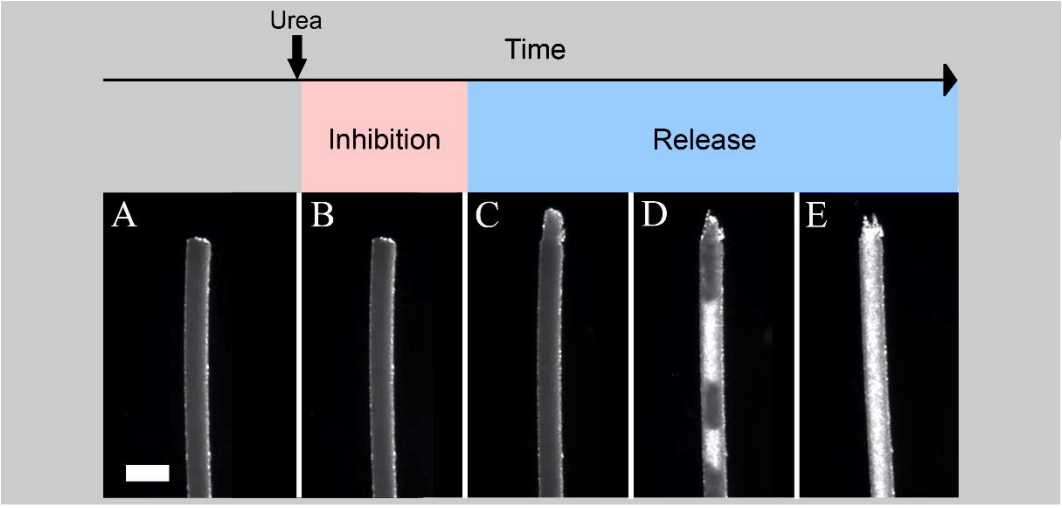


**Figure 4.14.** Still images taken from the video recordings showing the inhibition and release profiles of the fiber. (A) Fiber in acidic solution containing urease. (B) Urea is added in the acidic solution containing urease to initiate emulsion release from the fiber (Inhibition stage, $Time_{inibition}$ = 0 s). No release of emulsion droplets from the fiber. (C) Initial release of emulsion droplets from the fiber (Release stage, $Time_{release}$ = 0 s). (D) Continuous release of emulsion droplets from the fiber. (E) Fully empty fiber. Scale bar represents 500 µm.

The inhibition and release time profiles for 1 cm fiber at different concentrations of urease are shown **Figure 4.15 and Movie 4.2**.

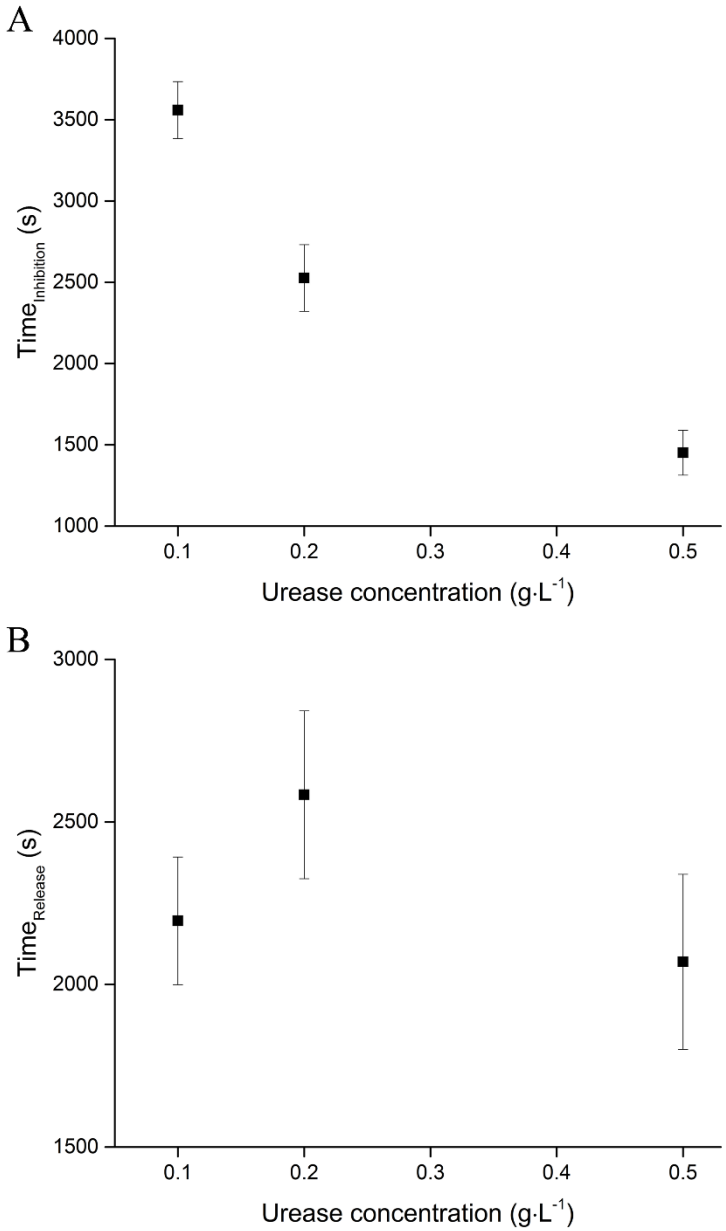


**Figure 4.15.** The inhibition (A) and release (B) times of emulsion droplets from a 1 cm fiber at different urease concentrations.

**Figure 4.15A** shows the inhibition time of the fiber decreases with the increase of urease concentration as there are more enzyme present for the generation of base, and hence, shortening the plateau time at low pH values. There was no release of emulsion droplets from the fiber for all the enzyme concentrations until the maximum pH value was reached (pH ~ 8.8) because hydrogen bonds are still acting between the pH-BCP, which in turn locks the emulsion droplets in the fiber structure. The release of emulsion droplets from the fiber was only observed once the system attained a pH value of ~ 8.8. At this pH value, only 0.01 % of the

carboxylic groups in the pH-BCP are protonated. The p$K_a$ of the pH-BCP was determined to be 6.46 by titration (Chapter 3.2.2). Therefore, there are only 0.01 % hydrogen bonding between the EG : MAA residues in the polymer, and as consequence, emulsion droplets are released from the fiber. It was observed that emulsion droplets were released as aggregates from the fiber and eventually disperses into individual droplets in the exterior medium with time. This is most likely due to the limited availability of $OH^-$ in the system and the slow rate of diffusion of $OH^-$ into the fiber. In contrast, there was no significant difference on the time required to fully empty a 1 cm fiber at different concentrations of urease as a 1 cm fiber will contain the same amount of emulsion droplets inside the fiber (**Figure 4.15B).** The release time values are within the error bars but large error bars were obtained. This might arise from the fact that the emulsion droplets are released from the fiber as aggregates rather than in a fluidic manner, and therefore, the release of emulsion droplets is not constant. We also considered whether the length of the fiber would have an influence on the inhibition and release time profiles of the fiber at the same urease concentration of 0.5 $g \cdot L^{-1}$ (**Figure 4.16 and Movie 4.3**). It was also observed that there was no release of emulsion droplets from the fiber below the pH value of ~ 8.8 and release only occurs at this pH value or above. As shown in **Figure 4.16A**, the inhibition time increases with increase in length of the fiber at the same enzyme concentration. This is because a longer fiber contains more pH-BCP compared to a shorter fiber, and hence, requires more $OH^-$ to deprotonate the carboxylic groups in the polymer, which in turn extends the inhibition time. In **Figure 4.16B**, the release time of the fiber increases in a linear fashion with the increase in fiber length at the same enzyme concentration. A longer fiber will contain a higher number of emulsion droplets in the internal structure of the fiber compared to a shorter fiber, and hence, requires more time to fully empty the fiber.

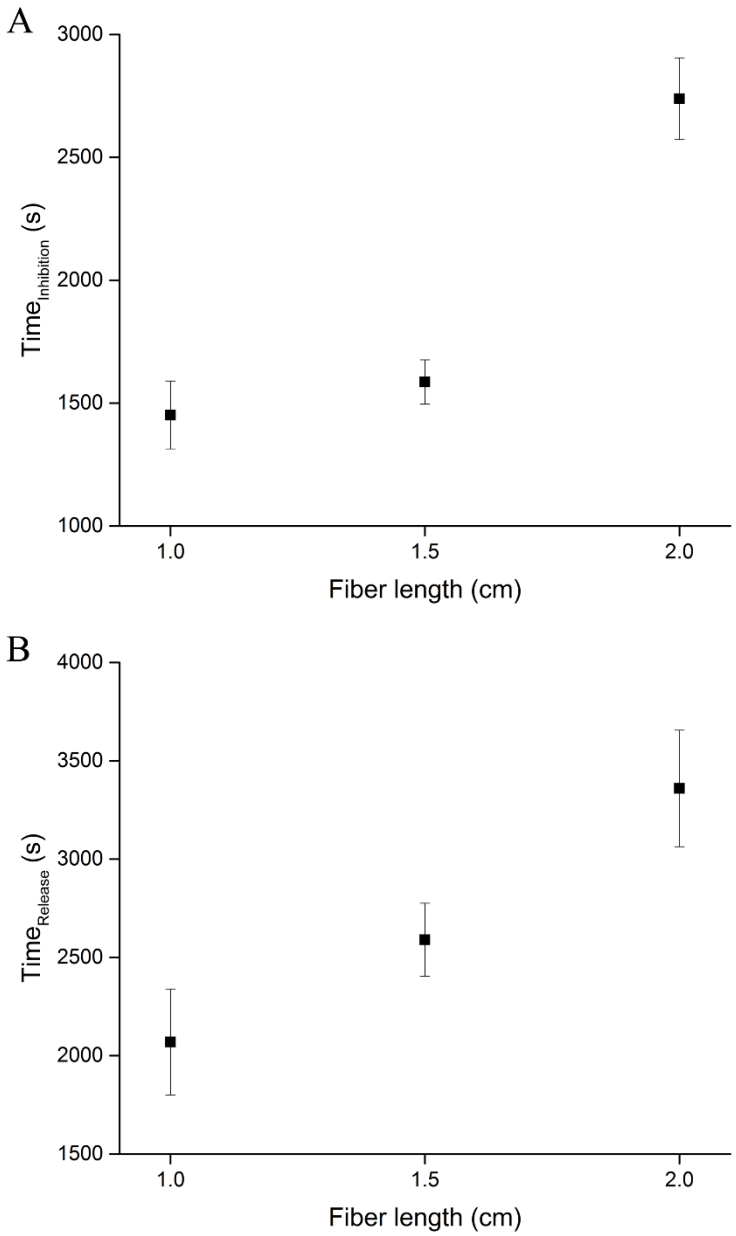


**Figure 4.16.** The inhibition (A) and release (B) times of emulsion droplets from different fiber lengths with the same concentration of urease.

### 4.2.5. Fabrication and Release Profile of 'Cake' Supracolloidal Macrostructure with Multiple Layers

Numerous supracolloidal structures with different shapes can be fabricated with the use of templates. Here, we demonstrate the fabrication a supracolloidal structure in the macro range size, coined 'cake', with the use of a cylindrical mold. The 'cake' contains three layers (red, white, and blue) and a cap (white). These layers were composed of concentrate Pickering oil-in-water emulsion stabilized with pH-BCP-Laponite. The red and blue layers were produced by encapsulating

dyes in the oil phase of the emulsion droplets, whereas the white layer did not contain any dye. On the other hand, the cap was composed of concentrate oil-in-water emulsions solely stabilized with pH-BCP. The layers and cap were set in place simultaneously with the addition of gluconic acid δ−lactone in the unset concentrated emulsions. Gluconic acid δ−lactone generates acid homogenously in the system, which is required for the production of hydrogen bonds between the EG : MAA residues in the pH-BCP. Once the layers and cap were set, the 'cake' was then dipped in a PVA acidic solution (pH 3, 3 w/v% PVA). The dipping process creates a composite polymer/clay film around the 'cake' except on the cap because Laponite clay is not present in the cap.

The release of emulsion droplets from the 'cake' was performed in an acidic solution (pH 3, adjusted with 1 M HCl) and was initiated with the addition of base (pH 10 – 11, adjusted with 1 M NaOH). **Figure 4.17 and Movie 4.4** show the release of emulsion droplets from the 'cake'.

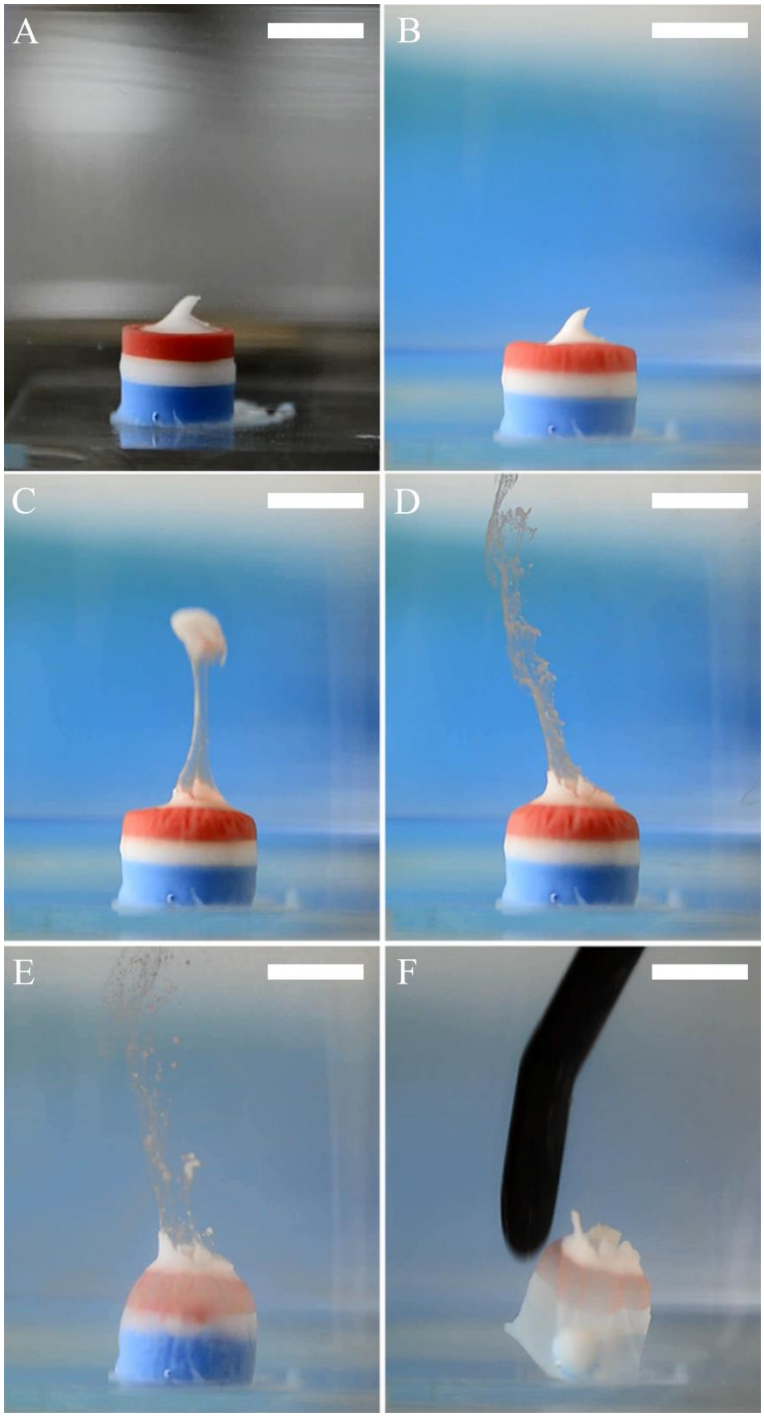


**Figure 4.17.** Still images taken from **Movie 4.4** showing the release of emulsion droplets from the 'cake'. The 'cake' in acidic (A) and basic (B-F) conditions. (A) No emulsion droplets released from the 'cake'. (B) Base is added to initiate release of emulsion from the 'cake'. (C) The cap comes off from the top of the 'cake', and allows the release of emulsion droplets from the 'cake' (D). (E) Two layers have been released from the 'cake' with time (red and white layers). (F) A composite film ('bag') remains after all the layers have been released from the 'cake'. A magnetic stirrer bar can be seen inside the composite film bag. It was used to add weight and to submerge the 'cake' in the acidic water. The magnetic stirrer bar was embedded in the 'cake' structure during the setting process of the layers. Scale bars represent 0.5 cm.

There was no release of emulsion droplets in acidic conditions (**Figure 4.17A**). There was also no release of emulsion droplets with the basification of the system (**Figure 4.17B**). Emulsion droplets were only released from the 'cake' once the cap came off from the top of the 'cake', which happened due to basification of the system. (**Figure 4.17C**). Layers were released simultaneously, in the order of red, white, blue layers, respectively. A flexible composite film was left after all the layers have been released from the 'cake' (**Figure 4.17D**).

## 4.3. Conclusions

We have shown that microfluidically spun supracolloidal fibers can act as a storage material for emulsion droplets, were emulsion droplets are locked in the fiber structure in acidic condition, and are released from the fiber upon basification of the system. The fiber was coated with a flexible composite clay/polymer film, which acts as a physical barrier between the emulsion in the fiber structure and the exterior medium, and only permits the outflow of emulsion droplets at the endpoints of the fiber. The release of emulsion droplets from the fiber was time-controlled by programming the transient acidic pH states of the system by combining a fast acidic promoter with a feedback-driven urease-catalyzed controlled slow generation of ammonia in a close system. These fibers show autonomous dynamics and self-regulation properties. Fabrication and release profiles of other supracolloidal structures, such as ‘matchstick’ fiber and ‘cake’ have been demonstrated, suggesting the versatility of the material.

## 4.4. Experimental

### 4.4.1. Materials

Poly(ethylene glycol) methyl ether methacrylate (PEGMA, $M_n$ = 1100 g·mol$^{-1}$, Sigma-Aldrich), methacrylic acid (MAA, 99 %, Sigma-Aldrich), ethylene glycol dimethacylate (EGDMA, 98 %, Sigma-Aldrich), 1−dodecanethiol (DDT, ≥98 %, Sigma-Aldrich) and (trimethylsilyl)diazomethane (2 M in hexane, Sigma-Aldrich). 2,2'−Azobis(isobutyronirile) (AIBN, BDH) was recrystallized from methanol prior to use. Deuterated chloroform and methanol were purchased from Sigma-Aldrich. All organic solvents were standard laboratory grade. Laponite RD (BYK), dodecane (≥99 %, Sigma-Aldrich), oil blue N (96 %, Sigma-Aldrich), oil red O (Sigma-Aldrich), nile red (technical grade, Sigma-Aldrich), D−(+)−gluconic acid δ−lactone (≥99 %, Sigma-Aldrich), mowiol 8−88 (PVA, $M_w$ ~ 67,000 g·mol$^{-1}$, Sigma-Aldrich), ammonium hydroxide (35 %, Fisher chemical), hydrochloric acid (37 %, Analar Normapur), sodium hydroxide pellets (Fisher chemical), urea (99 − 100.5 %, Sigma-Aldrich), acetic acid glacial (Laboratory reagent grade, Fisher Scientific), and sodium acetate anhydrous (>99 %, Sigma-Aldrich) were used as received. The urease was from Canavalia ensiformis (Jack bean) (Type III, 15000 – 50000 units/g solid, Sigma-Aldrich).

### 4.4.2. Synthesis of pH-Responsive Branched Copolymer

Refer to Chapter 3.4.2.

### 4.4.3. Characterization of pH-Responsive Branched Copolymer

Refer to Chapter 3.4.3.

### 4.4.4. Fabrication and Characterization of Emulsions

Refer to Chapter 3.4.5.

### 4.4.5. Fabrication of Microfluidic Device and Fibers

A glass capillary with an inner and outer diameter of 1.16 mm and 2.0 mm, respectively, forms the outer capillary of the device, and contains the sheath fluid. Within the outer capillary, two capillaries (injection and collection inner capillaries) with inner and outer diameters of 0.58 mm and 1.0 mm, respectively,

were tapered with a laser puller to allow flow focusing of the concentrated emulsion. The injection inner capillary and collection inner capillary has a diameter of ~ 110 μm and ~ 120 μm, respectively. The inner capillaries were aligned to produce a flow-focused junction where the fibers are fabricated. The optimum flow rates for the fiber fabrications were 0.1 $mL \cdot min^{-1}$ for the sheath fluid and 0.02 $mL \cdot min^{-1}$ for the concentrated emulsion. Harvard Apparatus PHD 2000 Infusion was used as the pumping system. The sheath fluid was a PVA acidic solution (3 w/v%) and was acidified by adding gluconic acid δ−lactone (3 w/v%). All fibers were collected in an acidic aqueous solution reservoir (pH 3, adjusted by addition of 1 M HCl). The photograph and light micrographs of the microfluidics device are show in **Figure 4.18A-Appx** and **Figure 4.18C-Appx**. The release was performed in an acidic solution (pH 3, adjusted with 1 M HCl), and initiated with the addition of 1 M NaOH (pH10 − 11).

### 4.4.6. Confocal Micrograph of Fibers

To image the fiber under confocal microscopy, Nile red (0.1 w/v%) was dissolved in the oil phase of the emulsion prior to the emulsification process. Nile red loaded fibres were imaged with a confocal laser scanning microscope (Leica TCS SP5, Leica Microsystems). Confocal micrograph (1024 x 1024 pixels, 8 bit pixel depth, 4.0x digital zoom, 1024 line average) was acquired on a Leica DMI6000 microscope using a HC PL FLUOTAR 40.0 x 0.75 dry objective lens, at a scan speed of 8000 Hz. Nile red (9-diethylamino-5-benzo-α-phenoxazinone) was visualised using a white light laser (λ = 549 nm, 67 % intensity) with a spectral detection window of 618 − 719 nm. Data was collected and analysed using the Leica LAS-AF confocal acquisition software.

### 4.4.7. Release of Emulsion Droplets from Fibers by Enzymatic Catalyzed Feedback-Driven Process

Fibers were submerged in a buffered-acidified solution containing urease (final concentration of 20 mM of acetic acid/sodium acetate buffer at 9:1 volume ratio, pH ~ 3.7). The concentrations of urease in the solution were 0.5 $g \cdot L^{-1}$, 0.2 $g \cdot L^{-1}$ and 0.1 $g \cdot L^{-1}$ for varying enzyme concentration with similar fiber length (1 cm) experiment. Urease concentration of 0.5 $g \cdot L^{-1}$ was used for varying fiber length (1 cm, 1.5 cm, and 2 cm) with constant enzyme concentration experiment. Fibers

were manually cut with a scissor to the specific length required. The release of emulsion droplets from the fiber was initiated with the addition of urea (to give a final concentration of 60 mM urea). The inhibition and release profiles of the fibers were recorded and analyzed using the camera of the droplet shape analyzer (KRUSS DSA 100).

### 4.4.8. Fabrication of 'Matchstick' Fibers

'Matchstick' fibers were fabricated by having two inlets to the injection inner capillary. The photograph and light micrographs of the microfluidics device are show in **Figure 4.18B-Appx** and **Figure 4.18C-Appx**. The flow parameters to fabricate uniform 'matchstick' fibers (0.1 cm in length) were *(i)* outer capillary contained PVA acidic solution at a flow of 0.1 $mL \cdot min^{-1}$ (similar solution concentration to the PVA acidic solution mentioned in Chapter 4.4.5), *(ii)* injection inner capillary inlet 1 contained nothing (air) at a flow rate of 0.01 $mL \cdot min^{-1}$, and *(iii)* injection inner capillary inlet 2 contained concentrated emulsions at a flow rate of 0.01 $mL \cdot min^{-1}$. The release of emulsion droplets from the 'matchstick' fiber was initiated with the basification of the solution (pH 10 − 11, adjusted with 1 M NaOH).

### 4.4.9. Fabrication of 'Cake' Supracolloidal Macrostructure with Multiple Layers.

The 'cake' was fabricated by setting the layers of concentrated emulsions in a cylindrical mold with a diameter of 0.7 cm (layers: red, white and blue colors). The layers were set simultaneously by dissolving gluconic acid δ−lactone (0.05 w/v%) in the concentrated emulsion. A magnetic stirrer bar was added to the layers before the layers set. The cap was applied on the top of the 'cake'. The emulsion droplets of the layers and cap were stabilized with pH-BCP-Laponite and solely pH-BCP, respectively. The red and blue colors originate from, oil blue N and oil red O dyes in the oil phase of the emulsion droplets. The 'cake' was removed from the mold and submerged in an acidic PVA solution (3 w/v% PVA and acidified with 3 w/v% of gluconic acid δ−lactone). The release was performed in an acidic solution (pH 3, adjusted with 1 M HCl), and initiated with the addition of 1 M NaOH (pH 10 − 11).

## 4.5. Appendix

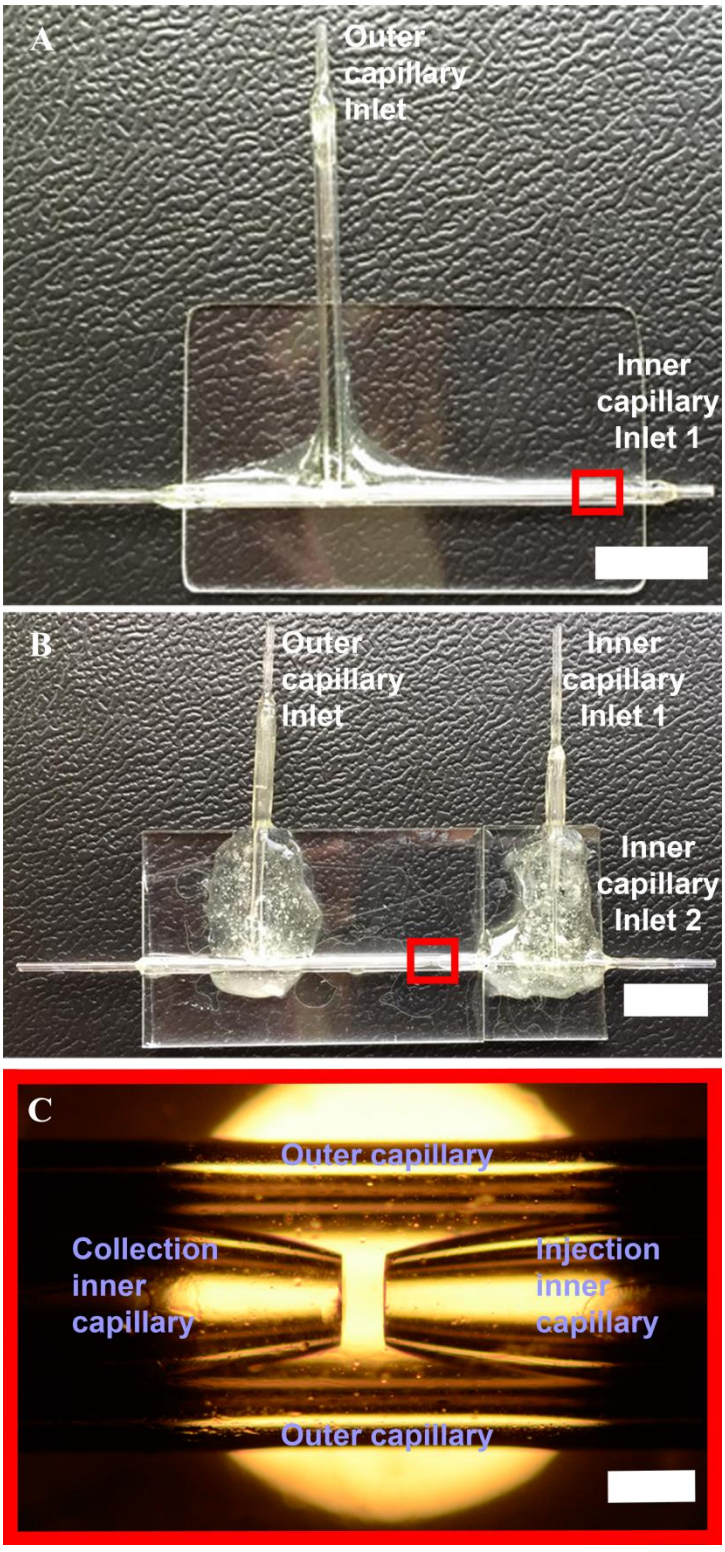


**Figure 4.18-Appx.** Photograph of microfluidics devices with one (A) and two (B) inlets to the injection inner capillary. Scale bars represent 1 cm. (C) The two inner capillaries (injection and collection inner capillaries) are aligned within the outer capillary to produce a flow-focusing junction. Scale bar represents 100 μm.

## 4.6. References


1 M. A. C. Stuart, W. T. S. Huck, J. Genzer, M. Müller, C. Ober, M. Stamm, G. B. Sukhorukov, I. Szleifer, V. V Tsukruk, M. Urban, F. Winnik, S. Zauscher, I. Luzinov and S. Minko, *Nat. Mater.*, 2010, **9**, 101.

2 Y. Bae, S. Fukushima, A. Harada and K. Kataoka, *Angew. Chem. Int. Ed.*, 2003, **42**, 4640.

3 E. R. Gillies, T. B. Jonsson and J. M. J. Fréchet, *J. Am. Chem. Soc.*, 2004, **126**, 11936.

4 M. Nakayama, T. Okano, T. Miyazaki, F. Kohori, K. Sakai and M. Yokoyama, *J. Control. Release*, 2006, **115**, 46.

5 Y. C. Chen, L. C. Liao, P. L. Lu, C. L. Lo, H. C. Tsai, C. Y. Huang, K. C. Wei, T. C. Yen and G. H. Hsiue, *Biomaterials*, 2012, **33**, 4576.

6 E. Amstad, S.-H. Kim and D. A. Weitz, *Angew. Chem. Int. Ed.*, 2012, **51**, 12499.

7 E. G. Bellomo, M. D. Wyrsta, L. Pakstis, D. J. Pochan and T. J. Deming, *Nat. Mater.*, 2004, **3**, 244.

8 M. Danial, C. M. N. Tran, K. A. Jolliffe and S. Perrier, *J. Am. Chem. Soc.*, 2014, **136**, 8018.

9 G. Ibarz, L. Dähne, E. Donath and H. Möhwald, *Adv. Mater.*, 2001, **13**, 1324.

10 G. B. Sukhorukov, A. A. Antipov, A. Voigt, E. Donath and H. M̈hwald, *Macromol. Rapid Commun.*, 2001, **22**, 44.

11 Y. Zhu, J. Shi, W. Shen, X. Dong, J. Feng, M. Ruan and Y. Li, *Angew. Chem. Int. Ed.*, 2005, **44**, 5083.

12 L. Y. Chu, S. H. Park, T. Yamaguchi and S. I. Nakao, *J. Memb. Sci.*, 2001, **192**, 27.

13 W. C. Jeong, S. H. Kim and S. M. Yang, *ACS Appl. Mater. Interfaces*,

2014, **6**, 826.

14 L.-Y. Chu, Y.-J. Liang, W.-M. Chen, X.-J. Ju and H.-D. Wang, *Colloids Surf. B. Biointerfaces*, 2004, **37**, 9.

15 A. Gutowskad, Y. H. Baea, J. Feijenb, S. W. Kim and I. May, *J. Control. Release*, 1992, **22**, 95.

16 H. Ghandehari, P. Kopecková and J. Kopecek, *Biomaterials*, 1997, **18**, 861.

17 P. D. Thornton, R. J. Mart and R. V. Ulijn, *Adv. Mater.*, 2007, **19**, 1252.

18 J. Bibette, F. L. Calderon and P. Poulin, *Rep. Prog. Phys.*, 1999, **62**, 969.

19 R. T. Woodward, R. A. Slater, S. Higgins, S. P. Rannard, A. I. Cooper, B. J. L. Royles, P. H. Findlay and J. V. M. Weaver, *Chem. Commun.*, 2009, 3554.

20 A. M. Mathur, B. Drescher, A. B. Scranton and J. Klier, *Nature*, 1998, **392**, 367.

21 S. Fujii, E. S. Read, B. P. Binks and S. P. Armes, *Adv. Mater.*, 2005, **17**, 1014.

22 Y. Liu, P. G. Jessop, M. Cunningham, C. A. Ekert and C. L. Liotta, *Science*, 2006, **313**, 958.

23 S. Khoukh, P. Perrin, F. Bes De Berc and C. Tribet, *ChemPhysChem*, 2005, **6**, 2009.

24 A. Vesperinas, J. Eastoe, P. Wyatt, I. Grillo, R. K. Heenan, J. M. Richards and G. A. Bell, *J. Am. Chem. Soc.*, 2006, **128**, 1468.

25 J. V. M. Weaver, S. P. Rannard and A. I. Cooper, *Angew. Chem. Int. Ed.*, 2009, **48**, 2131.

26 A. Y. C. Koh and B. R. Saunders, *Chem. Commun.*, 2000, **6**, 2461.

27 E. Garcia-Tunon, S. Barg, R. Bell, J. V. M. Weaver, C. Walter, L. Goyos and E. Saiz, *Angew. Chem. Int. Ed.*, 2013, **52**, 7805.

28 R. T. Woodward and J. V. M. Weaver, *Polym. Chem.*, 2011, **2**, 403.

29 A. L. B. Maçon, S. U. Rehman, R. V. Bell and J. V. M. Weaver, *Chem. Commun.*, 2016, **52**, 136.

30 T. Heuser, E. Weyandt and A. Walther, *Angew. Chem. Int. Ed.*, 2015, **54**, 13258.

31 C. Tang, R. V. Ulijn and A. Saiani, *Langmuir*, 2011, **27**, 14438.

32 S. Debnath, S. Roy and R. Ulijn, *J. Am. Chem. Soc.*, 2013, **135**, 16789.

33 J. Boekhoven, A. M. Brizard, K. N. K. Kowlgi, G. J. M. Koper, R. Eelkema and J. H. Van Esch, *Angew. Chem. Int. Ed.*, 2010, **49**, 4825.

34 R. V. Bell, C. C. Parkins, R. A. Young, C. Preuss, M. M. Stevens and S. A. F. Bon, *J. Mater. Chem. A*, 2016, **4**, 813.

35 P. Das, J. Malho, K. Rahimi, F. H. Schacher, B. Wang, D. E. Demco and A. Walther, *Nat. Commun.*, 2015, **6**, 5967.

36 W. Zhu, C.-H. Lu, F.-C. Chang and S.-W. Kuo, *RSC Adv.*, 2012, **2**, 6295.

37 J. Gaume, A. Rivaton, S. Thérias and J.-L. Gardette, *Polym. Degrad. Stab.*, 2012, **97**, 488.

38 M. Fidaleo and R. Lavecchia, *Chem. Biochem. Eng. Q.*, 2003, **17**, 311.

# Chapter 5

## Conclusions and Future Work

In this chapter, we discuss the conclusions of the work presented in this thesis and discuss future work and potential applications.

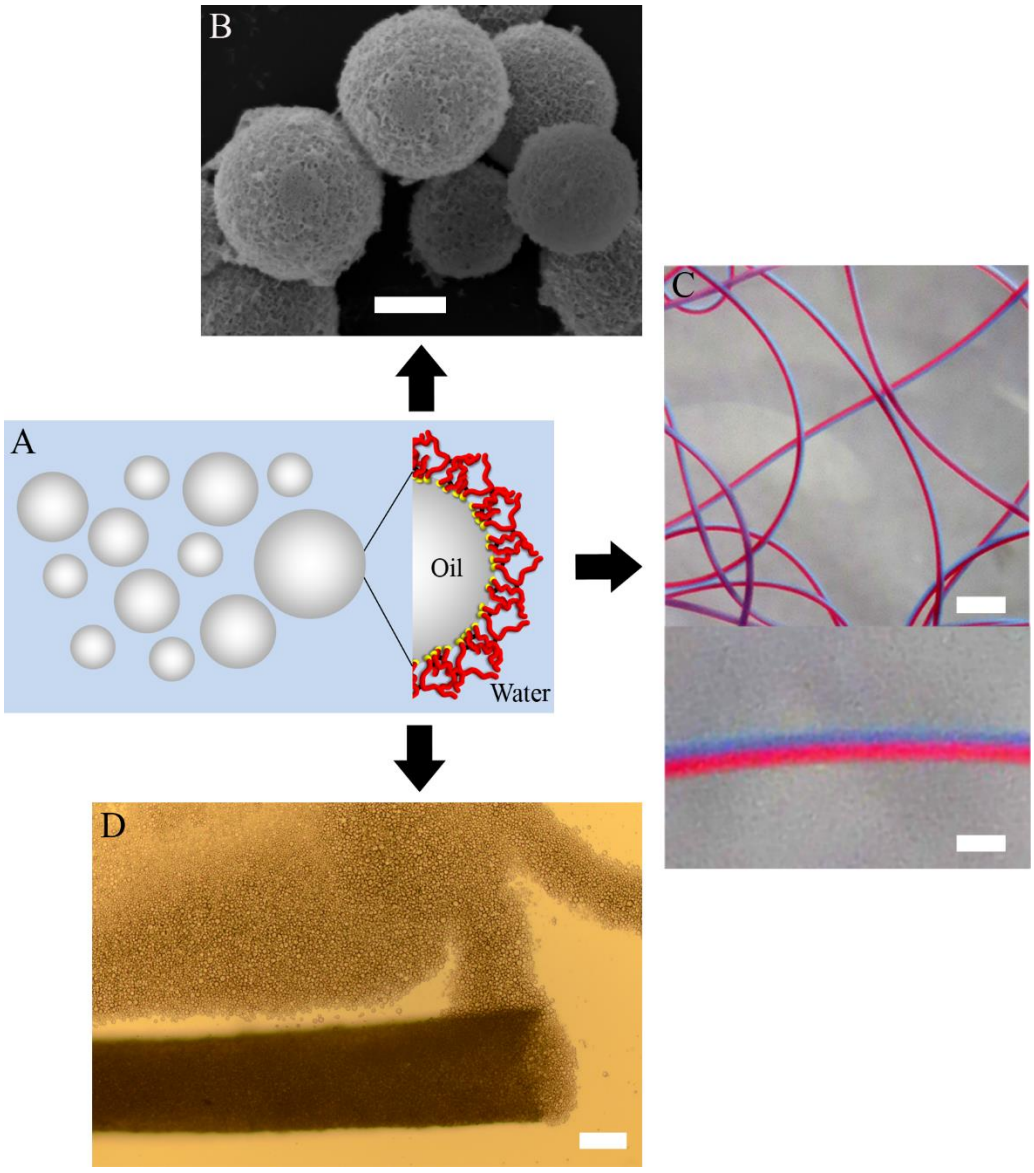


(A) Oil-in-water emulsion droplets stabilized with branched copolymers. These emulsion droplets were used as a platform to create novel emulsion-based supracolloidal materials. (B) Calcium phosphate microcapsules. Scale bar represents 5 µm. (C) Asymmetric Janus high internal phase emulsion fiber. Scale bars represent 0.1 cm (top) and 300 µm (bottom). (D) Supracolloidal fiber as a storage material for emulsion droplets. Emulsion droplets are released from the fiber upon basification. Scale bar represents 100 µm.

In this thesis, branched copolymers with the correct chemical composition and architectural structure were utilized as emulsifying agents for the production of oil-in-water emulsion. These emulsion droplets were utilized as a platform to create novel emulsion-based supracolloidal materials.

***Chapter 2*** reported on a versatile and time-efficient method to fabricate calcium phosphate (CaP) microcapsules by utilizing oil-in-water emulsion droplets stabilized with synthetic branched copolymer as templates. The branched copolymer was designed to provide a suitable architecture and functionality to produce stable emulsion droplets, and permit the mineralization of CaP at the surface of the oil droplet when incubated in a solution containing calcium and phosphate ions. The CaP capsules were made fluorescent by functionalizing the surface of the CaP shell with a fluorescein−bisphosphonate conjugate.

*Future work*: The oil phase of the CaP capsules can act as a compartment for hydrophobic materials and can be release on demand with sonication or acidification. Therefore, studies should be conducted on these CaP capsules to determine whether they can be utilized as drug/molecule delivery system. The CaP shells of the microcapsules were established to be calcium deficient hydroxyapatite with incorporated chlorine and carbonate species. Hydroxyapatite is well known for its biocompatibility and bioactivity so it would be good to see how these CaP capsules interact with cells. The composition of the CaP shell crystal structure can be further functionalized, by utilizing the ability of the apatite structure to accept numerous ionic substituents, for additional functionality. Incorporation of silver and fluoride, lanthanides, and iron ions provide anti-bacterial, fluorescent, and magneto-responsive properties, respectively. Furthermore, the surface of the CaP shell can be functionalized via addition of bisphosphonate−X conjugate (where X can be the desired functionality). The surface of CaP capsules can be decorated with interactive molecules (antigen : antibody, Avidin : biotin, cucurbituril : a pair of electron-rich and electron-deficient molecules, and 2-ureido-4[1H] pyrimidinone) for selective interactions between capsule to capsule and/or hosts. Also, polymers at the surface of the CaP capsule can be attached or grown for stimuli-responsive properties (such as temperature responsive polymer: poly(N−isopropyl acrylamides)), or to improve compatibility to polymer blends if CaP capsules are

added as an additive. Lastly, these CaP capsules are fragile materials and can be potentially added to self-healing materials. Upon impact of the self-healing material, these CaP capsules would absorb the impact energy and break, allowing the release of the material inside the capsules required to heal the self-healing material.

***Chapter 3*** illustrated that individual oil-in-water emulsion droplets which are stabilized by Laponite clay discs functionalized with pH-responsive branched copolymers can be assembled into fibers using a microfluidic wet spinning process. The proton diffusion into the stream of emulsion droplets induces the reversible self-assembly process leading to the formation of a continuous supracolloidal fiber. The production of stripy Janus type fibers (two and three stripes), magnetic fibers, and fibers of controlled length suggest the versatility of the material and method. These supracolloidal fibers can be used as a tool to delivery volatile compounds, where the evaporation rate of the volatile compounds can be tuned as a function of calcium ions concentration. The dried fibers produced are low-weight highly porous materials.

*Future work*: These supracolloidal fibers can potentially be used to make fabrics that have the ability to release active compounds in a time-controlled manner, such as, mosquito nets and clothing that release insect repellent, or fabric-based home accessories (carpets, curtains, and cushions) that release fragrances. The emulsion droplets in the fiber act as reservoirs for the active compounds and are release in a time-controlled manner. These reservoir droplets in the fiber can be refilled by simply soaking the fabric into a solution containing the active compounds. However, these supracolloidal fibers are not tough enough to create fabrics. Further studies are required to toughen these fibers. Some suggestions are *(i)* growing nylon polymer at the interface of the emulsion droplets throughout the fiber, or *(ii)* coating the fiber with polyester and chemically cross-linking it to fiber.

***Chapter 4*** shown that microfluidically spun supracolloidal fibers can act as a storage material for emulsion droplets, were emulsion droplets are locked in the fiber structure in acidic condition, and are released from the fiber upon basification of the system. The fiber was coated with a flexible composite

clay/polymer film, which acts as a physical barrier between the emulsion in the fiber structure and the exterior medium, and only permits the outflow of emulsion droplets at the endpoints of the fiber. The release of emulsion droplets from the fiber can be time-controlled by programming the transient acidic pH states of the system by combining a fast acidic promoter with a feedback-driven biocatalytically controlled slow generation of base in a close system. The ability to fabricate other supracolloidal structures, such as 'matchstick' fiber and 'cake' suggest the versatility of the material.

*Current studies are in progress*: It was determined that the enzyme (urease) can be incorporated inside the fiber structure. It was also observed that the pH-change (from acidic to basic) only occurred locally inside fiber and not the surrounding medium (In Chapter 4, the enzyme was added in the exterior medium, which in turn, changed the pH of the whole medium). Emulsions droplets are still released from the fiber at basic pH even after the fiber has been modified. Further studies are currently running to produce novel supracolloidal fibers as storage materials with more complexity.

*Future work*: Chapter 4 described the production of supracolloidal tube embedded with emulsion droplets. The aim in the future is to make these tubes 'constrict' and 'dilate' in response to stimuli. Some suggestions are *(i)* light- and pH-responsive tubes: Load the oil phase of the emulsion droplets embedded on the tube with photo-acids. Protons are released from the emulsion droplets when radiated with light, causing the tube to 'constrict' due to the presence of the pH-responsive branched copolymers, and *(ii)* temperature-responsive tubes: Replace the emulsion droplets with particles made of poly(N−isopropyl acrylamides) (temperature responsive polymer) stabilized by Laponite clay discs functionalized with pH-responsive branched copolymers. The tube will 'constrict' at high temperature and 'dilate' at low temperature (poly(N−isopropyl acrylamides) is hydrophobic at high temperature and hydrophilic at low temperature). These stimuli-responsive tubes can be used in transportation of particles from one area to another area.